Non-invasive optical monitoring of free and bound oxygen in humans

Krite Svanberg, Emilie

2016

Non-invasive optical monitoring of free and bound oxygen in humans

Emilie Krite Svanberg, MD

LUND
UNIVERSITY

DOCTORAL DISSERTATION
by due permission of Lund University, Faculty of Medicine
to be defended at Jubileumsaulan, Medical Research Centre,
Jan Waldenströms gata 5, Skåne University Hospital, Malmö, Sweden
on 18th March, 2016 at 9.15 a.m.

Faculty opponent:
Professor Eddie Weitzberg
Anesthesiology and Intensive Care Medicine, Karolinska Institute, Stockholm

Supervisor:
Professor Jonas Åkeson
Anesthesiology and Intensive Care Medicine

Co-supervisors:
Professor Stefan Andersson-Engels
Atomic Physics
Professor Vineta Fellman
Pediatrics

Organization	Document name
LUND UNIVERSITY Faculty of Medicine Department of Clinical Sciences Malmö Anesthesiology and Intensive Care Medicine	DOCTORAL DISSERTATION
	Date of dissertation March 18, 2016
Author: Emilie Krite Svanberg	Sponsoring organization

Title and subtitle: Non-invasive optical monitoring of free and bound oxygen in humans

Background: Possibilities of detecting oxygen - both in its free form, as gas in the lungs, and in its bound form, as oxygenated hemoglobin - have been explored in this thesis. Perfusion and oxygenation of vital organs (e.g., heart, brain and kidneys) may be severely compromised in critical illness or major trauma, which is why blood is rapidly diverted to those organs to improve chances of survival. Blood vessels in less important organs (e.g., skin, skeletal muscles and intestines) are constricted, leading to reduced regional perfusion and oxygenation in these organs. Non-invasive measurements of changes in tissue perfusion and oxygenation, in e.g., the forearm, might give an early indication of clinical deterioration.

Preterm infants are very vulnerable patients. Their organs, in particular the lungs, are not fully developed, and the respiratory distress syndrome (RDS) frequently occurs. The intestines may be affected by necrotizing enterocolitis (NEC). Complementary diagnostic and surveillance methods of RDS and NEC are desirable.

Aims: The overall aim of this thesis, which includes Studies I-IV, was to develop and evaluate non-invasive optical techniques, based on light at different wavelengths, to complement future bedside surveillance in critically illness or severe injury, for adults as well as for infants.

Methods: Changes in tissue oxygenation by near-infrared spectroscopy (I-II), blood perfusion by laser Doppler imaging (I) and blood volume by tissue viability imaging (I) in skeletal muscle and skin were studied, and continuous-wave and time-resolved near-infrared spectroscopy were compared (II) in healthy volunteers subjected to various defined regional physiological perturbations.

For the first time, gas in scattering media absorption spectroscopy (GASMAS) was used to detect alveolar water vapor (III-IV) and oxygen gas (IV), as well as intestinal water vapor (III) in newborn infants.

Main results: Near-infrared spectroscopy, laser Doppler imaging and tissue viability imaging provided valuable information on physiological changes in the microcirculation (I). Continuous-wave and time-resolved near-infrared spectroscopy techniques were both able to determine changes in tissue oxygenation, but the time-resolved technique provided more realistic values with smaller inter-individual differences (II). Alveolar (III-IV) and intestinal signals of water vapor (III), were readily detected, together with alveolar signals of oxygen gas (IV), non-invasively in newborn infants.

Conclusions: Optical techniques, being non-invasive and providing data in real-time, are attractive as potential tools for surveillance in critical illness or severe injury, in particular concerning the oxygenation. As an overall conclusion, we believe, that fully developed time-resolved near-infrared techniques have the potential to become an additional monitoring method of choice for surveillance of critically ill or severely injured patients.

Likewise, GASMAS has great potential for future monitoring of critically ill preterm or full-term infants, and might, ultimately, reduce the current use of X-ray imaging in these most vulnerable patients.

Key words: Intensive care, oxygenation, free gas, near-infrared spectroscopy, absorption spectroscopy, scattering

Classification system and/or index terms (if any)

Supplementary bibliographical information	Language: English
Lund University, Faculty of Medicine Doctoral Dissertation Series 2016:27	
ISSN and key title:1652-8220	ISBN: 978-91-7619-253-5
Recipient's notes / Number of pages: 109	Price
Security classification	

Non-invasive optical monitoring of free and bound oxygen in humans

Emilie Krite Svanberg, MD

LUND
UNIVERSITY

Cover photo, front: Sunrise at Klädesholmen – a lot of red, scattered light in fresh, oxygen-containing air!
Cover photo, back: Solar spectrum with Fraunhofer absorption lines (modified from Wikipedia).

Department of Clinical Sciences Malmö
Anesthesiology and Intensive Care Medicine
Faculty of Medicine
Lund University
Sweden

Lund University, Faculty of Medicine Doctoral Dissertation Series 2016:27
ISBN 978-91-7619-253-5
ISSN 1652-8220

Printed in Sweden by Media-Tryck, Lund University
Lund 2016

Rerum indagare naturas est cogitationes
Dei post Deum cogitare
(after Johannes Kepler 1571-1630)

To my beloved parents and little sister

To my wonderful family
– William, Valdemar, Ragnhild,
and my husband Martin

Table of contents

Original papers

The present thesis is based on the following original papers (**I-IV**), corresponding to four individual studies (**I-IV**), and referred to in the text by their Roman numbers:

I. Krite Svanberg E, Wollmer P, Andersson-Engels S, Åkeson J. Physiological influence of basic perturbations assessed by non-invasive optical techniques in humans. *Applied Physiology, Nutrition and Metabolism* 2011; 36: 946-957.

II. Krite Svanberg E, Shaharin A, Ellerström I, Subash AA, Khoptyar D, Andersson-Engels S, Åkeson J. Time-resolved versus continuous-wave near-infrared spectroscopy for determination of oxygen saturation in human skeletal muscle tissue. Manuscript.

III. Lundin P, Krite Svanberg E, Cocola L, Lewander Xu M, Somesfalean G, Andersson-Engels S, Jahr J, Fellman V, Svanberg K, Svanberg S. Noninvasive monitoring of gas in the lungs and intestines of newborn infants using diode lasers: feasibility study. *Journal of Biomedical Optics* 2013; 18: 127005-1-127005-8.

IV. Krite Svanberg E, Lundin P, Larsson M, Åkeson J, Svanberg K, Svanberg S, Andersson-Engels S, Fellman V. Diode laser spectroscopy for noninvasive monitoring of oxygen in the lungs of newborn infants. *Pediatric Research*, advance online publication 10 February 2016; doi:10.1038/pr.2015.267.

Summary

Oxygen in human tissue – both in its bound form, as oxygenated hemoglobin in the capillaries of skeletal muscle tissue, and in its free form, as oxygen gas in the alveoli of the lungs – has been explored in this thesis. All studies (**I-IV**) in this thesis are based on non-invasive optical measurements.

The overall aim of this thesis is to develop and evaluate techniques, based on light at different wavelengths, with potential of being compliments for bedside surveillance of critically ill or injured adult or pediatric patients.

Changes in tissue oxygenation of skeletal muscle under various physiological perturbations in adult subjects have been evaluated, and possibilities of detecting alveolar oxygen gas in newborn infants have been explored. The penetration of light through tissue is limited, leading to different applicability of the techniques studied depending on tissue layer thickness.

Each specific substance, appearing in bound or gaseous form, absorbs light at specific wavelengths. A "spectral fingerprint" is obtained – broad and more diffuse for bound substances, and sharper and easier to identify for free gases. This difference demands different experimental approaches – broad-band spectral light sources for detection of oxygen bound to hemoglobin, and narrow-band light (from semi-conductor laser sources) for detection of free oxygen gas. Since not only the content of oxygen in blood, but also the blood perfusion are important for oxygen transport, laser Doppler techniques have been employed to study the transport of bound oxygen in blood. The amount of blood available is of course another important factor, which is the reason why tissue viability imaging, a non-invasive technique providing estimates on regional blood volume, has also been evaluated.

In critical illness or major injury, where perfusion and oxygenation of vital organs (e.g., heart, brain and kidneys) may be severely compromised, blood is rapidly diverted to those organs to improve chances of survival. Blood vessels in less important organs (e.g., skin, skeletal muscle and intestines) are constricted, leading to reduced local perfusion and oxygenation. Non-invasively determined changes in regional tissue blood flow and oxygenation in e.g., the forearm, might hence indicate early medical deterioration. More central measurements, closer to vital organs, are certainly possible, but since the body struggles to maintain perfusion and oxygenation of these organs, such measurements could be expected to provide delayed information, compared with those in peripheral limbs. Moreover, central

measurements often demand varying degrees if invasiveness, e.g., central venous or pulmonary artery catheterization.

We have evaluated, in healthy volunteers, how tissue perfusion, blood volume and oxygenation respond to non-harmful, locally induced physiological perturbations, designed to resemble early medical deterioration (**I-II**). Doppler spectroscopy and the broad-band spectroscopic techniques tissue viability imaging and near-infrared spectroscopy, detect and reflect changes in tissue perfusion, blood volume and oxygenation in skin and skeletal muscle under various physiological conditions (**I-II**). The latter technique in its time-resolved version seems to be particularly promising, and might in the future serve as a valuable compliment in the surveillance of critically ill or injured patients.

Preterm infants are most vulnerable patients. Since their organs, in particular the lungs, are not fully developed at birth, much of the medical care aims at creating conditions for optimal respiratory function and oxygenation. We have shown that – by transmitting light at the right wavelength through the chest wall and detecting the diffuse light returning from the tissue – it is possible to detect free gas (**III-IV**), and in particular oxygen (**IV**), non-invasively in newborn infants. The results obtained provide guidance on how treatment could be improved, and the need of potentially harmful radiological examinations could be reduced.

Summary in Swedish

Syre i mänsklig vävnad - både i sin till blodet bundna form, som syresatt hemoglobin i perifer skelettmuskulatur, och i sin fria form, som gas i lungornas luftfyllda hålrum - har studerats i denna avhandling. I samtliga delarbeten har icke-invasiva optiska (ljusbaserade) tekniker använts.

Målet med avhandlingen är att finna och utvärdera tekniker, baserade på ljus vid olika våglängder, med potential att utgöra komplement för övervakning av svårt sjuka patienter, såväl vuxna som barn.

Avhandlingen är baserad på fyra delarbeten (**I-IV**), där den röda tråden är att studera syre i kroppen - från att det kommer ner i lungorna genom inandning tills det i bunden form når ut till kroppens vävnader.

Vi har undersökt hur syresättningen i skelettmuskulatur hos vuxna förändras under olika fysiologiska provokationer. Vidare studeras möjligheterna att kunna mäta och kvantifiera fri syrgas inne i lungans luftfyllda hålrum, i de aktuella fallen hos nyfödda barn. Ljus har begränsad genomtränglighet i vävnad, vilket gör att de använda mätmetoderna har olika tillgänglighet beroende på vävnadslagrens tjocklek.

Mättekniskt utnyttjas förhållandet, att varje specifikt ämne, vare sig det uppträder som gas eller i fast form, absorberar ljus vid för ämnet karakteristiska våglängder. Man får ett ”spektroskopiskt fingeravtryck”, som när det gäller fria gaser är ytterst skarpt och lättidentifierbart, medan fasta ämnen har bredare och mera diffusa strukturer. Denna skillnad leder till olikartade mättekniker - för syrgas utnyttjas smalbandig laserstrålning från en halvledarlaser, medan mer bredbandiga ljuskällor utnyttjas för vävnadsbundet syre. Eftersom inte enbart syrekoncentrationen i blodet, utan även själva blodflödet är av betydelse för syretransporten, har även laser-Doppler-teknik används för att studera transporten av det bundna syret.

Vid kritisk sjukdom, där livsviktiga organ (t ex hjärna, hjärta och njurar) hotas av dålig genomblödning och syresättning, omfördelas blodet snabbt i kroppen för att öka möjligheterna till överlevnad. Blodkärlen i mindre viktiga organ (t. ex. hud, skelettmuskulatur och tarmar) dras samman, så att blodflödet och syresättningen där minskar. Mätningar från kroppens utsida av hur blodflöde och syresättning i hud och muskulatur, t. ex. i underarmen, förändras, skulle tidigt kunna varna när kroppen är på väg in i ett mer kritiskt tillstånd. Att mäta mera centralt, nära de vitala organen görs idag i klinisk praxis, men då kroppen in i det sista kämpar för att upprätthålla god blodförsörjning dit, kommer dessa mätningar ge utslag senare än mätningar i armar eller ben. Ofta förutsätter dessutom centrala mätningar att man lagt in slangar i

stora kärl nära hjärtat. Vi har studerat hur blodflödet och syresättningen i huden och musklerna i underarmen förändras i samband med ofarliga provokationer hos friska frivilliga vuxna forskningspersoner (**I-II**). Vi har funnit att bredbandig optisk spektroskopi, speciellt om den genomförs med tidsupplöst teknik, kan registrera och följa syresättningen i muskelvävnad med hög noggrannhet och därför i framtiden skulle kunna bli ett användbart komplement för patientnära övervakning vid kritisk sjukdom eller omfattande kroppskada.

Barn, som föds för tidigt, är en mycket utsatt patientgrupp. Deras organ, framför allt lungorna, är inte fullt utvecklade, varför mycket av vården inriktas på att skapa förutsättningar för bästa möjliga andningsfunktion och syresättning för att minimera och helst helt förebygga skador på viktiga organ. Vi har - genom att lysa med ljus av rätt våglängd på bröstkorgens hudyta och samtidigt fånga upp det diffusa ljus som kommer tillbaka från vävnaden (**III-IV**) - kunnat visa att fri gas (**III**) och framför allt syrgas (**IV**) kan detekteras i lungorna på nyfödda barn. Resultaten ger vägledning kring hur dagens medicinska behandlingar skulle kunna förbättras och hur behovet av upprepade röntgenundersökningar på svårt sjuka spädbarn skulle kunna minskas.

Abbreviations

ABP	Arterial blood pressure
ADH	Antidiuretic hormone
ADP	Adenosine diphosphate
ANF	Atrial natriuretic factor
ATP	Adenosine triphosphate
ATT	Adipose tissue thickness
BE	Base excess
B-Hb	Blood concentration of Hb
BPD	Bronchopulmonary dysplasia
CO	Cardiac output
CO_2	Carbon dioxide
COHb	Carboxyhemoglobin
CPAP	Continuous positive airway pressure
CW-NIRS	Continuous-wave NIRS
2,3-DPG	2,3-diphosphoglycerate
DAP	Diastolic arterial pressure
DO_2	O_2 delivery
F_iO_2	Fraction of inspired O_2
GASMAS	Gas in scattering media absorption spectroscopy
Hb	Hemoglobin
HbA	Adult Hb
HbF	Fetal Hb
Hb^-	Deoxyhemoglobin
HbO_2	Oxyhemoglobin
HbT	Total Hb count
H_2O	Water
HR	Heart rate
IQR	Inter-quartile range
LDI	Laser Doppler imaging
MAP	Mean arterial pressure
MetHb	Methemoglobin
NEC	Necrotizing enterocolitis
NIR	Near-infrared
NIRS	Near-infrared spectroscopy
$PaCO_2$	PCO_2 in arterial blood
PaO_2	PO_2 in arterial blood

PCO_2	Partial pressure of CO_2
PO_2	Partial pressure of O_2
$P_{50}O_2$	PO_2 at which SO_2 is 50 %
PPG	Photoplethysmography
PTOFS	Photon time-of-flight spectroscopy
PVR	Peripheral vascular resistance
O_2	Oxygen
RDS	Respiratory distress syndrome
RH	Reactive hyperemia
SaO_2	Arterial SO_2
SAP	Systolic arterial pressure
$ScvO_2$	Central venous O_2 saturation
SO_2	Hb saturation of O_2
SpO_2	Percutaneous SaO_2
StO_2	Tissue oxygenation
SV	Stroke volume
SvO_2	Mixed venous O_2 saturation
SVR	Systemic vascular resistance
TVI	Tissue viability imaging
VO_2	O_2 consumption
WMS	Wavelength modulation spectroscopy

Preface

This thesis concerns oxygenation, a field of major importance in medicine, not the least in intensive care medicine - a field catching my interest as a medical student. The whole journey started as a diploma project, suggested by my present main supervisor, professor Jonas Åkeson. He wanted to explore possibilities and limitations of different commercially available non-invasive optical techniques in intensive care medicine. During the course of the project, certainly good opportunities were found, but also limitations. Absorption is normally used for optical quantification of chemical substances (oxyhemoglobin being one). A major challenge of human tissue is the simultaneous presence of extensive light scattering. To combat this, more advanced approaches are needed, calling for interdisciplinary collaboration. This became available through my co-supervisor professor Stefan Andersson-Engels, a physicist with long experience in optical spectroscopy in scattering media. In this way the most promising technique from the first study – continuous-wave near-infrared spectroscopy - could be compared with the more advanced time-resolved tissue spectroscopy technique in studies of relevant conditions in adults. A most fruitful interdisciplinary collaboration had started!

By coincidence, the physicists had at around this time started to get interested in free oxygen monitoring in tissue, mainly related to infection, like sinusitis. The idea emerged of closing the oxygenation loop in the thesis by combining - for the first time *in situ* in humans - monitoring of free alveolar oxygen within the lungs with studies of oxygen bound to hemoglobin.

Because of the limited penetration of light in tissue, the smallest individuals - newborn infants – seemed to be the most suitable starting point for optical lung monitoring. My other co-supervisor, professor Vineta Fellman, saw particular potential in such techniques, since lung problems are among the most severe in neonatology, a particularly demanding area of intensive care medicine. Free oxygen monitoring calls for quite different experimental techniques, but light scattering in tissue remained the major issue to address. Towards the end of this most rewarding interdisciplinary journey, monitoring of free alveolar oxygen also in adults – based on internal administration of light - emerged as a future possibility.

I sincerely hope that results reported in this thesis might serve as a base for improved management of severe disease, and ultimately make a real difference for somebody.

Background

Clinical aspects

Since various aspects of tissue oxygenation are of central importance in the present thesis, an overview of the complex and interlaced processes is first given as a general background.

Oxygen is a prerequisite for life. The lungs need to be filled with air with its vital oxygen crossing alveolar-capillary membranes to enter the blood stream. Proper expansion of the alveoli in the lungs and short diffusion distances are mandatory for successful transportation of oxygen. Inhomogeneous distribution of air and thickened membranes in respiratory diseases in newborn preterm infants lead to a poor oxygenation. Reduced oxygenation of peripheral tissues (e.g., skin and skeletal muscle) could be an early indicator of medical deterioration (e.g., in hemorrhagic shock), reflecting early reduction of peripheral tissue perfusion to improve perfusion of more vital organs and tissues.

Oxygen

Oxygen is a chemical element with atomic number 8 and atomic weight 16. It exists as an odorless and colorless diatomic gas (O_2) in the lower atmosphere and also as triatomic oxygen (O_3), ozone, in particular in the upper atmosphere. Oxygen is a reactive element and an oxidizing agent that readily forms compounds (primarily oxides) with most elements.

Oxygen makes up 21 % of air by volume. It was discovered independently by the Swedish pharmacist Carl Wilhelm Scheele (1742-1786) (Fig. 1) in 1771 [1-3], and by the English chemist Joseph Priestley in 1774 [2, 3]. It was also studied by the French chemist Antoine Laurent de Lavoisier, who explained the process of combustion [2, 3].

Figure 1.
Carl Wilhelm Scheele (1742-1786). From [3]; reproduced with permission from John Wiley & Sons, Inc.

Oxygen is essential for cellular respiration in humans and animals, where carbon dioxide (CO_2) is formed [4, 5]. Conversely, CO_2 is consumed and O_2 is created by photosynthesis in plants.

Microcirculation

In the year of 1661, Marcello Malpighi (1628-1694), using the recently invented light microscope, solved the mystery of how the peripheral arteriovenous connections are arranged, by discovering the capillaries [6]. Before this, the scientific knowledge on how blood circulated in the human body from arteries to veins by motions of the heart, was based on a description in 1628 by William Harvey (1578-1657), leaving out the detailed connection between the two systems [7].

Our blood circulation serves the purpose of providing all tissues with oxygen, nutrients and fluid, and to carry away waste products from the metabolism. The capillary bed plays a key role in the exchange between the blood stream and the tissues. There are approximately 25 x 10^9 capillaries in the body, with approximately 6 % of the total blood volume in systemic, and 3 % in pulmonary capillaries. About 80 % of the total microvascular blood volume is located in the capillaries, venules and veins [8]. The diameter of capillaries ranges from 5 to 10 µm and the average length is about 1 mm. The capillary wall is only one cell layer thick, enabling diffusion distances of only about 0.5 µm. Due to the enormous amount of capillaries, their total surface area is 800-1000 m^2 and no cell is more than 20-30 µm away from a capillary [9, 10].

Oxygen transport

Free and bound oxygen

Oxygen in its gaseous form, present in the air surrounding us, is inhaled during breathing. It moves by convection along our airways to reach the alveoli of the lungs, still in its gaseous form. The alveoli are in close contact with the capillaries of the lungs - only approximately 0.5 µm apart. Oxygen passively diffuses along its concentration gradient to the low-oxygen containing blood of the lung capillaries, while CO_2 diffuses along its gradient from capillary blood to alveoli and is then exhaled. Transfer of O_2 across the alveolar-capillary membrane depends on the diffuse conductance for oxygen, and under basal conditions occurs within one-third of the capillary transit time for red blood cells (erythrocytes) [5]. Inside the bloodstream, almost all (97-98 %) O_2 binds to hemoglobin (Hb) within erythrocytes, thus now existing in its bound form [10]. The small amount of O_2 dissolved in blood is directly proportional to the partial pressure of O_2 (PO_2) of blood, and is 0.003 ml/100 ml blood/millimeter mercury at 37 ℃. At normal arterial PO_2 (PaO_2) of 13.3 kPa (equal to 100 mmHg) the dissolved amount is 0.3 ml of O_2/100 ml blood [11]. Oxygen is then being transported as oxygenated Hb (HbO_2) in the erythrocytes to capillaries of different organs and tissues. Here O_2 is released from Hb, moves by diffusion over the capillary membrane across the interstitial fluid space and cell membranes, to finally reach the mitochondria inside the cells, where it has a crucial role in the respiratory chain. At the same time CO_2, a waste product of cell metabolism, rapidly diffuses in the opposite direction to the capillaries, from which it is transported, 60 % as bicarbonate, 30 % bound to Hb (and plasma proteins) and 10 % physically dissolved in the plasma fluid, back to the lungs by the venous bloodstream [11].

Hemoglobin and the dissociation curve of oxygen

Our bone marrow produces about two million erythrocytes per second [12]. This production, erythropoiesis, is a highly prioritized process in the human body. The erythrocyte is an anuclear biconcave disc, on average 7.5 µm wide and 2 µm thick, with a large surface area relative to its volume, promoting gaseous diffusion into the

cell. Hemoglobin, a red-colored pigment in the erythrocytes, is essential for O_2 transport in the human body. Normal adult Hb (Hb A) consists of four sub units, two α and two β polypeptide chains, while fetal Hb (Hb F) consists of two α and two γ chains. One heme moiety, a porphyrin derivate, containing one iron ion in its ferrous (Fe^{2+}) state, is bound to each chain. Each iron ion can reversibly bind one O_2 molecule, whereby deoxygenated Hb (Hb^-) shifts to HbO_2. Each Hb molecule can bind four O_2 molecules, and 1 g of Hb (if totally pure) can bind 1.39 ml of O_2. However, since methemoglobin (metHb) and carboxyhemoglobin (COHb), both unable to bind O_2 as further discussed below (p. 30), make up some percentage of total Hb in the human body, the physiological oxygen-binding capacity is 1.34 ml per g of Hb (Huffner´s constant). This capacity is proportional to the hematocrit level (concentration of erythrocytes) in the blood. In Hb^- the sub units are held in a tense conformation by electrostatic bonds, leading to low affinity for oxygen. However, when one molecule of O_2 binds, the linkages between α and β chains are broken, leading to an increased affinity of Hb for further binding of O_2 [13, 14] (Fig. 2).

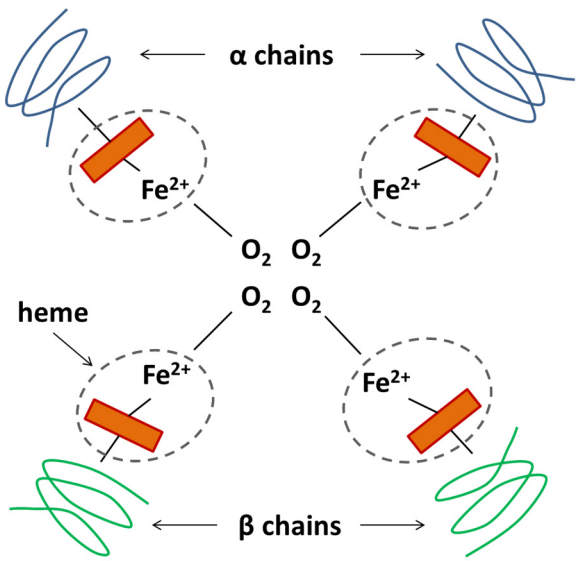

Figure 2.
Schematic drawing of a fully oxygenated molecule of adult hemoglobin (HbA). Modified from [12].

This cooperative nature of O_2 binding to Hb results in a sigmoidal dissociation curve of oxygenation, where O_2 affinity is reduced by increased temperature, partial pressure of carbon dioxide (PCO_2), acidity (Bohr effect) and concentration of 2,3-diphosphoglycerate (2,3-DPG) [15] (Fig. 3). The PO_2 at which binding sites of Hb for O_2 are half-saturated (at 50 %) is referred to as $P_{50}O_2$. HbF has a greater affinity for O_2 than HbA, which is an essential aspect of intrauterine oxygenation [16]. Hb^- has a higher affinity for CO_2 than HbO_2 (Haldane effect) [17]. As mentioned, when O_2 is delivered to organs and tissues, approximately 30 % of CO_2 reversibly binds to

amino groups of polypeptide chains to form carbaminohemoglobin, whereas most of it is transported as bicarbonate (60 %) or dissolved (10 %) in plasma [11].

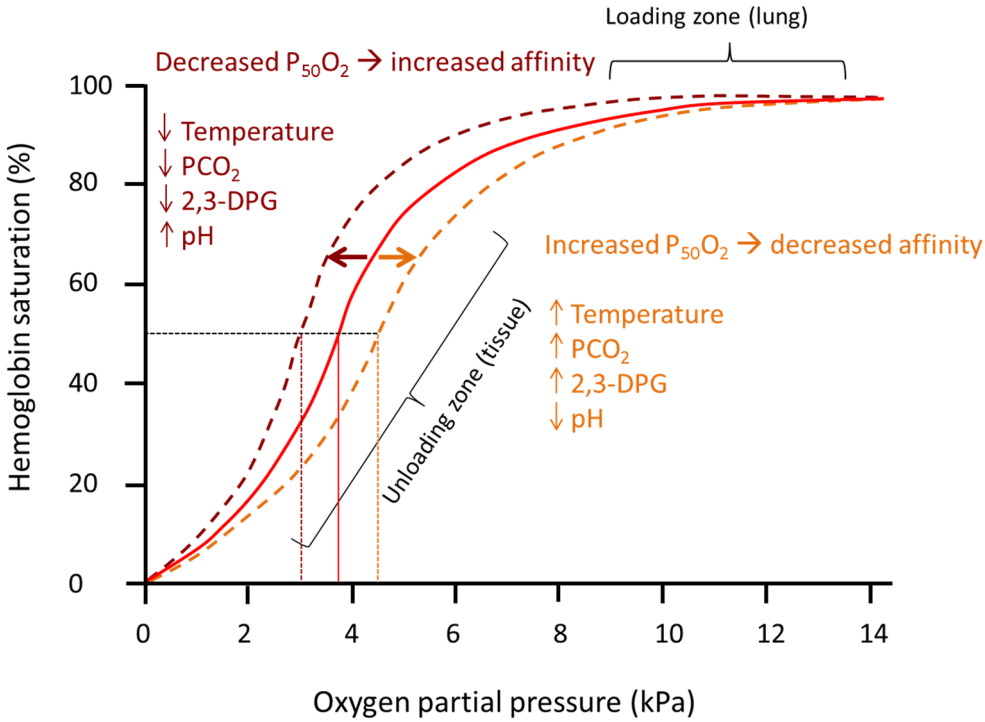

Figure 3.
The sigmoidal oxygenated hemoglobin dissociation curve. Influence of temperature, partial pressure of carbon dioxide (PCO_2), 2,3-diphosphoglycerate (2,3-DPG), and pH on the oxygen (O_2) affinity for hemoglobin is shown by vertical arrows. $P50O_2$ is the partial pressure of O_2, for which hemoglobin is half-saturated (at 50 %). For normal conditions, the solid red curve, $P50O_2$ is 3.6 kPa, as indicated. Modified from [18].

The driving gradient of PO_2 determines O_2 flux by diffusion across membranes and barriers in lungs and various organs and tissues The non-linearity of the O_2 dissociation curve promotes maximal diffusion of O_2 across alveolar-capillary membranes at the higher levels of PO_2 in the lungs. Accordingly, lower levels of PO_2 in other organs and tissues promote unloading of O_2 (Fig. 3).

The rates of loading and unloading of O_2 are slow, since erythrocytes are "squeezed" through the narrow capillaries in the tissues, the capillary diameters are 5-10 µm, while the diameter of an erythrocyte is 7.5 µm. Diffusion constant values are approximately 100 000 times higher in alveolar gas than in tissue. Unless diffusion in the lungs is compromised by prolonged diffusion distances, as in pulmonary edema or interstitial lung disease, tissue unloading of O_2 is the limiting factor in O_2 transportation.

Tissue oxygenation

Adequate tissue oxygenation (StO_2) is the fundamental purpose of the respiratory and cardiovascular system in humans (Fig. 4). Factors determining StO_2 are discussed in the following section.

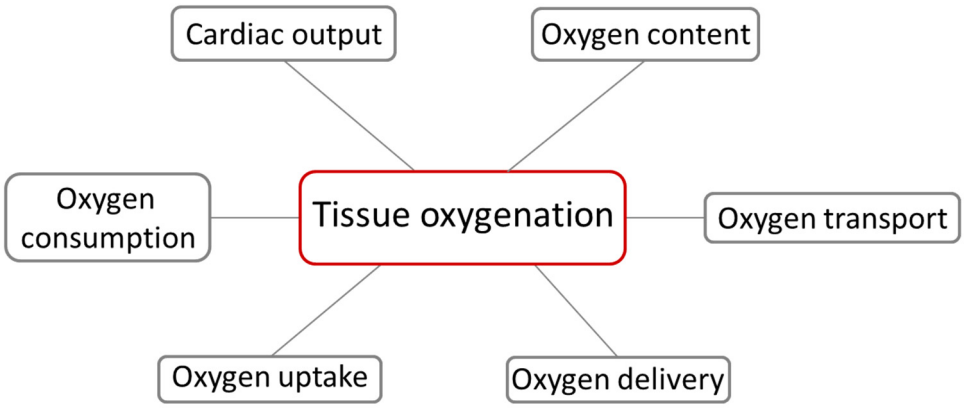

Figure 4.
Schematic figure of factors determining tissue oxygenation (StO_2).

Efficient supply of O_2 and substrates is essential for aerobic cellular respiration. A single enzyme, cytochrome C oxidase, accounts for more than 90 % of O_2 consumption in the human body. This is the final enzyme complex of the cellular respiratory chain in the mitochondria. It oxidizes cytochrome C, whereby O_2 and H^+ are reduced to form water (H_2O). Energy needed in our cells is obtained from high energy phosphate bonds in adenosine triphosphate (ATP). Oxidative phosphorylation with glucose as a substrate and molecular O_2 as the terminal electron acceptor is the most efficient way of producing ATP, primarily from adenosine diphosphate (ADP). In total 38 molecules of ATP are generated per molecule of glucose under aerobic (compared with 2 ATP under anaerobic) conditions [5].

Continuous and adequate supply of O_2 and substrates (e.g., glucose) to different tissues in the body relies on proper function of the respiratory, cardiac, and macro- and microvascular systems. At rest, there are normally wide margins between arterial delivery of O_2 (DO_2) to organs and tissues (approximately 1.0 l/min) and their uptake (VO_2) of O_2 (approximately 0.25 l/min). This allows for maintenance of aerobic respiration and VO_2 also when DO_2 is considerably reduced.

Oxygen delivery is determined by the cardiac output (CO), blood concentration of Hb (B-Hb), and arterial saturation of O_2 (SaO_2) according to a somewhat simplified equation,

$$DO_2 = CO \times B\text{-}Hb \times SaO_2 \times 1.34, \quad (1)$$

where the O_2 dissolved in arterial blood (0.003 x PaO_2) under normobaric conditions is considered to be negligible. The normal adult value of CO, calculated as heart rate (HR) times stroke volume (SV), is approximately 5 l/min. Reference ranges of B-Hb are 123-153 g/l in female, and 140-175 g/l in male adults [19]. Normally, SaO_2 is above 95 %. The factor 1.34 (Huffner´s constant) denotes the volume of O_2 (in ml) approximately carried by each g of Hb under clinical conditions (as mentioned, the theoretical maximum capacity is 1.39 ml/g).

Contents of O_2 in arterial (CaO_2) and mixed venous (CvO_2) blood are calculated as

$$CaO_2 = B\text{-}Hb \times SaO_2 \times 1.34 \quad (2)$$

$$CvO_2 = B\text{-}Hb \times SvO_2 \times 1.34, \quad (3)$$

where SvO_2 is the mixed venous saturation of O_2.

According to Fick´s principle it is possible to calculate total tissue VO_2 as

$$VO_2 = CO \times (CaO_2 - CvO_2). \quad (4)$$

Accordingly, uptake of O_2 by a specific organ or tissue corresponds to its regional blood flow times its regional arteriovenous gradient of O_2 content.

The pathway of O_2 from gas in the atmosphere to the respiratory chain in the mitochondria of human cells contains several steps. The diffusion of O_2 in the pulmonary system is extremely efficient, keeping the arterial blood well saturated (around 95 %) also during maximal work [20]. However, trained individuals, who are able to increase their CO up to 40 l/min (compared with 25 l/min in less trained individuals), may undergo arterial desaturation during intense exercise. This occurs since the transit time of erythrocytes in the pulmonary capillaries falls below the time required (approximately 0.25 s) for saturation to be completed [21].

The arterial blood pressure (ABP) is determined by CO and the systemic vascular resistance (SVR) according to the equation

$$ABP = CO \times SVR. \quad (5)$$

At rest, approximately 5 % of CO is distributed to the heart, 15 % to the brain, 20 % to the kidneys, 20 % to the muscle tissues, 25 % to the liver, and 15 % to other organs and tissues [10]. Maximal VO_2 correlates to CO and regional blood flow,

where the latter determines the rate of convective transport of O_2 to different organs and tissues.

Both DO_2 and VO_2 are directly affected by lowered concentrations of Hb. Also, according to the Hagen-Poiseuille law (stating that the laminar flow through a cylinder (e.g., a vessel) is directly proportional to the fourth power of the radius and inversely proportional to the viscosity of the fluid) - reducing the concentration of Hb (which normally determines 70-80 % of the blood viscosity) will increase CO and regional blood flow [5].

The microvascular system is under rigorous physiological control, where the distribution of blood flow is determined by coordinated interaction between arteriolar, capillary and venular vessels according to local and regional metabolic demands. Skeletal muscle tissue has a wide dynamic range of blood flow, where, due to interaction between regulatory events, blood flow can increase almost 100-fold during intense aerobic exercise compared with the situation at rest. The vascular reactivity determines the distribution of DO_2 between and within organs and tissues, where dilation of terminal arterioles increases the capillary surface area for diffusion to increase tissue extraction of O_2. The venules, by diffusion of metabolites, provide additional feedback [22, 23].

A particular example of acute control of regional and local blood flow (of particular importance in this thesis) is reactive hyperemia (RH), defined as a transient increase in organ or tissue blood flow in response to a brief period of recent ischemia (induced by e.g., arterial occlusion). This vascular response is proposed to result from both myogenic and local metabolic factors [24]. In RH regional or local blood flow increases by four to seven times over a period of time lasting from few seconds (if the interruption of blood flow has been quite short) to several minutes. During a period of hypoperfusion or vascular occlusion, regional ischemia with tissue hypoxia induces progressive local acidosis with release of vasoactive metabolites (like prostaglandins and adenosine), which dilate arterioles and reduce the vascular resistance to improve tissue perfusion [25]. When the occlusion is released and the perfusion pressure is rapidly restored, the reduced vascular resistance will allow a higher blood flow. The high peak capillary velocity after a short period of occlusion suggests involvement of myogenic control mechanisms [24]. The increased blood flow during RH normally lasts long enough to re-establish StO_2 and wash out acid and vasodilating metabolites from the tissue [10].

Clinically available measurement techniques

In clinical practice, most bedside techniques evaluate global parameters of oxygenation to estimate StO_2. Furthermore, varying degrees of invasiveness are often required to retrieve this information. This section discusses some techniques available for measurements of vital physiological parameters, some of which can also be used for estimation of regional StO_2.

Pulmonary artery catheterization

Pulmonary artery catheterization is an almost 40 years old invasive technique, using a flow-directed balloon-tipped catheter, to evaluate hemodynamics in critically ill patients [21]. The catheter is inserted through the right internal jugular vein, passes through the right atrium and ventricle and is positioned inside the pulmonary artery. Information can be obtained on right atrial, ventricular and pulmonary (mixed venous) tensions of O_2 and CO_2, on SaO_2 and SvO_2, right atrial and ventricular pressures, and on arterial pulmonary and capillary wedge pressure, right ventricular ejection fraction and CO. Information obtained can be used to calculate VO_2 according to Eq. 4 (p. 25). This technique enables bedside measurements, and has previously been widely used. However, severe complications may arise, e.g., infections, mechanical damage to cardiac valves or the pulmonary artery, pulmonary thromboembolism and infarction [26, 27], and observational studies have indicated that the technique is associated with increased risks of death compared to controls with illness of similar severity [28].

Transpulmonary thermodilution

Transpulmonary thermodilution is another invasive technique for CO measurement. An indicator solution (e.g., cold saline 0.9 %), injected through a central venous catheter, passes through the right heart, lungs and left heart to be detected in a central arterial catheter, e.g., in the femoral artery. The Stewart-Hamilton equation [29] is then used to calculate CO.

Pulse pressure analysis

Many systems combine thermodilution with pulse pressure analysis for continuous trend monitoring of CO. This technique also enables levels of preload volume and extravascular lung water content to be estimated [30].

Pulse pressure variation

Another approach, based on variations in the arterial pressure curve measured with a catheter in e.g., the radial artery, has been used to estimate CO and SV levels for hemodynamic bedside guidance in critically ill patients. However, this technique requires mechanical ventilation for appropriate function [31, 32].

Central venous oxygen saturation

Measurement of central venous O_2 saturation ($ScvO_2$) is a less invasive option, useful for estimations of DO_2, CO and StO_2 in various clinical settings [27, 33, 34]. Ideally, SvO_2 reflecting mixed venous oxygenation from the whole body, in blood obtained from the right ventricle or the pulmonary artery, should be determined. However, this requires pulmonary artery catheterization, described above. However, $ScvO_2$ has been shown to correlate well with SvO_2 [33]. The normal value for $ScvO_2$ is approximately 70 %, and lower levels may reflect too low levels of CO, B-Hb or SaO_2 to meet tissue demands for O_2.

Indirect calorimetry

Indirect calorimetry is a non-invasive method, where the metabolic rate is estimated from measurements of O_2 consumption and CO_2 production. Briefly, VO_2 is calculated from differences in concentrations and volumes of O_2 and CO_2 between inspired and expired gases. However, this technique needs specific equipment and careful calibration. Moreover, for correct measurements no volume loss is allowed. This leads to particular problems in neonatal care settings, where un-cuffed endotracheal tubes are often used [35, 36].

Gastric tonometry

Gastric tonometry is a monitoring technique, based on tonometric determination of PCO_2 in the stomach, and on determination of arterial content of bicarbonate. Information obtained is used to calculate gastric intramucosal pH [37]. A recent meta-analysis suggests that treatment guided by gastric tonometry is associated with lower overall mortality in critical care patients, but more investigations are needed [38].

Esophageal Doppler

Determination of blood flow in the descending thoracic aorta by esophageal Doppler techniques is another method for monitoring of CO to guide decisions in e.g., volume replacement and the need for inotropic or vasopressor support [39]. The principles behind the Doppler effect are described under Technical aspects (pp. 57-58). Perioperative studies, e.g., in cardiac [40] and abdominal surgery [41, 42], have reported improved outcome when esophageal Doppler monitoring has been used.

Base excess and lactate

Blood analyses can also be used to detect and follow-up clinical deterioration. When there is an imbalance between O_2 supply and demand, anaerobic respiration will start and metabolic acidosis develops, shown as reduced blood levels of base excess (BE) and as increased blood levels of lactate levels, indicating poor StO_2. Although blood levels of BE and lactate are both considered as good markers of clinical outcome, they respond slowly to tissue hypoxia [43].

Near-infrared spectroscopy

All techniques mentioned above enable assessment of vital physiological bedside information of potential use for optimization of critical care in severe illness or major injury. However, none of them directly determines regional StO_2 or blood flow. Near-infrared spectroscopy (NIRS) is a non-invasive optical technique providing continuous or frequent values of StO_2 in e.g., skeletal muscle or brain. This technique is described in detail below (pp. 49-53). Two studies (**I-II**) in this thesis focus on determination of StO_2 in muscle tissue, and on how reduced perfusion and oxygenation in peripheral organs or tissues might be used to detect clinical deterioration at an early stage in critical illness.

Tissue oxygenation in critical illness

Maintenance of aerobic metabolism depends on adequate StO_2. There is an essential link between microcirculatory function and adequate DO_2 and thus normal organ function. Tissue blood supply is a crucial indicator of injury and disease [44]. Low DO_2 may occur despite normal levels of mean arterial pressure (MAP) and HR, both used for basic hemodynamic monitoring [27]. Tissue hypoxia occurs when too little O_2 is available due to abnormal key determinants of O_2 transport. Regulatory mechanisms in the cardiovascular and respiratory systems, and in the blood, all aim at ensuring adequate oxygenation of organs and tissues.

In major trauma or critical illness, blood flow is redistributed from less vital organs (e.g., skin, skeletal muscle, intestines) to more vital organs (e.g., brain, heart, kidneys) to increase the possibilities of adequate StO_2 and hence individual survival. Therefore, detection of reduced peripheral StO_2 resulting from hypoperfusion might be used to early detect, and hence improve initial management of clinical deterioration in severely ill or injured patients [45]. In clinical practice today, StO_2 is often indirectly assessed by invasively measuring global parameters of oxygenation, as described above (pp. 27-28).

Tissue hypoxia may have several causes, depending on where in the chain of O_2 transportation the problem is located. The following section describes the four most common types of tissue hypoxia.

Stagnant hypoxia

Stagnant hypoxia occurs when the blood flow is abnormally low e.g., in ischemia or due to reduced CO. In terms of O_2 transport, hypoperfusion is the primary limitation, and hence, cardiovascular problems lead to inadequate DO_2 [46]. The amount of O_2 extracted from the blood must now increase in order to meet the tissue demands, and SvO_2 will fall. The PaO_2 remains unchanged, so respiratory chemoreceptors (carotid bodies) do not sense any decrease. Increasing the inspired O_2 fraction (F_iO_2) does not correct stagnant hypoxia, and instead bedside interventions to improve CO or regional blood flow are required [14].

Hypoxic hypoxia

When the PaO_2 falls, hypoxic hypoxia is present. This may occur at high altitudes, where the inspired PO_2 is lower than normal. In clinical settings, hypoxic hypoxia is mostly due to respiratory problems, e.g., hypoventilation, ventilation-perfusion mismatch, pulmonary edema (impaired diffusion) or shunting of blood. The key problem is respiratory, and low arterial oxygenation limits proper StO_2. Physiological responses to reduced tissue PO_2 comprise dilation of precapillary arterioles (resistance vessels) increasing perfusion, and opening of additional capillaries to reduce diffusion distances and increase the total area available for diffusion of O_2, all leading to an increased DO_2. SvO_2 is decreased due to higher tissue extraction of O_2. Respiratory chemoreceptors promote respiration by sensing arterial hypoxemia. Increasing the

F_iO_2 helps to restore the balance between supply and demand of O_2, except in severe pulmonary shunting [14].

Anemic hypoxia

In anemic hypoxia, the carrying capacity of O_2 is reduced, because of fewer Hb molecules or O_2 binding sites. The most common reason is anemia, but anemic hypoxia also occurs in carbon monoxide poisoning (carboxyhemoglobinemia). When carbon monoxide poisoning occurs, O_2 is outrivaled by carbon monoxide with more than 200 times higher affinity to heme-binding sites. Carboxyhemoglobinemia also inhibits tissue delivery of O_2 by shifting the dissociation curve to the left, thereby increasing the affinity of O_2 to Hb [47] (Fig. 3).

In methemoglobinemia, the iron ion of heme is oxidized from the normal ferrous (Fe^{2+}) to the ferric (Fe^{3+}) (normally <1 %) state, which leads to inability of binding O_2 and also to a shift of the dissociation curve to the left. Nitrates and prilocaine are examples of drugs which may induce methemoglobinemia [48]. Hemodynamic responses to anemic hypoxia include arteriolar dilation, increased capillary perfusion and increased tissue extraction of O_2 with lower levels of SvO_2. Since PaO_2 is maintained, anemic hypoxia is not sensed by respiratory chemoreceptors. The only cause of this kind of hypoxia where high levels of F_iO_2 can help, preferably at hyperbaric pressures, is in carbon dioxide poisoning, where O_2 may competitively more easily replace carbon monoxide at the binding sites [14].

Histotoxic hypoxia

The fourth case of reduced tissue oxygenation is histotoxic hypoxia, induced mainly by cyanide, with a tragic record of genocide and in prohibited warefare, and also released in industrial disasters and by the drug sodium nitroprusside [49]. Histotoxicity makes cells unable to utilize delivered O_2, since its mitochondrial reaction with cytochrome C oxidase is blocked, leading to a reduced production of ATP and subsequent energy depletion. Oxygen extraction and consumption decreases, resulting in progressive tissue hypoxia with metabolic acidosis and increased lactate levels, and increased levels of SvO_2. Respiratory chemoreceptors are stimulated, but respiratory stimulation or increasing the F_iO_2 does not help, since there is already enough O_2 in the circulatory system, but the cells are unable to utilize it [14, 50]. Treatment involves rapid administration of amyl nitrate, sodium thiosulfate and sodium nitrate (the cyanide antidote kit). If smoke inhalation is the cause of cyanide poisoning, hydroxocobalamin is the antidote of choice [49].

Tissue oxygenation in hemorrhage

A significant loss of blood volume, enough to reduce ABP below normal baseline levels, is referred to as hemodynamically relevant hemorrhage. The immediate physiological effect is a reduction in venous return to the right heart, whereby CO

and MAP are both reduced. The decrease in CO reduces blood flow to all tissues, leading to a fall in DO_2. In massive hemorrhage, the DO_2 might fall to levels too low to support oxidative phosphorylation in the tissues, forcing anaerobic metabolism to take over. Poor tissue blood flow, with increased production of lactate, severely compromises cellular function. Multiple compensatory mechanisms are activated, to redistribute CO for optimal oxygenation of vital organs by change of vascular resistance in other organs and tissues.

The brain, heart and kidneys are under autoregulation to maintain appropriate regional blood flow levels. Autoregulation is able to maintain adequate perfusion of the brain and heart as long as the MAP does not fall below approximately 70 mmHg. The systolic arterial pressure (SAP) must be 75-170 mmHg to maintain autoregulation in the kidneys. Compensatory mechanisms in hemorrhage start almost immediately by reduced signaling rate of baroreceptors in the carotid sinus region, in response to the decrease in ABP, whereby activation of the vasomotor inhibitory center in the brainstem decreases and the vasomotor center is activated [14, 51].

Vasomotor activation reduces inhibitory vagal baseline influence on the sinoatrial node, whereby HR increases towards its internal basic level of approximately 100 min^{-1}. In addition, sympathetic activation induces higher myocardial contractility and HR, and also arteriovenous vasoconstriction, to maintain CO. Arterial vasoconstriction increases SVR and also, by precapillary vasoconstriction, reduces the capillary hydrostatic pressure to increase fluid absorption from the interstitial volume. This reabsorption may increase intravascular blood volume by up to one liter.

Other hormonal responses to hemorrhage include reduced release of atrial natriuretic factor (ANF) from the right atrium in response to decreased venous return. Reduced blood levels of this hormone promote release of antidiuretic hormone (ADH) from the posterior pituitary gland. Renal vasoconstriction increases the release of renin activating the renin-angiotensin pathway, which leads to increased release of aldosterone. Both ADH and aldosterone promote renal reabsorption of sodium and water to restore intravascular volume at the expense of dilutional anemia. Within few days the kidneys increase their production of erythropoietin to stimulate erythrocyte maturation, whereas protein synthesis in the liver is promoted by lower levels of plasma proteins [14, 51], resulting from dilution of the plasma volume.

Since one of the early compensatory mechanisms in hemorrhage is powerful peripheral vasoconstriction, measurements of changes in the peripheral circulation could be helpful in detecting early hypovolemia [52].

Diseases affecting newborn infants

Respiratory distress syndrome

Infants born preterm (before 37 weeks of gestational age) are most vulnerable patients, accounting for 75 % of perinatal mortality and for more than 50 % of long-

term morbidity [53]. Infants born before 32 weeks of gestational age account for two thirds of perinatal deaths. Reported rates of preterm delivery are 12-13 % in the USA and 5-9 % in Europe [54]. Overall numbers of preterm births seem to increase, for complex reasons [55]. Most organs in a preterm infant are immature, and the lungs and brain are especially vulnerable [56, 57]. The lungs are not fully mature until after approximately 35 weeks of gestation. Infants born in gestational weeks 24-28 have lungs where development of distal alveoli and capillary beds has just begun [58]. Surfactant, a complex lipid and protein aggregation lowering the alveolar surface tension, is normally detected in fetal lungs at 24 weeks of gestation, although in very low concentrations [59, 60].

Respiratory distress syndrome (RDS) is a lung disease, caused by a combination of insufficient amounts of surfactant and structural immaturity. The prevalence is approximately 1 % of all live births, but the incidence strongly increases with lower gestational age at birth. Approximately 90 % of infants born in gestational weeks 22-28 are affected, while around 50 % develop the disease if delivered in weeks 30-31 [61, 62]. An infant born in gestation week 25 with RDS is shown in Fig. 5. The pathophysiology of RDS is explained by surfactant-deficient alveoli with high surface tension, prone to collapse during expiration, resulting in atelectatic regions with ventilation-perfusion mismatch, hypoxemia and hypercarbia, and in lung injury associated with required mechanical ventilation [63]. Epithelial lung damage and leakage of plasma proteins into the alveoli result in development of hyaline alveolar membranes, a characteristic histopathological finding, with impaired conditions for diffusion of O_2. The disease presents shortly after birth with tachypnea, cyanosis, grunting, and sternal and intercostal recession, and deteriorates within the first two days of postnatal life. Chest X-ray (Fig. 6) shows inhomogeneous aeriation, with pathognomonic findings including “ground-glass” appearance of the lung fields and air bronchograms [64]. Management of RDS begins before birth, by administration of steroids to the mother, which significantly reduces neonatal mortality [65].

Cornerstones in the treatment of RDS are exogenous surfactant administered into the trachea and continuous positive airway pressure (CPAP) to prevent the lungs from collapsing [66]. Great effort is taken to avoid O_2 toxicity, barotrauma and retinopathy of prematurity. If possible, mechanical ventilation (conventional or high-frequency (3-15 Hz; oscillatory) is avoided, since it can be associated with pneumothorax or pulmonary interstitial emphysema, and, in the long run, also with bronchopulmonary dysplasia (BPD) [64]. A large clinical trial, where preterm infants were randomized to CPAP treatment or intubation with surfactant treatment, did not show significantly different rates of mortality or BPD between the two study groups [67]. A proposed way of avoiding prolonged mechanical ventilation in infants requiring surfactant, is the INSURE technique, including *in*tubation, instillation of *su*rfactant and *r*apid *e*xtubation, followed by CPAP [68, 69].

Figure 5.
Image of an intubated preterm infant with respiratory distress syndrome (RDS) born in gestational week 25. Note the pen for comparison of size. From Bild-Zeitung/Udo Weger.

Figure 6.
X-ray image showing the lungs of a preterm infant with respiratory distress syndrome (RDS) under mechanical ventilation via an endotracheal tube positioned with the tip above the tracheal bifurcation. Note the symmetrical ground-glass (whitish) appearance of the lung fields making it difficult to distinguish the heart and air bronchograms, i.e. the air in the bronchi makes them visible. (Case courtesy of Radiopaedia.org, rID: 11510).

To assess the severity of RDS, especially regional areas with hyperinflation and atelectasis, remains difficult even though preterm infants in intensive care units are continuously monitored with sophisticated equipment. Information on O_2 delivery, ventilator settings, SpO_2, StO_2, and various vital parameters are examples of data needed in surveillance. Therapeutic effects of ventilator adjustments are evaluated mainly by arterial and venous blood gas assessments. Recently, ultrasonography for non-invasive assessments of various air-filled spaces and tissues within the body has been proposed as a diagnostic tool in neonatal lung diseases [70-72]. However, an important drawback of this technique is that different constituents of the pulmonary gas mixture cannot be identified.

Pulmonary X-ray is today the diagnostic method of choice for RDS to evaluate the air content in the lungs, and is also used to follow the clinical course of the disease. However, it is well known that repeated exposure to ionizing radiation is potentially harmful, and more so in infants and young children than in adults. Exposition to a standard dose of radiation in a one-year-old child compared with a 50-year-old adult, is considered to be associated with 10-15 times higher life-risk of developing malignant neoplasia [73]. Nevertheless, the number of radiographic computerized tomographic examinations increased by approximately 25 % in a large children´s hospital over a five-year period between 1998 and 2003 [74]. In neonatal intensive care, currently aiming at more non-invasive diagnostic and therapeutic strategies, an important goal is to limit the number and extent of potentially harmful radiological examinations.

Necrotizing enterocolitis

One of the most severe gastrointestinal complications in newborn infants is necrotizing colitis (NEC), with a prevalence of up to 7 % in preterm infants weighing 500-1500 g [75]. This is an acute inflammatory disease, where portions of the intestine undergo necrosis, carrying high risk of perforation. The mortality rate is 15-30 %. Approximately 90 % of the NEC cases occur in premature infants. Low birth weight (<1500 g) and gestational age are associated with higher risk of developing NEC. In contrast to RDS, NEC mainly affects premature infants who have survived the early postnatal period and constitutes a new threat to survival [76].

The disease hardly occurs in infants who have never been fed; and over 90 % of the cases are seen after enteral feeding has been provided [77]. However, human breast milk has been shown to be protective, with a three- to ten-fold risk reduction compared with formula milk [78]. The pathogenesis is still not fully understood, but immaturity of the immune defense, the circulatory regulation, gastrointestinal motility, intestinal barrier function, and digestive ability, could be of importance for disease development. Hypoxic/ischemic injury, colonization by pathological bacteria and formula milk feeding are also potential risk factors for development of NEC [79-82]. The “diving reflex” might be a possible explanation for the hypoxic/ischemic injury, since this reflex leads to redistribution of blood from less vital organs and tissues to organs necessary for survival. Predisposing or underlying diseases, like

perinatal asphyxia, respiratory distress or congenital heart disease, are often associated with development of NEC in full-term infants [76].

Initial clinical signs include intolerance to feeding, gastric residuals, abdominal distension and bloody stools. The diagnosis is based on patient history, clinical assessment and X-ray imaging (Fig. 7), where pneumatosis intestinalis (intramural gas) and intrahepatic gas, dilated bowel loops, paucity of gas and pneumoperitoneum are typical findings. Treatment includes gastric decompression, bowel rest, rehydration, and correction of deranged electrolytes and metabolic acidosis. Frequent laboratory analyses and radiological examinations are needed to follow the clinical course. Surgical treatment may be required if there is severe deterioration with bowel necrosis and even perforation [83]. Acute complications are wound infection, intra-abdominal abscess formation and sepsis, and the most common long-term complications are intestinal stricture and short gut syndrome [84]. To improve clinical outcome, prompt recognition of early clinical signs is essential. Furthermore, infants on enteral nutrition should preferably be fed with breast-milk, and surgical intervention should be avoided if possible.

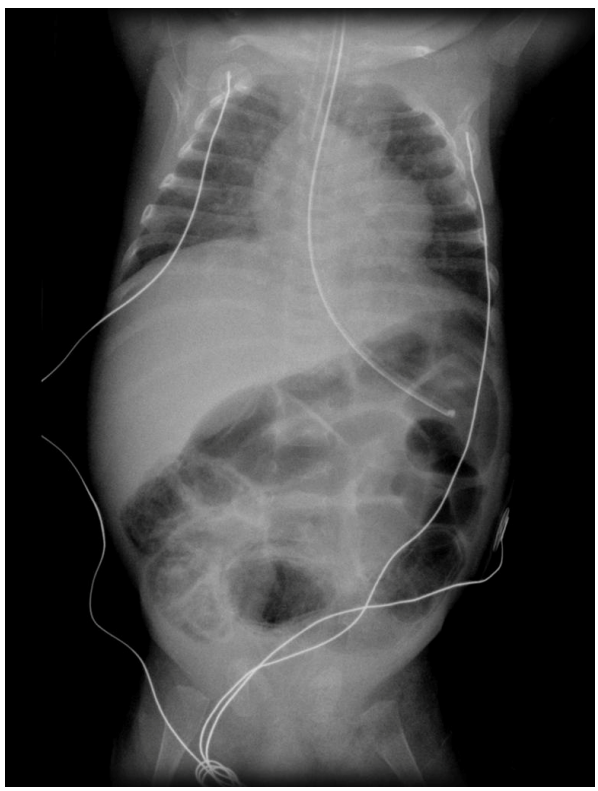

Figure 7.
Abdominal X-ray image at two months of age in a premature infant born at 27 weeks of gestation. The image shows multiple distended bowel loops, with prominent intramural gas. (Case courtesy of Prof. Frank Gaillard, Radiopaedia.org, rID: 5961).

In the context of intestinal conditions it should be mentioned that colic is well-known to most parents. Although far from life-threatening it renders sleepless nights and considerable worry. Colic affects both preterm and full-term infants. It is reported in 10-20 % of infants [85], and is defined as excessive crying for more than three hours a day, more than three days a week, and for more than three weeks, in otherwise healthy and thriving infants. The onset is usually within the first weeks of life, and spontaneous termination occurs within three to four months of age [86]. The etiology is not fully understood, but according to several investigators, abdominal pain is induced by large volumes of intestinal gas [85].

Technical aspects

Spectroscopy, the science about how light interacts with matter, is the technical cornerstone of this thesis. The aim of this chapter is to provide a technical background on basic concepts, and a broad review of the spectroscopic techniques used to study detection of free O_2 gas, tissue perfusion, blood volume, and StO_2.

Some physics of optical spectroscopy

Optical spectroscopy, as employed in this thesis, regards visible light (400–700 nm) and near-infrared (NIR) radiation (700-1000 nm). As shown in Fig. 8, this region constitutes a small part of the entire electromagnetic spectrum of radiation, with wavelengths stretching from 0.001 nm (gamma rays), to several 100 m (radio waves).

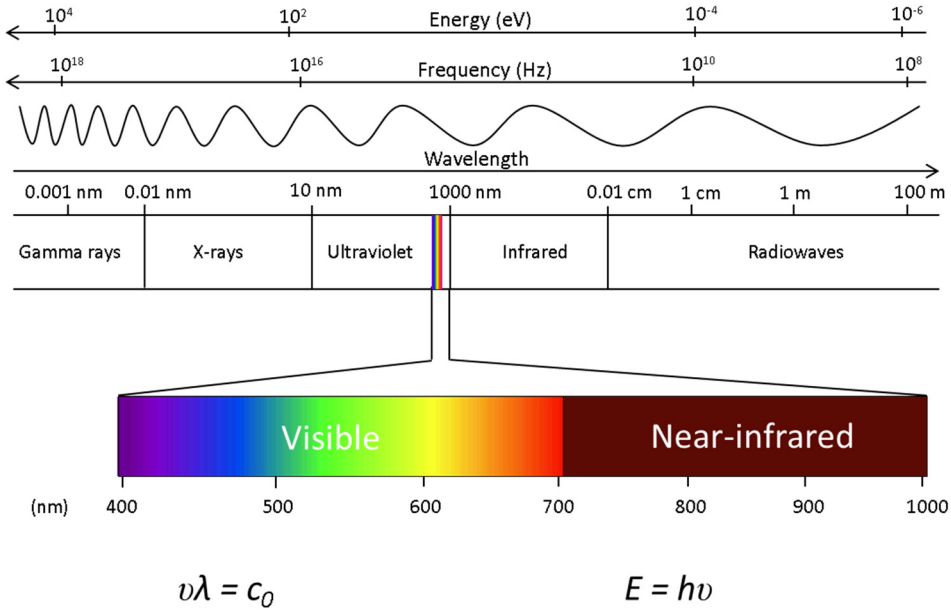

Figure 8.
Wavelength ranges of electromagnetic radiation. Corresponding frequencies and photon energies are also given. Note that the wavelength scale is logarithmic. The visible and near-infrared regions are enlarged on a linear scale. Fundamental relations between energy (E), frequency (υ) and wavelength (λ) are given. c_0 is the speed of light in vacuum, and h is Planck´s constant.

Energy levels and optical transitions in atoms and molecules

There are about 90 stable elements in the periodic table. Many of them are of interest in the medical field, some as key constituents in human tissue, and some as hazardous compounds.

Atoms are built up by a positive nucleus, containing positive protons and neutral neutrons, surrounded by negatively charged electrons. The electrons are arranged in shell structures around the nucleus. A configuration of electrons in different shells leads to a specific internal energy of the atom. This internal (or binding) energy is quantized in specific allowed energy levels that the atom can configure itself in. The electrons in the outer shell contribute least to this binding energy (they are furthest away from the nucleus and thus more weakly bound). Consequently, they are the ones that easiest participate in interactions with the surrounding, leading to a change of the atomic energy level [87]. Charges of atoms are balanced, and the net charge equals zero. If the atom loses or gains an electron in interactions with the surrounding, it becomes a charged ion. Free atoms are very rare in human tissue and instead they combine into free molecules (gases) or condensed matter (tissue), being the corner stones of proteins and amino acids, lipids, carbohydrates and of the water in body fluids. However, ions, such as Na^+, K^+, Mg^{2+}, Ca^{2+} and Cl^-, appear dissolved in body fluids and are of major importance for many physiological processes [88].

Molecules, consisting of arrangements of atoms bound together by electrons, also show energy level structures, but much more complicated because of vibrational and rotational motions. Free atoms and gases exhibit sharp energy levels and correspondingly sharp transitions of energy. However, in liquids and solid matters the energy levels smear out because of perturbations from neighboring molecules, and energy transitions are correspondingly much broader. Atoms and molecules change energy levels by absorption and emission of photons, with energy corresponding to the energy change [87]. Fig. 9 shows a typical Jablonski diagram of energy levels and transitions including the fundamental relationships between energy, frequency and wavelength.

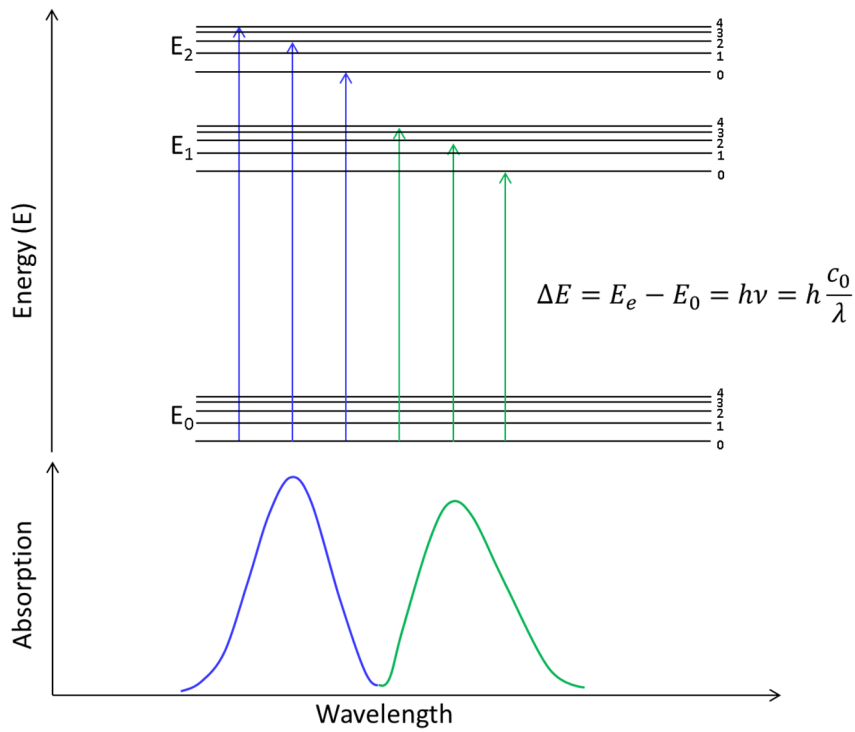

Figure 9.
Jablonski diagram of absorption, showing energy levels and corresponding spectra. Solid blue and green arrows represent radiative transitions. Absorption following irradiation of light occurs in response to transitions from a lower to a higher energy level. Return to lower energy levels normally occurs on the nanosecond scale, with emission of fluoroscence light (not shown), or by collisions leading to temperature increase. E_0 is the ground state and E_e (E_1 or E_2) higher electronic states, h = Planck´s constant, ν = frequency, λ = wavelength and c_0 = speed of light in vacuum.

Light absorption

When light absorption occurs, the energy of a photon is taken up by the constituent, which in our case could be a free O_2 gas molecule or HbO_2. For this to occur, the wavelength of light must precisely match the energy difference of the involved energy

levels of the molecule. The extinction coefficient $\sigma(\lambda)$ defines at a given wavelength (λ) how strongly a substance absorbs light per molar concentration and cm path length of the light.

Examples of optical absorption spectra of particular relevance to the present work are given in Fig. 10. Different substances have different absorption lines, making identification possible. Note the much broader (approximately 20 nm) absorption bands of HbO_2 and Hb^- (Fig. 10a) compared to the extremely sharp (exact to the 6^{th} digit) absorption lines of gaseous O_2 (Fig. 10b).

At about 800 nm the absorption curves of HbO_2 and Hb^- cross at the isobestic point [89]. At shorter wavelengths HbO_2 has lower, and at longer wavelengths higher absorption of light than Hb^-. This wavelength-dependent difference in absorption is used to calculate the O_2 saturation of Hb, either in arterial blood by pulse oximetry or in tissue by NIRS, as evaluated in Papers **I** and **II**.

At around 760 nm there are some extremely sharp, narrow lines, corresponding to the absorption of free O_2 gas. Detection of approximately ten thousand times sharper absorption lines, reflecting presence of free O_2 inside tissue cavities, calls for another experimental technique; "gas in scattering media absorption spectroscopy" (GASMAS), evaluated in Papers **III** and **IV**.

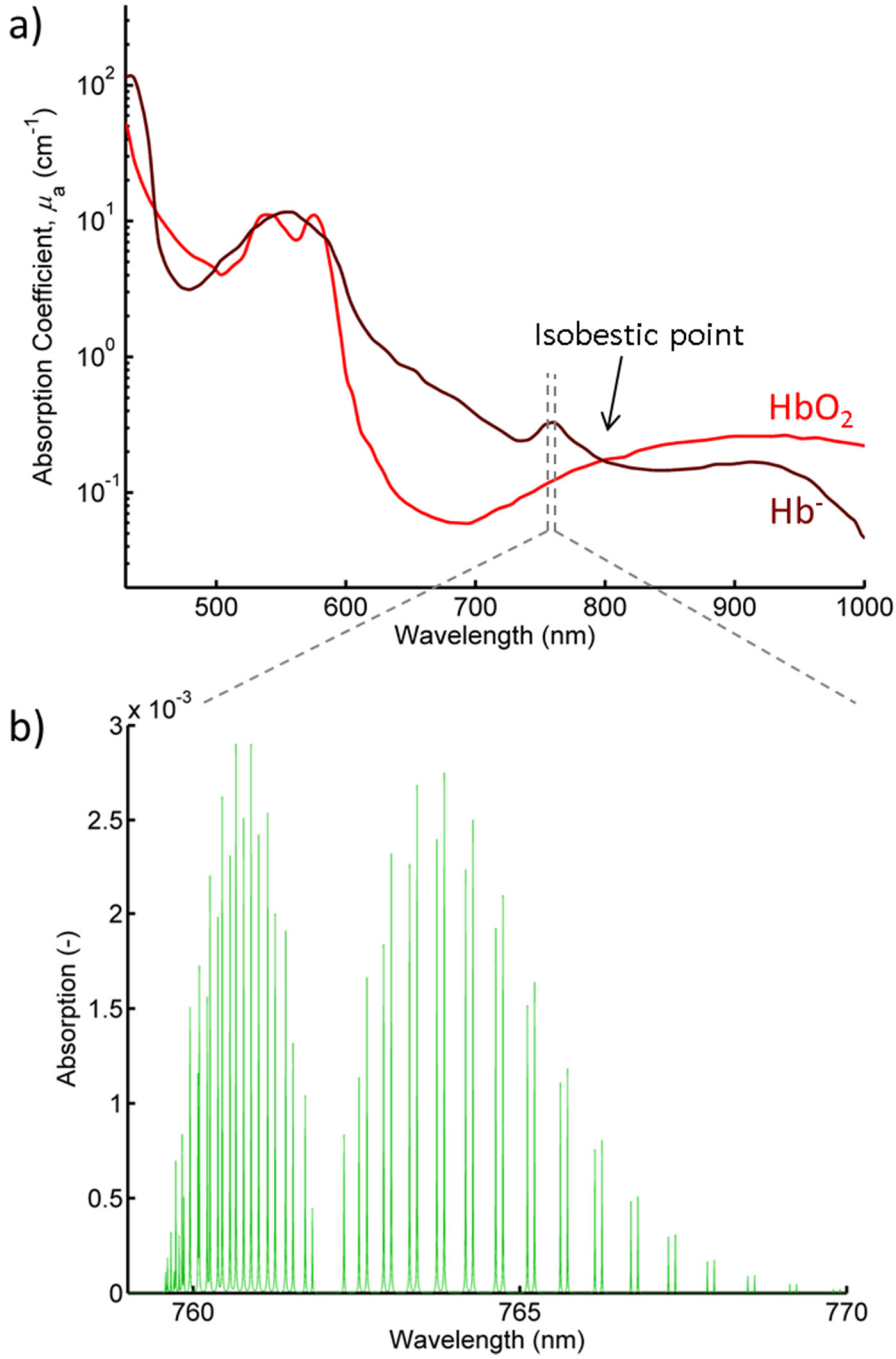

Figure 10.
Absorption of light by molecules of HbO_2 (bright red line) and Hb^-(dark red line) is shown in (a), and by oxygen (O_2) gas around 760 nm (oxygen A-band) in (b). HbO_2 and Hb^- have identical absorption of light at the isobestic point (approximately at 800 nm). The absorption lines of free O_2 gas are approximately 10 000 times sharper than those of HbO_2 and Hb^- molecules.

Light scattering

Scattering occurs when light interacts with structures, where there are changes in refractive index. Tissue is a perfect example of a highly scattering medium, where typical scattering structures are lipids, collagen, cells, or cell organelles such as mitochondria [90]. Some typical biological structures scattering light are presented in Fig. 11. The strength of the scattering is expressed by the reduced scattering coefficient ($\mu_s'(\lambda)$). Scattering typically increases for shorter wavelengths in the wavelength range of interest in this work. In practical spectroscopy, scattering often reduces the amount of light reaching the detector.

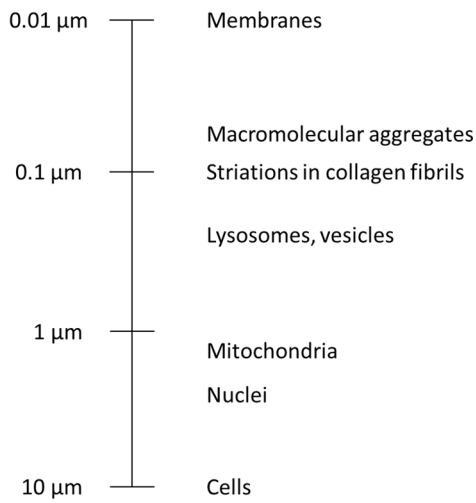

Figure 11.
Biological structures of various sizes causing photon scattering. Modified from [90].

Tissue optical window

The tissue optical window refers to a portion of the visible and NIR region of the electromagnetic spectrum covering wavelengths from 600 to 1400 nm. In this window the tissue is relatively transparent, so light can reasonably well be transmitted without major absorption to gain spectroscopic information on the tissue interior. However, within the tissue optical window, light scattering is still very strong, leading to multiple scattering and light attenuation [91]. Major tissue absorbers are shown in Fig. 12. Proteins strongly absorb light at short wavelengths (in the ultra-violet region). Below 600 nm Hb dominates the absorption [92] and beyond 1400 nm liquid water absorbs massively [93], leading to a very shallow penetration depth. Melanin, giving the natural coloring of human skin, shows continuously lower absorption towards the NIR region [94].

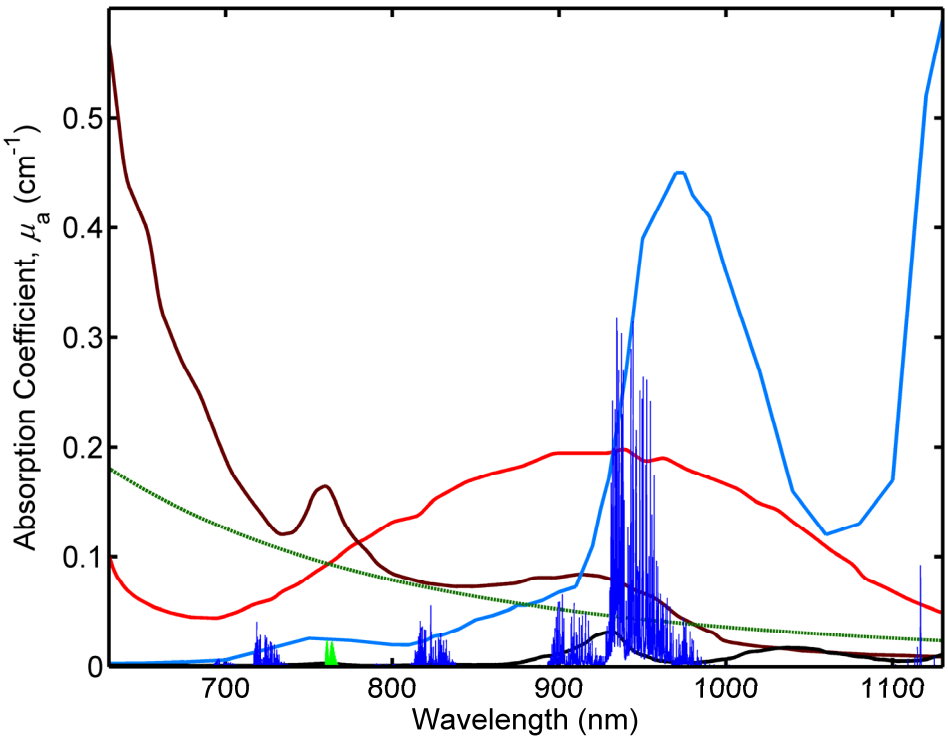

Figure 12.
Diagram showing the tissue optical window with absorption spectra of major tissue constituents, with concentrations approximately corresponding to skin-covered muscle. Indicated are: HbO_2 (bright red curve), Hb^- (dark red curve), liquid water (blue curve), melanin (green dashed curve) and lipids (black curve). In addition, sharp lines due to free oxygen (O_2) gas (green lines) and water (H_2O) vapor (dark blue lines) are shown.

The Beer-Lambert-Bouguer law

The relation between attenuation of light and properties of the material through which the light is travelling is given by the Beer-Lambert-Bouguer law. Pierre Bouguer described the law in 1729 and Johann Heinrich Lambert stated that the absorbance (A) of a material sample is directly proportional to its thickness, the path length of light (l). About twenty years later, August Beer discovered that the absorbance of light by a compound in a sample is proportional to its concentration [95]. This law (commonly named the Beer-Lambert law) states that the remaining light ($I(\lambda)$) after passage through the sample is determined by both the concentration (C) of the compound and l, in an exponential way [87],

$$I(\lambda) = I_0(\lambda)e^{-\sigma(\lambda)Cl}, \qquad (6)$$

where $I_0(\lambda)$ is the initial light intensity and the extinction coefficient $\sigma(\lambda)$ is a constant, characteristic of the specific transition. A mathematically equivalent way of expressing this law is

$$A = ln\left(\frac{I_0(\lambda)}{I(\lambda)}\right) = \sigma(\lambda)Cl \quad (7)$$

where A is the absorbance introduced by Beer and Lambert. Since absorbance is normally expressed as the ^{10}logarithm (log), rather than as the natural logarithm (^{e}log = ln), the above expression should be multiplied by the factor 0.434. We note that the product of the C and l determines the amount of absorption. Sometimes the absorption coefficient ($\mu_a(\lambda)$), with

$$\mu_a(\lambda) = \sigma(\lambda)C \quad (8)$$

is preferred to express the absorption, especially when dealing with complex matter, like tissue, containing many kinds of molecules with various concentrations and extinction coefficients. Thus,

$$I(\lambda) = I_0(\lambda)e^{-\mu_a(\lambda)l} \quad (9)$$

Since the exponent does not have any unit, the unit for $\mu_a(\lambda)$ is cm^{-1} (if l is expressed in cm) and that for $\sigma(\lambda)$ is molar^{-1}cm^{-1} (if C is given in molar (mol/l) and l in cm).

If the absorption through the sample is small (as in our gas measurements (**III-IV**)), then

$$I(\lambda) = I_0(\lambda)(1 - \sigma(\lambda)Cl) \quad (10)$$

since $e^{-x} = 1 - x$ for small values of x. Eq. 10 can then be written

$$\frac{\Delta I}{I_0} = \sigma(\lambda)Cl \quad (11)$$

where $\Delta I = I_0(\lambda) - I(\lambda)$.

Scattering, characterized by the reduced scattering coefficient ($\mu_s'(\lambda)$), with unit cm^{-1}, also leads to a reduction of a collimated light beam:

$$I(\lambda) = I_0(\lambda)e^{-\mu'_s(\lambda)l} \quad (12)$$

As mentioned, scattering increases at shorter wavelengths (also explaining the general observation that the sky is blue on a clear day).

Within the tissue optical window, where spectroscopic measurements on bulk tissue are possible, the optical properties of tissue lead to that, on average, a photon travelling in tissue will change its direction completely approximately ten times per cm ($\mu'_s \approx 10$ cm^{-1}). This leads to a greatly prolonged path length as light is propagating through tissue from the position of light injection to its detection. Approximately 10-40 % of the light is absorbed per every centimeter of path length ($\mu_a \approx 0.1$-0.4 cm^{-1}), while approximately 10 % remains after diffusely propagating through 1 cm of tissue according to

$$\phi(\lambda) = \phi_0(\lambda)e^{-\mu_{eff}(\lambda)l}, \quad (13)$$

where $\phi(\lambda)$ is the light fluence rate and μ_{eff} is the effective diffuse attenuation coefficient ($\mu_{eff} \approx 1.7$-3 cm^{-1}) [96].

According to the Beer-Lambert law, concentrations of e.g., a specific gas can be calculated from a transmission measurement as long as the geometry of the sample is well defined and scattering events are absent (the path length of the detected light is known). The law is universally used in chemistry when analyzing different solutes/gases with regard to their concentration. However, when the absorbing molecules of interest are located inside a scattering medium, such as human tissue, certain modifications are required, since the path length of the transmitted light now becomes undefined, due to scattering [97, 98] The path length (l) may then be replaced by an effective path length (l_{eff}), relating to scattering as well as geometry.

These general principles can be applied in spectroscopy of the human body to assess bound as well as free molecules. The absorption line widths are very different, calling for quite different experimental approaches, which will be described in detail below.

Tissue viability imaging

Tissue viability imaging (TVI) enables estimation of the blood volume by polarization spectroscopy, with illumination in the visible spectral region (400-700 nm). White linearly polarized light is emitted by an electronic photo flash towards the skin surface. Due to Fresnel reflection, related to the change in refractive index (n), approximately 4 % of the light is directly reflected by the skin surface, with maintained linear polarization [99]. Light penetrating into deeper dermal layers, becomes diffusely scattered and hence randomly polarized. By using a crossed polarizer in front of a camera the linearly polarized light from the surface is prevented to reach the detector, enabling monitoring of the microcirculation in deeper dermal layers through the skin surface [100], as shown in Fig. 13.

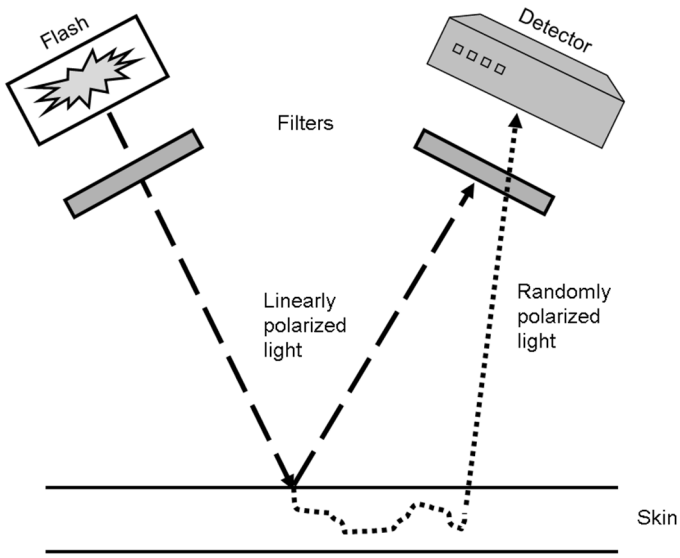

Figure 13.
Linearly polarized white light from an electronic photo flash becomes depolarized when scattered inside skin tissue. By using a crossed linear polarization filter in front of the detector, directly reflected light from the skin surface (with maintained polarization) is blocked out, whereas randomily polarized light scattered from deeper tissue structures is detected and available for analysis. Assessment of skin blood volume is done by comparing absorption in the red and green spectral regions, selected by optical filters. Modified from Paper **I**.

This quite new optical non-invasive technique is based on wavelength-dependent differences in spectral absorption between erythrocytes and surrounding tissue. Absorption varies between different tissue components (Fig. 12), and green components of the scattered light are highly absorbed by the erythrocytes (blue even more), whereas red components are much less absorbed (Fig. 14). This is of course related to the obvious observation that blood is red! Surrounding tissue structures

have similar absorption spectra in the green and red regions (Fig. 14). Relative estimations of erythrocyte concentrations, indirectly reflecting the regional blood contents or volume, can be obtained with TVI by applying an algorithm, where the light intensity recorded in the green spectrum for every picture element of the camera is "subtracted" from the corresponding element recorded in the red spectrum [101].

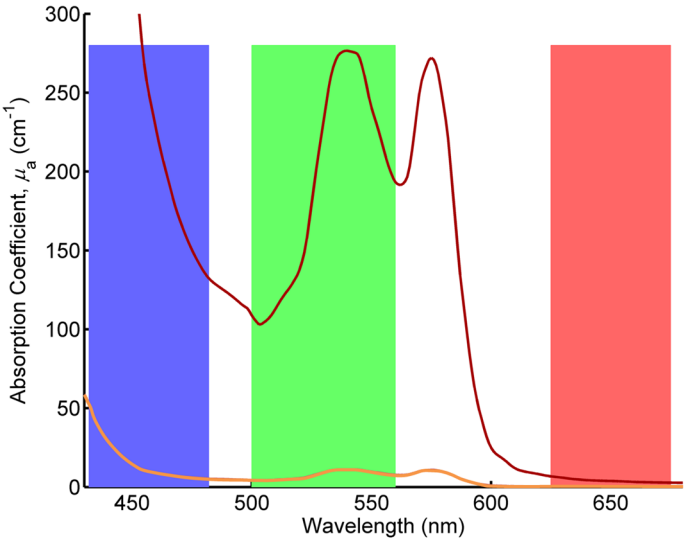

Figure 14.
Wavelength dependency of light absorption by blood (red curve), and by surrounding tissue (orange curve). Blue, green and red bands of the visible spectrum of light are also indicated.

The technique has been used to assess and quantify skin erythema (vasodilation), blanching (vasoconstriction) and RH [101-103], and was recently proposed as a promising tool for detection of venous stasis [104].

Pulse oximetry

Pulse oximetry has, since its introduction about 30 years ago, become an essential bedside tool for non-invasive estimation of arterial O_2 saturation (SpO_2). For comparison, saturation determined in arterial blood by blood gas co-oximetry is referred to as SaO_2. Pulse oximetry is today routinely used in almost all clinical settings, and is of particular interest in critically ill, injured and/or anesthetized patients [105].

SaO_2 is defined by the concentration (C) ratio of oxygenated C_{HbO_2} (frequently denoted [HbO_2], etc) to total hemoglobin ($C_{HbO_2} + C_{Hb^-}$) concentrations according to the equation

$$SaO_2 = \frac{C_{HbO_2}}{C_{HbO_2}+C_{Hb^-}} \times 100. \qquad (14)$$

Throughout the arterial vascular system SaO_2 has the same value, since extraction of O_2 only occurs in the capillaries (pp. 21, 23). Note that O_2 dissolved in arterial blood is measured by PaO_2. PaO_2 is routinely measured by an arterial blood gas analyzer, but can also be measured non-invasively, by a transcutaneous PaO_2 electrode. However, this method has low accuracy and requires warming of the skin to 43-44 ºC [106]. The correlation between SaO_2 and PaO_2 is determined by the sigmoidal oxygenated hemoglobin dissociation curve (Fig. 3).

A recent thorough review of pulse oximetry is given in [107]. This technique is briefly described below, since it shares some fundamental principles with NIRS - a technical cornerstone in this thesis. Pulse oximetry was also used for SpO_2 monitoring in Papers **I** and **II**.

Pulse oximetry is based on the different light absorption spectra for HbO_2 and Hb^- in the visible red and near-infrared wavelength region (Fig. 10a). In most pulse oximeters, two wavelengths are used, e.g., 660 and 940 nm. To be able to determine the oxygenation in arterial blood only, pulse oximetry uses photoplethysmography (PPG), to measure increases in light absorption resulting from systolic increases in arterial blood volume, leading to a decreased intensity of the transmitted light [108] (Fig. 15).

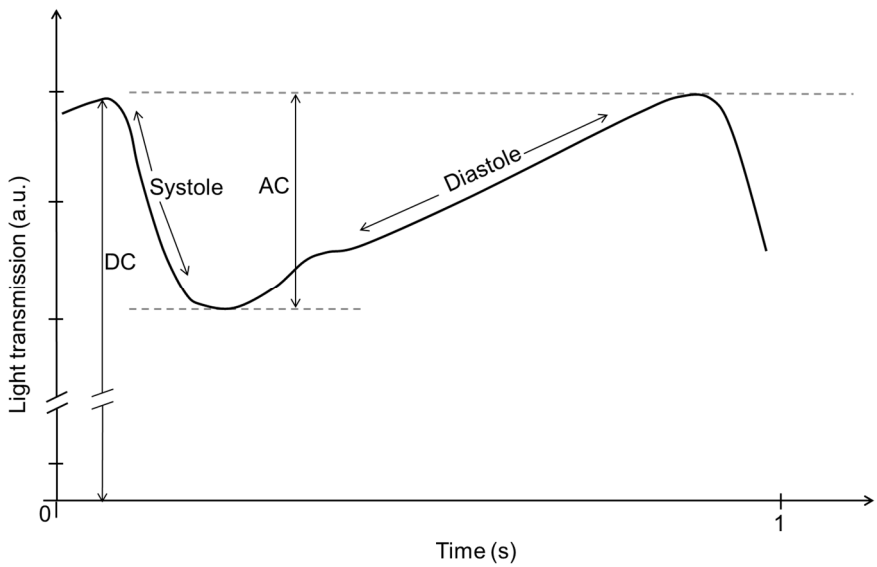

Figure 15.
The photopletysmography signal at a particular wavelength. DC refers to the signal baseline and AC to the pulse amplitude. Light transmission is given in arbitrary units (a.u). Modified from [107].

By recording curves like this one at two suitably selected wavelengths, the SpO_2 can be calculated and presented on the pulse oximeter. The signal from the pulsatile arterial blood flow is divided by its baseline level, representing light transmitted

through tissue, venous blood and non-pulsatile arterial blood flow, in order to obtain the PPG signal amplitude, which is related to the maximum blood volume change during systole [109]. The ratio of the transmitted pulsatile light (the PPG signals) at the two wavelengths, sensitive to the degree of oxygenation, is calculated and then compared with stored calibration curves derived in healthy subjects, to give an estimate of SpO_2. Since the technique utilizes the pulsations, pulse rate is also automatically obtained.

Typical locations of probe positioning are fingertips and earlobes, since light transmission through the tissue is used. These locations yield PPG pulses with a high signal-to-noise ratio, since blood flow, because of its role in heat regulation, normally exceeds that required for baseline metabolism [107].

For ethical reasons it is not possible to reduce SpO_2 below 80 % in healthy volunteers, and since empirical calibration of pulse oximeters has been based on values obtained on healthy volunteers, inaccuracy of SpO_2 measurements has been shown in critically ill patients, with lower levels of arterial oxygenation [110], and particularly so in pediatric patients [111]. However, it is important to accurately assess not only hypoxia but also hyperoxia (high PaO_2), since excessive administration of O_2 may be harmful [112], especially to infants. Detecting hyperoxia by pulse oximetry is problematic, since the dissociation curve is almost flat in the upper range (>95 %) of SaO_2, leading to small changes in SaO_2 for large changes in PaO_2. Preterm infants are particularly vulnerable in this respect, since hyperoxia may induce retinopathy of prematurity [113]. A recent meta-analysis of three large studies comprising 4911 preterm newborns concludes that SpO_2 should be targeted at 90-95 % in preterm infants born before 28 gestational weeks [114].

Conventional pulse oximeters, using only two wavelengths, are based on the assumption that HbO_2 and Hb^- are the only absorbers of light in blood. However, COHb and metHb (p. 30) also absorb light at the wavelengths used in pulse oximetry, causing potential errors in SpO_2 readings. Recently introduced pulse oximeters using more wavelengths can make it possible to differentiate between various kinds of hemoglobin [115].

Perfusion of the fingertips or earlobes might be low in intensive care patients, often because of low CO with reduced PPG signals, leading to reduced accuracy in the measurements. Local vasoconstriction with low perfusion decreases the PPG signal and is associated with an increase in the SpO_2 value obtained [116, 117]. Conversely, vasodilation is associated with a decrease in the SpO_2 value, probably due to altered transmission of the arterial pulsations to the venous blood in the finger [116, 118].

Reflection pulse oximetry, where light is injected and detected on the same surface of the skin, provides more options for probe positioning, and has been reported to be more reliable when peripheral perfusion is low [119]. Forehead reflection sensors have been found to be as accurate as standard finger-tip sensors in well-perfused pediatric patients [120]. Reflection pulse oximetry also enables mucosal SpO_2 measurements in e.g., the larynx, trachea and esophagus [121-123].

Near-infrared spectroscopy

Near-infrared spectroscopy (NIRS) is a non-invasive optical technique, used to monitor non-pulsatile StO_2 - in contrast to pulse oximetry, where the arterial pulsatile oxygenation is in focus.

In 1977 Frans Jöbsis first reported non-invasive detection of myocardial and brain StO_2 in the near-infrared wavelength region by transillumination spectroscopy [124]. This was the starting point for NIRS as a tool for measuring StO_2 non-invasively.

Many interventions, in various fields of medicine, aim to maintain, restore or optimize StO_2 [125]. It therefore remains important to directly assess StO_2. Systemic arterial and venous (central/mixed) oxygenation can on a routine basis be measured with established techniques like pulse oximetry, blood gas analysis and central venous or pulmonary artery catheters. Methods are required to allow for early detection of regional hypoxia and to guide therapy to restore oxygenation, since concealed regional ischemia, non-detectable systemically, is considered to contribute to mortality and severe morbidity in critical illness or major trauma [126]. Also, hyperoxia should be avoided, as it might be deleterious (p. 48). To optimize critical care management, monitoring of regional oxygenation is essential.

NIRS can provide an optical non-invasive tool, enabling estimation of local StO_2. The following sections discuss fundamental principles of the technique, and two specific ways of measuring StO_2 - by using continuous light or ultra-short pulses of light - and their advantages and limitations.

The NIRS technique is based on specific wavelengths (700-1000 nm) of near-infrared light [89]. Human tissue is quite transparent within this spectral range - falling in the tissue optical window. Light that has travelled as far as few cm through the tissue can be detected. The corresponding distance for visible light is restricted to less than 1 cm, because of the strong absorption by hemoglobin in this spectral region. At wavelengths above 1000 nm, water starts to become a heavy absorber, preventing deeper penetration into tissue [93].

Light injected into human tissue is highly scattered, some is absorbed and some finds its way to the detector. Approximately 80 % of the total attenuation of light is due to scattering and 20 % due to absorption [127]. Light travels through tissue in a "banana-shaped" distribution, with maximum penetration depths approximately one-third to half of the surface distance between the light source and the detector [128]. Detection of light at different distances from the point of injection favors different ray paths.

Absorption of light in the tissue, causing attenuation, depends on different compounds (chromophores). Each chromophore has its particular absorption spectrum, where the specific extinction coefficient is expressed as a function of wavelength ($\sigma(\lambda)$) in Eq. 6 on p. 42) (Fig. 12). The extent of light absorption, mainly by the chromophore hemoglobin, is influenced by its oxygenation. Other chromophores, such as myoglobin, are generally assumed to contribute less to the

total absorption of light [129] (discussed below, pp. 83-84). Melanin has a high absorption of light at shorter wavelengths (e.g., 400 nm), with gradually reduced absorption at longer wavelengths [94] (Fig. 12). The influence of melanin is discussed in Papers **I-II**.

A modified Beer-Lambert law, considering absorption as well as scattering (Eq. 13, p. 44) can be used to calculate StO_2 by matching the measured spectrum with reference spectra at known levels of saturation [97]. By using at least two defined wavelengths of light, with different values of absorption for HbO_2 and Hb^- (Fig. 10a), their relative content can be determined, and StO_2 calculated (Eq. 14, p. 46). Since the absorption of light by HbO_2 and Hb^- is the same at the isobestic point (Fig. 10a), it can be used to calculate hemoglobin concentration regardless the level of oxygenation [89].

Light is completely absorbed by vessels above 100 µm diameter. Values obtained with NIRS therefore reflect the O_2 saturation within the microcirculation only, and mainly so in capillaries and venules, since only about 15-20 % of the hemoglobin is located in arterioles [130].

As noted, a challenging issue, when attempting quantitative measurements of StO_2 with NIRS, is that human tissue represents a highly scattering medium (typically responsible for 80 % of light attenuation). Today, most commercially available clinical devices are based on non-time-resolved continuous-wave techniques (CW-NIRS), providing relative values of StO_2. However, with CW-NIRS, it is not possible to separate light attenuation resulting from scattering and from absorption, rending full interpretation difficult. Instead empirical calibration has to be applied.

There are two major strategies for differentiation of tissue scattering from absorption - frequency domain NIRS and time-resolved NIRS. In frequency domain NIRS, sinusoidally intensity-modulated near-infrared light is used. The signal received is observed with a phase shift and a demodulation, which depend on tissue optical properties and the modulation frequencies used (~100 MHz), enabling independent quantitative analysis of tissue absorption and scattering [131]. In time-resolved NIRS the tissue is instead exposed to ultrashort pulses of light, and the time-dispersion of the detected light is recorded, enabling differentiation between scattering and absorption [132]. Time-resolved NIRS is of central importance in Paper **II**, and is described in detail below.

During the last three decades numerous studies have been conducted using NIRS, in adults mainly in skeletal muscle or brain tissue [133]. Available studies in human skeletal muscle and cerebral physiology have recently been summarized [129, 134]. NIRS has also been evaluated as a possible tool for StO_2 assessments in sepsis [135], trauma [125], and during resuscitation in hemorrhagic shock [136]. In the pediatric field, NIRS has mainly been used to assess cerebral oxygenation [137], but also postoperatively to measure renal oxygenation/perfusion [138]. A recent multinational clinical trial has evaluated possibilities to guide treatment in extremely preterm infants, based on cerebral oxygenation values obtained by NIRS, in order to reduce

brain injury [139]. Primary outcome results [140] propose that cerebral NIRS, combined with evidence based treatment guidelines [141], can stabilize cerebral oxygenation in extremely preterm infants.

Continuous-wave near-infrared spectroscopy

Continuous-wave NIRS uses continuous near-infrared light emitted by e.g., light emitting diodes with a typical spectral width of 20 nm. Values of regional StO_2 are calculated from relative levels of tissue absorption by oxygenated and total (oxygenated and deoxygenated) hemoglobin [89]. Detection of light at different distances (e.g., 3 and 4 cm) from the point of injection, allows for both less and more tissue penetrating light to be examined (Fig. 16). Values of deeper regional StO_2 can be calculated by taking signal levels measured at both 3 and 4 cm distance into account. Although CW-NIRS is unable to provide absolute values of StO2 [142, 143], since time-resolved information on the photons is required to determine the relative extent of scattering and absorption of light in the tissue [144], the technique may still be used to monitor intra-individual changes in StO_2 over time [143, 145].

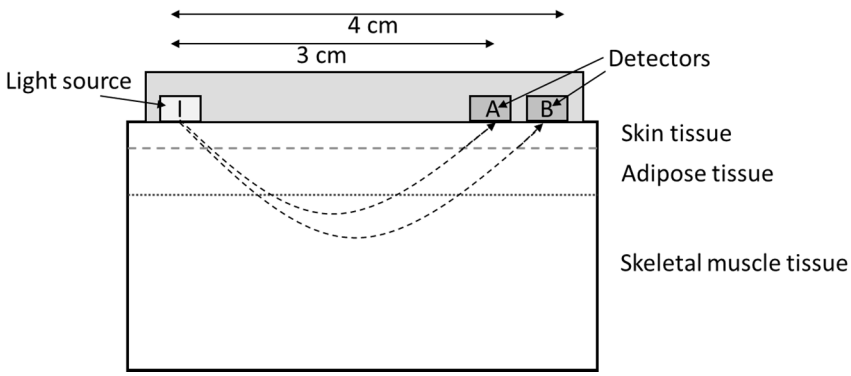

Figure 16.
Schematic picture showing fundamental principles of continuous-wave near-infrared spectroscopy. Light at two defined wavelengths is injected (I) through skin and subcutaneous adipose tissue into skeletal muscle tissue. Relative values of tissue saturation (StO_2) are obtained by comparing corresponding extents of absorption by oxygenated (Hb^-) and deoxygenated hemoglobin (HbO_2) at the two wavelengths. Emerging light reflecting deeper locations of tissue is detected further away (B) from the injection point, whereas detection closer (A) to the injection point favors shallower ray paths. Modified from Paper **II**.

Time-resolved near-infrared spectroscopy

Time-resolved near-infrared spectroscopy, sometimes called photon time-of-flight spectroscopy (PTOFS), measures light intensity as a function of time as the photons travel through the tissue. Later arrival times at the detector for photons from a pulsed laser source correspond to longer path lengths through tissue given the defined velocity of light in tissue [146]. According to the Beer-Lambert law (Eq. 6, p. 42) the transmission of light ($T=I(\lambda)/I_0(\lambda)$) depends on C and l, which in turn is given by $l=ct$,

where c is the speed of light in tissue of refractive index n ($c=c_0/n$), and t is the observed time delay. Clearly, there is such transmission expression for each time delay, and the net absorption in a scattering medium becomes a complicated sum of different contributions.

For clear solutions, absorption is more predictable, since there is almost no scattering or variation in l. The challenging issue of scattering media, like human tissue, is the presence of both shorter and longer l in the same measurement (Fig. 17). By emitting photons in laser pulses of ultrashort (≤ 10 ps) duration, and detecting the differences in the photon arrival times at the detector, histograms can be obtained with arrival time on the x-axis and number of photons on the y-axis [146] (Fig. 17).

According to the Beer-Lambert law, absorption is most prominent for the delayed photons that have travelled longer distances within the tissue. As a consequence, the absorption modifies the recorded curve shape and a larger absorption especially attenuates the tail of the curve. Likewise, with increased scattering the peak of the curve is delayed. By analyzing the shape of the curve with mathematical models of light propagation in scattering materials (i.e. photon migration), the distribution of photon time-of-flights can be used to determine the absorption and scattering properties separately, hence allowing their relative contributions to be individually assessed [147]. The absorption spectrum, free from scattering artifacts, can be used to accurately estimate absolute values of HbO_2 and Hb^- concentrations, from which a much more robust and precise calculation of StO_2 can be made [148].

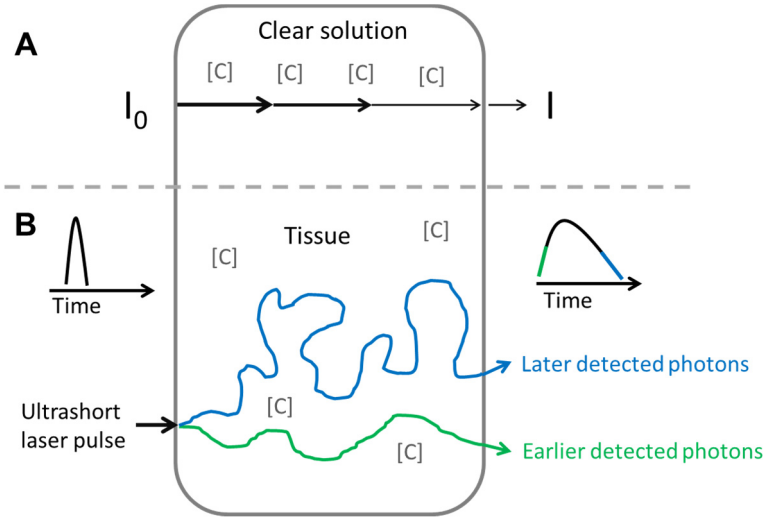

Figure 17.
Schematic illustration of the transmission of light through clear (A) and scattering (B) media. In the upper part (A), an injected short pulse of light with input intensity I_0, propagates through a sample with a clear solution, exiting with the output intensity I. Since the path length ($l=ct$) is the same and known for all photons (no scattering), the absorption is determined by the concentration ($[C]$) of the solute according to the Beer-Lambert law. Below, (B), a short pulse of light is injected into a highly scattering medium (human tissue), where the photons have different path lengths. A distribution of arrival times will be obtained because of the scattering. In the histogram of photon arrival times earlier arriving photons are marked in green, while later arriving in blue color. From Paper **II**.

Within the medical field, PTOFS and the frequency modulated technique have e.g., been used to study characteristics [149] and detection possibilities [150] of breast cancer, optical properties of the brain in adults [151] and infants [152], and skeletal muscle physiology during exercise [153, 154]. The technique has also found many applications in other areas, e.g., to determine scattering properties of pharmaceutical tablets [155].

Gas sensing in human tissue

Due to the huge differences in line width for absorption of light between gaseous and solid matter, gas pockets enclosed in highly scattering solid tissue can be examined. Biological tissue, solid or liquid, exhibits quite broad spectral structures of absorption, with absorption peaks seldom narrower than 20 nm (pp. 39-40). Hence, the demand for light at extremely well defined wavelengths (monochromatic light) is low and e.g., LEDs can be used.

For measurements on free gas, where the line width of the absorption line is only determined by the magnitudes of Doppler and pressure broadening, related to

molecular motion and collisions [87], respectively, the light beam must have a wavelength precision better than the 6th digit.

Various techniques for breath analysis are used in established clinical fields to assess gas properties. Capnography is routinely used to estimate exhaled concentrations of CO_2 [156], in cardiopulmonary resuscitation [157] and during anesthesia [158, 159], and in intensive care medicine [160]. This is done by infra-red or mass spectroscopy, and requires extraction of gas from the airways or the breathing circuit [156].

More recently, minor gas constituents, related to different medical conditions, have been studied by laser absorption spectroscopy on expired gas [161]. A further example of gas analysis outside the human body is investigations on nitrous oxide produced in the sinus cavities [162]. However, laser spectroscopy can also be used to monitor free gas, *in situ*, inside highly scattering tissue, with the technique "gas in scattering media absorption spectroscopy" (GASMAS), introduced in 2001 [163], and discussed in more detail below.

Gas in scattering media absorption spectroscopy

The main difference between GASMAS studies and studies for monitoring of solid or liquid tissue constituents is that the demands on the light source are much higher. The line width of a free O_2 transition is about 0.001 nm (1 pm, corresponding to 10^9 Hz), calling for a light source, with more narrow line width than this (pp. 39-40). Single-mode semiconductor lasers used have a typical line width of 10^7 Hz. High-resolution laser spectroscopy, where the wavelength of the laser is continuously changed, has been much employed for studying atmospheric pollution gases [164] and GASMAS is an extension of such techniques [163, 165]. The GASMAS method has also been used in many non-medical applications, e.g., for studying food packaging [166], fruits [167], wood drying [168], pharmaceutical tablets [169] and ceramics [170].

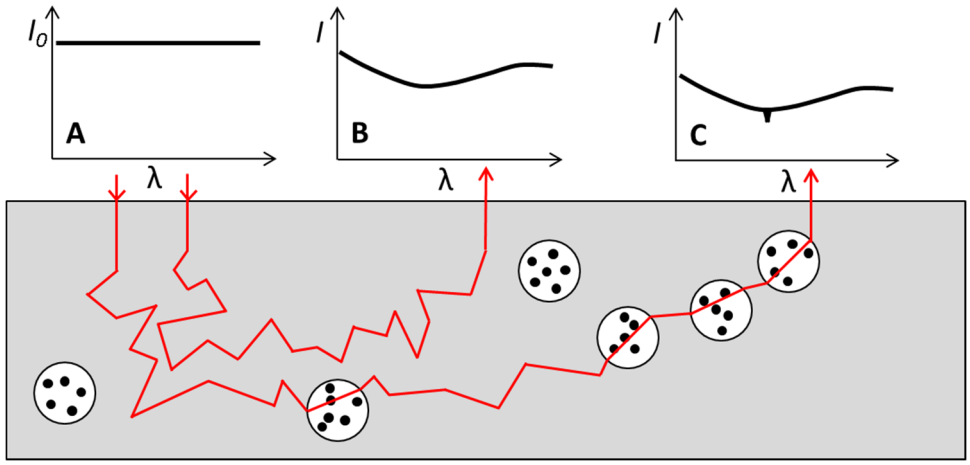

Figure 18.
Schematic figure showing basic principles of gas in scattering media absorption spectroscopy (GASMAS). Light with the intensity I_0 is injected into tissue (A). If the light only encounters solid matter, there is a broad decrease in intensity (B), resulting from absorption and scattering. If the light also passes through gas-filled cavities, there is also a sharp drop in intensity in the detected light (C) in addition to the broad decrease.

The principles are shown in Fig. 18. Laser light is sent into tissue, which contains cavities and pores, filled with gas. Because of tissue scattering (p. 41), photons travel in complicated pathways through the tissue and some of them will reach the light detector, placed at a certain distance from the point of injection. The similarity to NIRS should be noted. The detected light will have a slow intensity variation, when the wavelength of the laser is changed (scanned) – basically the broad-band structures of the heavily absorbing bound molecules, discussed in the preceding sections, are observed. However, light, which has passed through the gas-filled cavities will in addition have a very sharp imprint, due to absorption by the gas (Fig. 19). The gas absorption signals, which were studied in the present work for the case of O_2 and H_2O vapor, are very weak; only about 0.1 % or less of the detected laser light intensity is absorbed at the peak of the absorption line. In order to detect such a small signal in the weak light reaching the detector, so called lock-in techniques can be used, requiring a fast modulation of the laser wavelength. This leads to the detection of signals, which resemble the mathematical derivatives of the absorption curve, as indicated in Fig. 19. There are advantages of using the 2nd derivative of absorption, as frequently occurring in Papers **III** and **IV**.

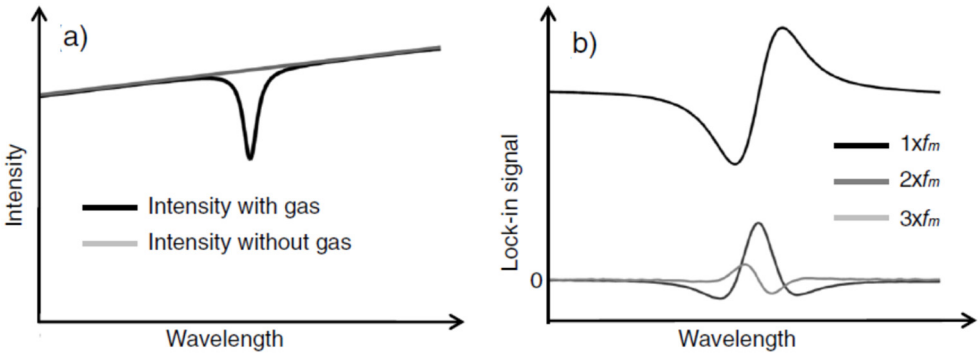

Figure 19.
Spectroscopic signals from a molecular absorption line. a) shows the sharp symmetrical intensity reduction, when the laser is tuned through the absorption line. The background is sloping, since the tuning is done by increasing the current. b) shows the 1st , 2nd and 3rd derivatives (approximately) of a symmetric absorption signal, as recorded by a lock-in amplifier. The 2nd derivative was used in Papers **III** and **IV**. From Paper **III**.

However, like in broadband spectroscopy (NIRS), gas concentration measurements become complicated due to the absence of a well-defined path length of the detected light, and a corresponding straight-forward Beer-Lambert law. Instead, GASMAS results are frequently expressed as equivalent path lengths (l_{eq}), which would give rise to the same fractional absorption for light travelling through an atmospheric gas with a known concentration, e.g., O_2 at 21 %. Only the *product* of path length and concentration occurs in the Beer-Lambert law.

The path length problem could in principle be solved by PTOFS, as described above (pp. 51-53). However, PTOFS measures the total path length between the light source and the detector. In order to determine the concentration of gas, e.g., O_2, the actual path length through the gas only must be known. Different approaches to solve this problem have been proposed [171]. One way is to normalize the O_2 signal to a simultaneously measured H_2O vapor signal. In a gas volume embedded in tissue, containing liquid water, the relative humidity will be close to 100 %, and the concentration of the H_2O vapor is then determined by the temperature only (known for the human body), through the Arden-Buck relation [172]. The path length can thus be calculated from the H_2O vapor signal, and - assuming similar path-lengths for light providing O_2 and H_2O vapor data - be used to derive the O_2 concentration. These aspects will be discussed more closely in the Methods section.

In the medical field, GASMAS has already been applied successfully for monitoring of gas in the human sinus cavities [173-175] and mastoid bone [176]. Model experiments for measurements of GASMAS signals through the ear drum have also been carried out [177].

Laser Doppler spectroscopy

The laser Doppler technique has an interesting status with regard to broadband and narrow-band spectroscopy. Very small frequency shifts are measured, suggesting that extreme laser frequency control would be needed, like in narrow-band spectroscopy. However, since shifts rather than absolute frequencies are being measured, the demands on the laser are much relaxed. Hence, like for non-time-resolved broadband spectroscopy (p. 51), equipment based on the laser Doppler principle is rather simple.

Laser Doppler spectroscopy is an optical technique, where laser light is used to non-invasively monitor superficial perfusion. The most common light source is a continuous helium-neon laser with a wavelength of 633 nm or a dark red NIR diode laser (wavelength 630-690 nm). The frequency shift of light emitted into the tissue observed between photons scattered by fixed structures, and by moving particles in the tissue, is determined. In the human skin, erythrocytes are the main moving particles, and their speed can be determined from the frequency shift. The reflected light will have a higher frequency than the irradiated light (positive Doppler shift) if the particle moves towards the laser beam and a lower frequency (negative Doppler shift) if it moves away from the beam [178].

In the capillary bed, however, all flow directions are present, leading to registration of a signal, symmetrically broadened around the laser frequency. The signal magnitude and size of the Doppler shift are related to the concentration and speed, respectively, of the erythrocytes, and the perfusion is defined as the product of erythrocyte concentration (erythrocyte volume fraction, or hematocrit) and average speed in the volume probed. The output signal gives information on relative perfusion, expressed in arbitrary units [179].

The technique uses the Doppler equation, relating the frequency shift ($\Delta\upsilon$) to the speed of the erythrocytes (v_x) in the direction of the impinging photon along the x-axis:

$$v_x = \left(\frac{\Delta\upsilon}{\upsilon}\right) c, \tag{15}$$

where υ is the emitted frequency, and c is the speed of the laser light. A rough estimate of $\Delta\upsilon$ for visible light (with $v_x \approx 2$ mm/s) is approximately 10^4 Hz. The frequency shift is thus very small, and can only be measured through registrations of the beat frequency between the originally emitted and the frequency-shifted light, using the so called heterodyne technique [178]. Fundamental principles are shown in Fig. 20.

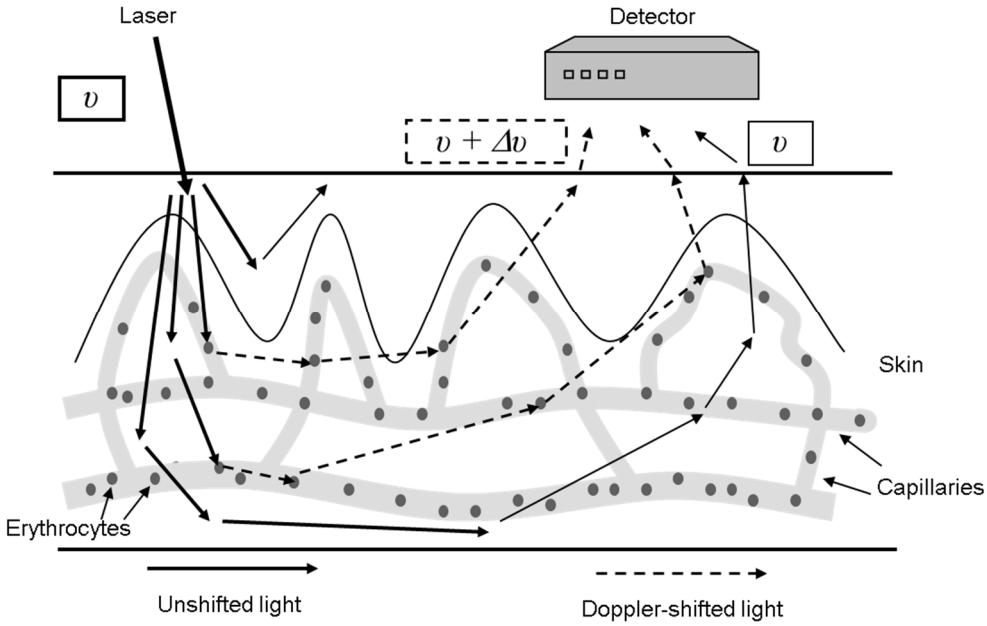

Figure 20.
Schematic illustration of fundamental principles of the laser Doppler technique. The frequency of the injected light (υ) is changed by moving red blood cells. Blood perfusion of the skin is estimated from the frequency shifts ($\Delta\upsilon$) between the injected light (solid arrows) and the light reflected by red blood cells in the vessels (dashed arrows). Modified from Paper **II**.

Primarily, measurements based on the laser Doppler principle provide information from single investigated spots - laser Doppler flowmetry [178]. However, information from extended areas can be obtained by using a laser beam scanned over the area with sequential measurements in multiple points – laser Doppler imaging (LDI). Clearly, this takes time, resulting in lower time resolution [180].

Laser Doppler measurements in medicine constitute a well-recognized and established technique for studying skin perfusion. The method has been used for nearly 30 years to monitor blood flow in the microcirculation, e.g., in burn wounds, transplanted flaps, wound healing and endothelial (dys)function [181, 182].

Aims

A general aim of this thesis, based on studies in humans (**I-IV**), was

- to optimize and evaluate spectroscopic techniques, based on light at different wavelengths, with potentials of being non-harmful complements for surveillance in critical illness or severe injury.

Specific aims of the thesis were

- to evaluate to what extent values of StO_2, capillary perfusion, and blood volume, obtained by CW-NIRS, LDI and TVI techniques, respectively, reflect defined hemodynamic perturbations in dermal and skeletal muscle tissue, and how those techniques can provide complimentary information (**I**).
- to compare CW-NIRS and PTOFS techniques under defined physiological conditions, with respect to accuracy, appropriateness and individual dependence of values of muscle StO_2 obtained (**II**).
- to test the GASMAS technique for non-invasive detection of alveolar and intestinal gas in healthy newborn infants (**III**).
- to explore opportunities and limitations of the GASMAS technique for non-invasive detection of alveolar O_2 in newborn healthy infants (**IV**).

Methods

Details on study design, subjects, and methods applied in this thesis are given in each paper (**I-IV**). Here a summary of the methods used is presented.

Tissue oxygenation, perfusion and blood volume (**I-II**)

Capabilities and limitations of three established non-invasive optical techniques – NIRS (**I-II**), LDI (**I**) and TVI (**I**), presented above (pp. 49-53, 57-58, 45-46) – for determination of regional StO_2, tissue perfusion and blood volume, respectively, - were evaluated and systematically compared in healthy volunteers, subjected to experimentally induced regional vasodilation, vasoconstriction, increased venous return, tissue edema and impaired arterial inflow. Two NIRS techniques – the established CW-NIRS (**I-II**) and the newer PTOFS (**II**) – were evaluated.

Subjects

The studies were approved by the Regional Ethics Review Board of Lund University, Lund, and carried out at the Department of Clinical Physiology, Skåne University Hospital, Malmö (**I**), and the Department of Physics, Lund University, Lund (**II**), Sweden. Eighteen (**I**) and 21 (**II**) healthy volunteers were included after individual informed consents. For technical reasons, four subjects were excluded, from the volunteers enrolled in Study **II**. Another two subjects had to be discarded due to a software bug in the CW-NIRS system. Hence, the study results in Paper **II** were based on 15 and 17 volunteers for CW-NIRS and PTOFS, respectively.

Preparations and monitoring

As shown in Fig. 21, the volar side of the proximal forearm was used for dermal and muscle tissue measurements (**I-II**). Similar values of muscle StO_2 can be determined over extended skin areas within this region [183], the adipose tissue thickness (ATT) covering the muscle is relatively low, and skin surface is quite flat [45] (making probe attachment easier). The forearm is subjected to early regional vasoconstriction in

systemic hemodynamic distress [184], and has been reported to respond more readily than the thenar region in this respect [52].

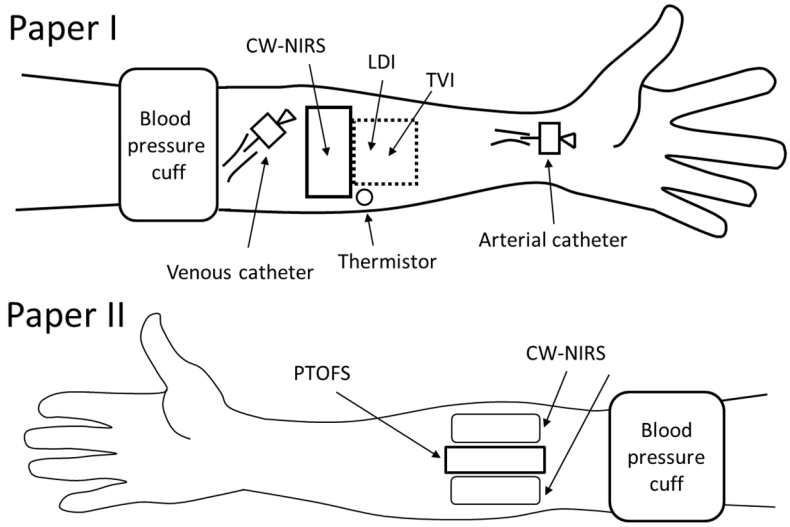

Figure 21.
Schematic illustration of technical arrangements for optical measurements in Paper **I** (upper drawing) and Paper **II** (lower drawing). From Papers **I** and **II**.

At high ATT, measurements of muscle StO_2 by NIRS are often influenced, since light probing then is limited mostly to the fat layer only [185]. Hence, many studies on muscle StO_2 based on NIRS have been restricted to slim male subjects [129]. In contrast, LDI and TVI techniques, both probing at tissue depths of 0.5-1 mm, are not considerably influenced by ATT. Skinfold thickness was determined by slide caliper measurements; half of that value was used as an estimate of ATT (**I-II**) [185]. The subjects were divided into three groups with regards to ATT – low (<9 mm), moderate (10-17 mm), or high (>18 mm) (**II**).

The Fitzpatrick scale [186] was used to classify all subjects into five groups (1-5) according to skin content of melanin (**II**). Five subjects differing in relative levels of ATT and melanin content were chosen for comparison of individual study recordings (**II**).

Teflon cannulas were positioned in the ipsilateral radial artery and medial cubital vein (**I**), for determination of individual arterial (baseline) and venous (baseline, and after each study event) levels of pH, PO_2, PCO_2 and base excess (BE). Blood pressure was monitored invasively by the arterial catheter (**I**).

All subjects were monitored by transcutaneous pulse oximetry on a finger of the contralateral hand (**I-II**) to detect any decrease in SpO_2.

Two different, commercially available CW-NIRS devices were used - InSpectra™ (**I**; Hutchington Technology Inc, Arnhem, Netherlands), and INVOS™ 5100C (**II**; Somanetics, Troy, Michigan, USA) – providing values on StO_2 (**I-II**), and total hemoglobin count (HbT), reflecting regional tissue blood volume (**I**); see Table 1. Our PTOFS system (**II**) used a broad-band, short-pulse light source and a tunable filter to select the wavelength bands employed. Time-resolved photon-counting detection was used to generate the time dispersion curves. Time-resolved measurements with this technique were done at 30 and 40 mm source-to-detector distances to provide technical conditions similar to those used by the CW-NIRS system (**II**).

A PIM III Laser Doppler Perfusion Imager (Perimed, Linköping, Sweden), employing imaging areas of 15 x 15 mm, was used for the LDI measurements (**I**).

For TVI measurements, a TiVi600 tissue viability imager (Wheelsbridge AB, Linköping, Sweden), including a standard digital camera (Canon S80, Canon Inc., Tokyo, Japan), was used (**I**). The same 15 x 15 mm region of interest as used in LDI measurements was subjected to TVI image analysis.

Table I.
Features of the two commercially available CW-NIRS devices used (**I-II**). Cyt AA3 = cytochrome AA3, Hct = erythrocyte volume fraction (hematocrit).

	InSpectra™	**INVOS™ 5100C**
Wavelengths employed (nm)	680, 720, 760, 800	730, 810
Source-to-detector distance (mm)	25	30, 40
Measurement intervals (s)	3.5	6
Parameters presented	StO_2, HbO_2, Hb^-, HbT, Cyt AA3, Hct	StO_2

Study design and measurements

Study designs (**I-II**) are shown in Fig. 22. The study events (marked by italic Roman numbers *I-III* or *I-IV* in the figure) were designed to resemble pathophysiological conditions in the clinical setting. Efforts were made to arrange those perturbations in chronological order, starting with the least demanding ones. The study protocols (**I-II**) have one study event - gradual venous-through-arterial occlusion (*III* in Fig. 22) - in common.

- Elevation and lowering of the arm above and below heart level – to evaluate the effects of "non-intentional" repositioning of the limb subjected to measurements (**I**:*I*).
- External cooling (at 21 ºC) and heating (at 39 ºC) of the forearm to evaluate effects of regional cooling/vasoconstriction and warming/vasodilation on the measurements (**I**:*II*).
- Induction of gradual venous-through-arterial occlusion (at 30, 60, 90, 120 and 150 mmHg, and on cuff release) by inflation of a cuff around the upper arm – to evaluate effects on gradually compromised venous outflow and arterial inflow (resembling development of compartment syndrome with increased tissue edema and decreased nutritional flow), and of RH (**I-II**:*III*).
- Elevation of both legs at 60-degree angle - to evaluate effects of increased central venous blood flow (**II**:*I*).
- Instant regional venous occlusion (at 60 mmHg) by inflation of the cuff around the upper arm – to evaluate effects of a situation resembling a moderate regional fluid overloading (**II**:*II*).
- Instant regional arterial occlusion (at 150 mmHg) by inflation of the cuff around the upper arm – to evaluate effects of a situation resembling arterial thromboembolism, external compression, injury, or major vasoconstriction (**II**:*IV*).

Values of SpO_2 (**I-II**), pulse rate (**I-II**), heart rate (**I**) and invasively measured blood pressure (**I**) were recorded together with the study measurements, which are indicated by arrows in Fig. 22.

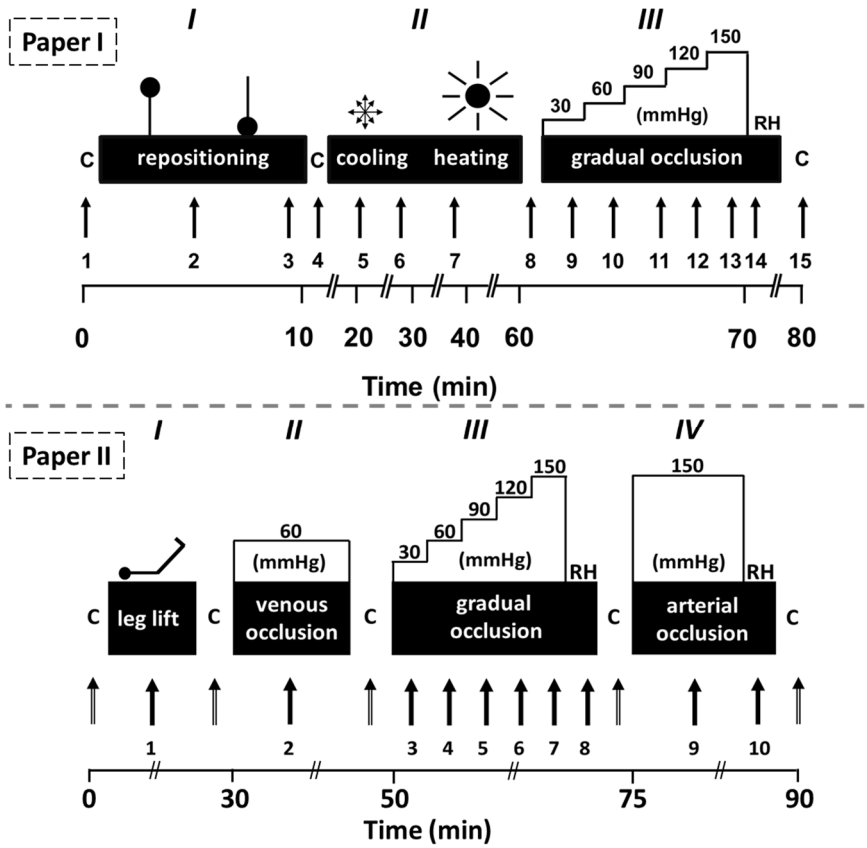

Figure 22.
Schematic study designs (**I-II**). The Roman numbers in italic (*I-III*) and (*I-IV*) indicate the different provocations in Study **I** and **II**, respectively. Determinations of tissue oxygenation (StO_2) (**I-II**), perfusion (**I**) and blood volume (**I**) were done during every physiological provocation and in between, as indicated by arrows. Denotation C indicates baseline measurements and RH reactive hyperemia. Modified from **I-II**.

Data handling and statistics

Results obtained with the CW-NIRS, LDI and TVI techniques (**I**) were normalized to the median value of baseline measurements in each subject. No such normalization was done when comparing data obtained with the CW-NIRS and PTOFS techniques (**II**).

Non-parametric statistics were employed since optical results obtained were not normally distributed (**I-II**). Optical results are reported as median with interquartile range (IQR) (**I-II**) and range (**I**). The Wilcoxon signed ranks test was used (**I-II**) for statistical comparisons. *P* values <0.05 were considered to be statistically significant.

Detection of oxygen gas and water vapor (III-IV)

Here the GASMAS technique was used to enable and evaluate non-invasive detection of free gas in the lungs (primarily O_2) and intestines (H_2O vapor) in newborn infants (**III-IV**).

Subjects

The studies were carried out at the Department of Physics, Lund University, as a pilot study (**III**), and at the Postnatal ward, Skåne University Hospital, Lund (**IV**) after approval by the Regional Human Ethics Review Board of Lund University, Sweden. Informed consents were obtained from the parents. Three full-term infants aged 19-36 days (**III**) and 29 newborn full-term infants (**IV**) were included.

Preparations

The infants were either resting in the arms of a parent or sleeping in a cot. Clothes were removed from areas of measurement, to allow free access for the optical measurements. Ambient light was dimmed. Optical components in direct contact with the child were enclosed in disposable plastics to avoid contamination. The measurements were performed on a time scale where maximum attention was put on the infant´s needs.

Study design and measurements

Since non-invasive gas monitoring in young infants was a new aspect of optical diagnostics and monitoring, both studies were by necessity exploratory. Finding optimal locations for initial gas detection was an important aspect of Study **III**. Although detection of O_2 in the lungs was of primary interest, the presence of H_2O vapor was also investigated. Water vapor measurements are useful to enable determination of absolute O_2 gas concentrations in the lungs (since the vapor concentration in closed volumes at 37 ^oC is known), and for assessing gas-filled volumes in the lungs, intestine interior and walls, and possibly other intra-abdominal locations.

Relative difficulties associated with detection of O_2 gas and H_2O vapor were assessed with respect to line strengths and absorption of tissue. Most promising locations for lung measurements in Study **IV**, as suggested in Study **III**, are indicated in Fig. 23. The investigation (**IV**) was mainly directed at detecting O_2 gas with sufficient recorded signal-to-noise ratios (SNR). Since the gas signals correspond to approximately 0.1 % or less of the recorded light intensity (also very much attenuated

compared to the laser light injected), signal recording times of typical several tens of seconds were chosen. Considering that multiple recordings were done, the typical investigation time for each infant was about 20 min.

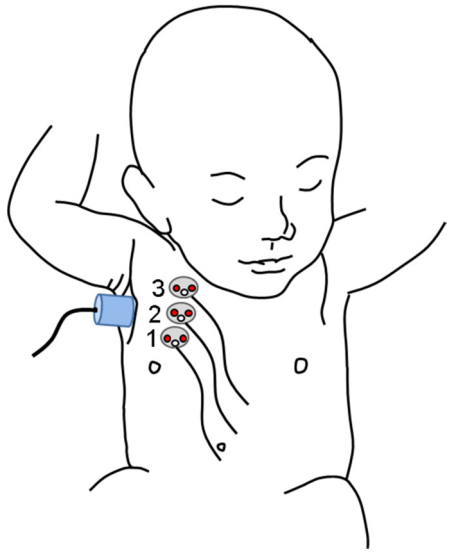

Figure 23.
Preferred localizations for light injection (red dots) along the midclavicular line (1-3) for non-invasive optical gas measuremens on lungs in newborn infants (**IV**). The detector (blue cylinder) was placed in the armpit. From Paper **IV**.

Two tunable semiconductor lasers emitting at around 760 nm for O_2, and 937 nm for H_2O vapor, were used (**III-IV**). Their linewidth was about 0.01 pm in order to enable accurate monitoring of the narrow absorption lines. The output power of the O_2 probing laser was about ten times higher in the later study (**IV**), to enable detection of O_2 in the lungs (~30 mW compared with ~4 mW). For convenience, outputs from both lasers were transmitted from the same optical head, and then recorded by a single detector. Still, the two signals could be separated by using different frequencies for the wavelength modulations, necessary for recording of the faint signals, employing lock-in techniques. This technique provides signal shapes, which resemble mathematical derivatives (see Fig. 19). The reason for choosing the 2^{nd} derivative is that it is less sensitive to fluctuations in light intensity.

To ensure proper functioning of the system, measurements through a block of polystyrene foam, containing large amounts of air, were used to confirm the expected presence of signals, while measurements through an adult forearm were accordingly used to confirm absence of gas signal.

Data handling and statistics

Recorded signals were fitted to reference signals of very high SNR, as registered from O_2 and H_2O vapor in normal air, without scattering (**III-IV**). In the curve fitting the product of concentration and path length is obtained, according to the Beer-Lambert law (Eq. 11, p. 43). A problem in scattering tissue is that the path length is unknown (p. 56), preventing the concentration to be directly determined. Therefore, we can evaluate our results as an equivalent path length (l_{eq}) which could be the distance needed in normal air, (containing 21 % O_2) for the case of O_2 detection, or air of known temperature and humidity for the case of H_2O vapor, to produce the same fractional signal, as recorded from the air-containing tissue. From Eq. 11 (p. 43) we have the experimentally measured signal S as:

$$S = \frac{\Delta I}{I_0} = \sigma(\lambda)Cl \ , \tag{16}$$

and thus with our chosen definition of l_{eq}:

$$C_{unknown} \times l_{unknown} = C_{ref} \times l_{eq} \ , \tag{17}$$

where C_{ref} can be the concentration of O_2 in normal air (21 %). For H_2O vapor the l_{eq} would primarily relate to ambient (e.g., 22 °C and 40 % relative humidity) conditions. However, it can be more physiological to recalculate the l_{eq} to human *in situ* (37 °C and 100 % relative humidity) conditions (**III**). Alternatively, measured results can be expressed by directly reporting the product of C and l in percentage meters (%m) (**IV**). Clearly, to be clinically useful we must have the O_2 concentration in %, i.e. the path length through gas must be determined. As discussed above, this is difficult, but could be achieved by normalization to H_2O vapor. Based on Eq. 16 experimental signals from O_2 (S_{O_2}) and H_2O vapor (S_{H_2O}) form the ratio:

$$\frac{S_{O_2}}{S_{H_2O}} = \frac{\sigma_{O_2}}{\sigma_{H_2O}} \frac{C_{O_2}}{C_{H_2O}} \frac{l_{O_2}}{l_{H_2O}} \tag{18}$$

Here the signal ratio is measured, the extinction coefficient ratio is known and C_{H_2O} is known for air at 100 % humidity of given temperature through the Arden-Buck relation [172]. The path lengths l are unknown, but if they can be assumed to be the same they cancel each other, and the unknown O_2 concentration (C_{O_2}) can then be calculated. This approach to the concentration problem is discussed in the original Papers **III** and **IV** and further addressed in the Discussion section below (pp. 84-85).

Since possibilities of detecting O_2 gas in infants was an open question (it was not observed in **III**), our refined study (**IV**) focused on the quality of the O_2 signals (which were actually detected). This is why the observed signal-to-noise ratio (SNR), defined as the ratio between the amplitude of the best fitted reference curve to the typical noise, expressed by the standard deviation, was given much attention and used in the evaluation (**IV**). In addition, O_2 signals were expressed, now in %m rather than l_{eq}. This means that for 21 % oxygen, 1 %m corresponds to a path length of approximately 4.8 cm.

Purely explorative findings (**III**) were not tested statistically. Other results obtained (**IV**) were not normally distributed and are reported as median values with IQR and range. Group differences were analyzed with the Mann-Whitney U-test. Differences between groups were considered statistically significant for P values <0.05.

Results

Tissue oxygenation, perfusion and blood volume (**I-II**)

All three study techniques provided valuable information on physiological changes in the microcirculation (**I**). Important to keep in mind is that LDI and TVI both provide information on superficial (dermal) tissue, while CW-NIRS provides information on deeper (skeletal muscle) tissue. Results obtained with the three optical techniques are given in Fig. 24.

Figure 24 shows that skin perfusion (measured by LDI) responded prominently to limb repositioning, whereas muscle StO_2 (measured with NIRS) did not change. On lowering of the arm, HbT (also measured by NIRS) and blood volume (estimated by TVI) both increased significantly. Skin perfusion and blood volume both increased considerably on local cooling (at 21°C), while no change in StO_2 or HbT was seen. Local heating (at 39 °C) was associated with a ten-fold increase in perfusion and a smaller increase in StO_2, HbT and blood volume. The perfusion and StO_2 levels decreased on gradual venous-through-arterial occlusion, and approached baseline levels on release of the occlusion, with an overshoot of the StO_2 (RH). On progressive occlusion, HbT and blood volume levels increased at first, and then decreased until full arterial occlusion had been achieved.

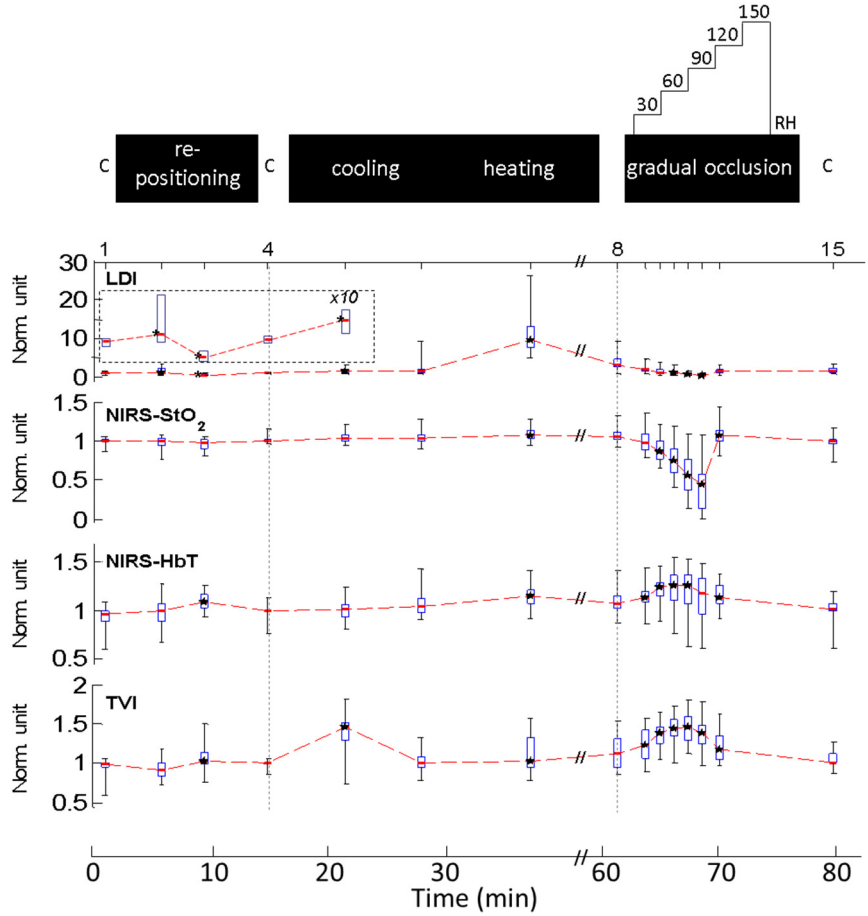

Figure 24.
Results obtained by laser Doppler imaging (LDI), continuous-wave near-infrared spectroscopy (CW-NIRS), yielding StO_2 and HbT, and tissue viability imaging (TVI) under three different physiological study conditions (separated by vertical dashed lines) (**I**). All data has been normalized to individual baseline levels. The graphs show median values with 1st and 3rd quartiles (box) and range (bar). Statistically significant differences from baseline levels (P <0.05) are indicated by black stars. For clarity, left parts of the upper diagram (within dashed lines) have been expanded 10-fold. From Paper **I**.

One volunteer, with higher skin melanin content, had higher TVI values, however with relative responses to various perturbations similar to those of other subjects. In contrast, results obtained by LDI and CW-NIRS were less influenced by melanin content.

Invasive blood pressure recordings showed that systolic and diastolic blood pressure levels gradually approached each other during gradual venous-through-arterial occlusion (*III*), and also that complete occlusion was preceded by transiently higher diastolic arterial pressure (DAP) levels (Fig. 25). Reduced outflow of blood from a tissue compartment, resulting from moderate venous occlusion, increases hydrostatic

transcapillary pressure levels with loss of fluid from intravascular to interstitial compartments. By external vascular compression, higher tissue pressure resulting from this fluid shift increases local diastolic pressure levels. These alterations were accompanied by an approximately 30 % decrease in venous oxygenation levels (representing outflow of blood from the occluded limb). The other measurements on systemic influence during the study yield that HR and SpO_2 remained unchanged.

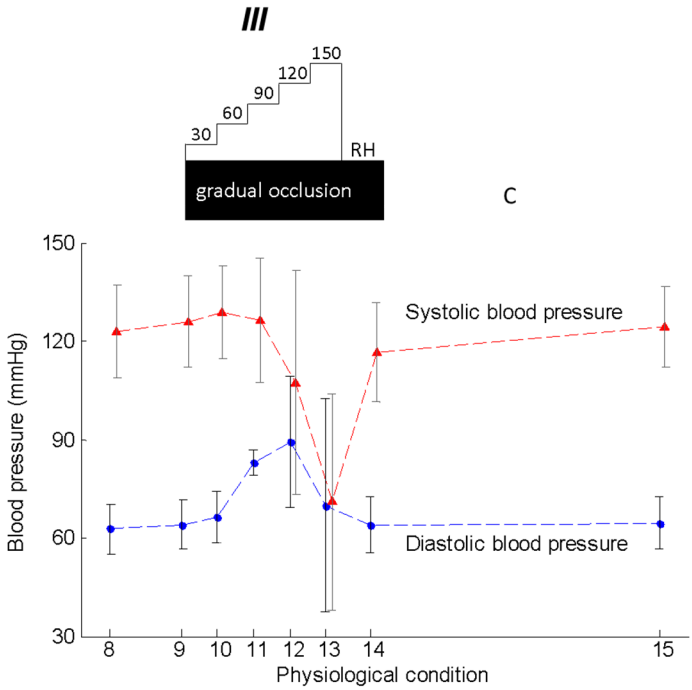

Figure 25.
Arterial systolic and diastolic blood pressures levels (mean ± SD) at wrist level before, during, and after gradual vascular occlusion achieved by inflation of a blood pressure cuff fitted around the left upper arm (**I**). The pulse pressure level, i.e. the difference between the systolic and diastolic blood pressures levels, gradually approached zero as the venous-through-arterial occlusion proceeded, and was rapidly restored on release of the cuff pressure. From Paper **I**.

Levels of StO_2 determined by either NIRS technique (Fig. 26) reflected various experimentally induced regional physiological conditions (**II**). However, values obtained by PTOFS (compensated for tissue scattering) were judged to be more accurate with smaller inter-individual differences, also when taking different subcutaneous ATT and cutaneous melanin content levels into consideration.

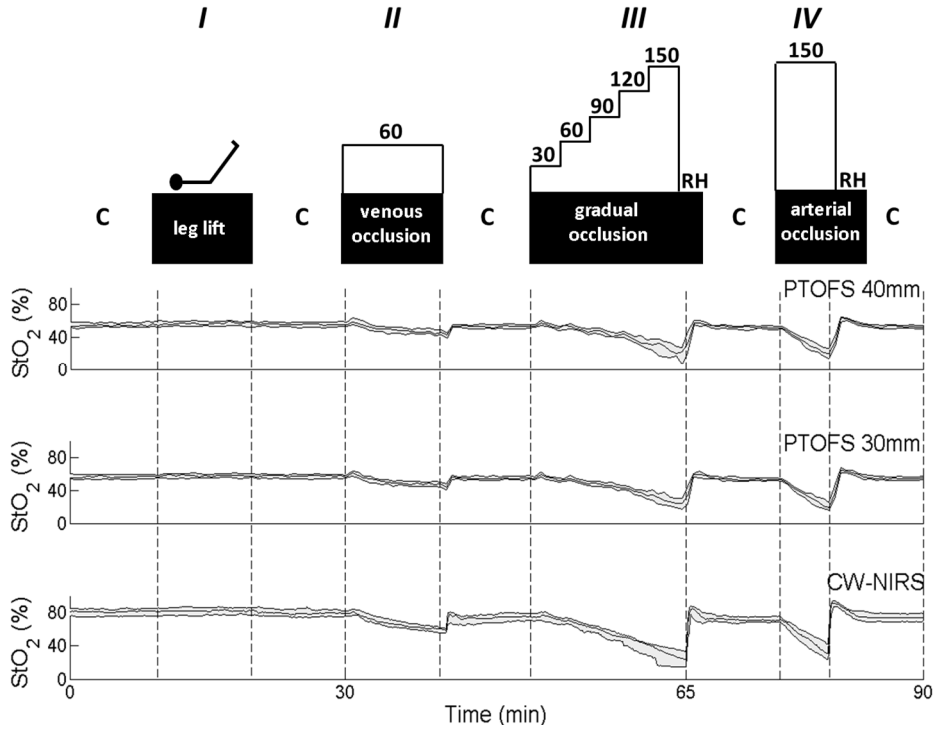

Figure 26.
Median values and interquartile ranges (in light shaded grey) of muscle tissue oxygenation (StO_2) obtained by photon time-of-flight near-infrared spectroscopy (PTOFS; upper curves) in 17 adult subjects (including those 15 below) and by continuous-wave near-infrared spectroscopy (CW-NIRS; lower curve) in 15 subjects. The volunteers were subjected to four different physiological study events (*I-IV*), separated by vertical dashed lines. Denotations PTOFS 30 mm and PTOFS 40 mm indicate values obtained at corresponding emission-to-detection distances. Baseline periods are labeled by C and reactive hyperemia by RH. From Paper **II**.

Elevation of the legs did not influence StO_2 values obtained by CW-NIRS and PTOFS (**II**). Venous occlusion was associated with lower, venous-through-arterial occlusion with gradually reduced, and RH with higher values of StO_2, obtained by either technique (**II**). Accordingly, instant arterial occlusion rapidly reduced StO_2 values, and the RH following immediately on the release of cuff pressure was observed as an increase in StO_2 values, obtained by CW-NIRS and PTOFS (**II**).

Values of SpO_2, obtained by contralateral pulse oximetry, were >95 % in all subjects throughout the study protocol.

To better understand potential influence of inter-individual differences on values of StO_2 obtained with the two study techniques (**II**), we also compared those results between subjects, which were considerably differing in subcutaneous ATT and cutaneous melanin content (Fig. 27).

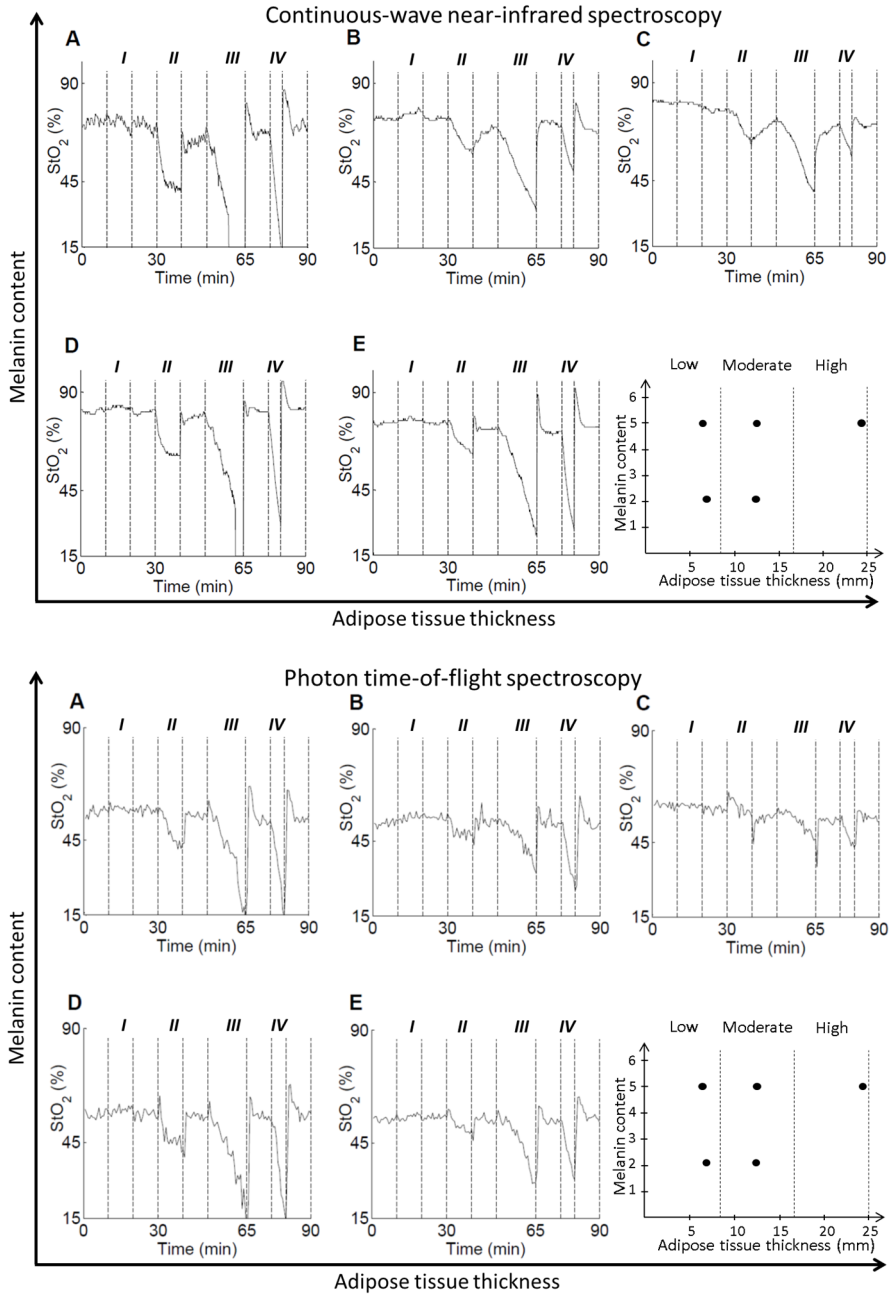

Figure 27.
Diagrams showing influence of skin content of melanin and adipose tissue thickness in five individual recordings of StO_2 with continuous-wave near infrared spectroscopy (upper) and photon time-of-flight spectroscopy (lower) techniques under various experimentally induced regional physiological conditions (*I-IV*). Subject characteristics, corresponding to curves A-E, are shown in the lower right part of each diagram. From Paper **II**.

There were considerable inter-individual differences in StO_2 levels obtained (**II**). Whereas values obtained by both techniques were influenced by high ATT levels, the PTOFS technique seemed less sensitive to high melanin content at moderate ATT levels (**II**).

Detection of oxygen gas and water vapor (III-IV)

Clear pulmonary and intra-abdominal H_2O vapor signals were detectable with the GASMAS technique in full-term infants (**III**). Typical signal recordings with acceptable SNR are shown in Fig. 28. The SNR values for the lung measurements were considerably lower than those for the abdomen. Lung signals were weak and 60-second integration time was required for these measurements, while 10 seconds was enough for intra-abdominal recordings.

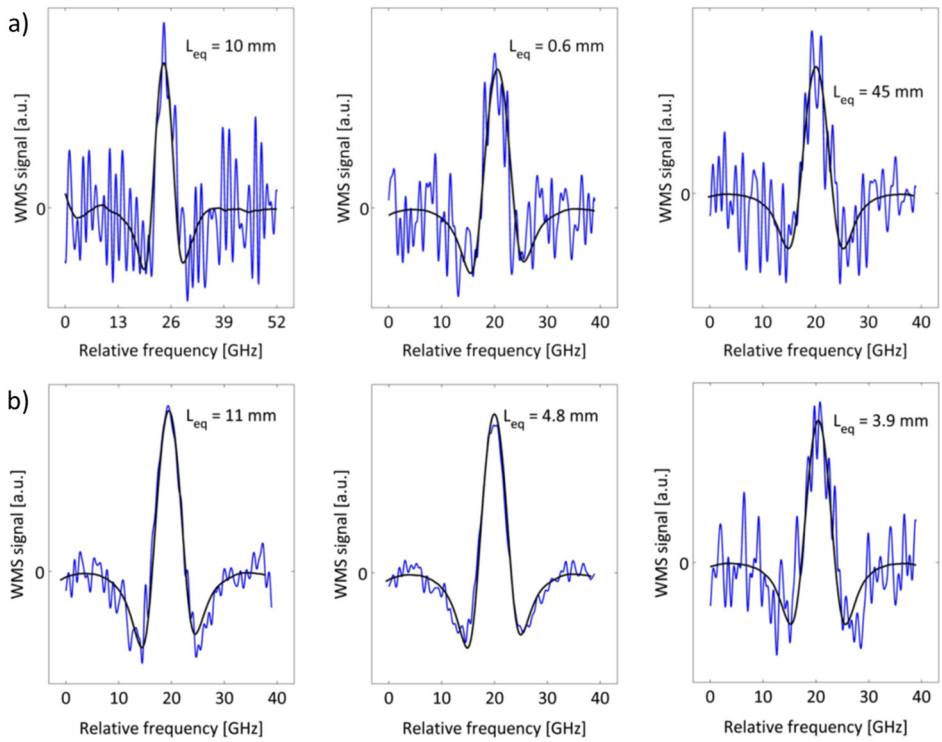

Figure 28.
Wavelength modulation spectroscopy (WMS) signals for water (H_2O) vapor in the lungs (a) and intestines (b). Curves for each subject and each location are shown (**III**).

However, no O_2 signals were detectable (**III**), mainly related to the weaker absorption strength ($\sigma(\lambda)$) for this gas, as further discussed below (p.84). Tissue thickness aspects were also very relevant, as studied by standard ultrasound techniques.

By using considerably higher laser power (30 mW) in the following study, distinct O_2 signals could be detected (**IV**). Typical lung recordings (of O_2 gas and H_2O vapor) and a recording on forearm muscle (expected to yield zero signal) are shown in Fig. 29. Oxygen signals with a reasonable SNR ≥3 were obtained at least once in each infant (and in 60 % of in total almost 400 measurements). If higher SNR thresholds were set, fewer "successful" measurements were obtained, e.g., 24 of the infants yielding a SNR ≥5. Data of similar quality was recorded at all three midclavicular positions proposed for light injection (Fig. 23), and optimal signal quality was obtained at approximately 15 mm source-to-detector distances (**IV**). No differences in signal quality or absorption magnitude were found between the right and left sides, nor any effect of gender (Fig. 30) or body weight (within the 3-4 kg range).

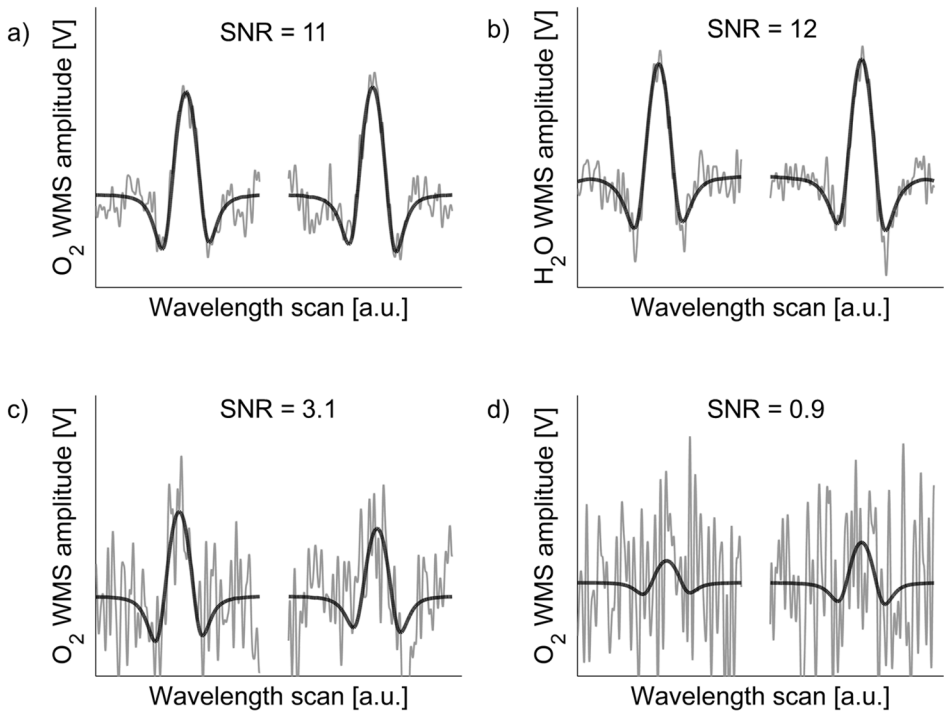

Figure 29.
Examples of wavelength modulation spectroscopy (WMS) curves with different signal-to-noise ratios (SNR). a) High quality (SNR = 11) alveolar recording of oxygen (O_2). b) Corresponding high-quality (SNR = 12) alveolar recording of water (H_2O) vapor. c) Moderate-quality (SNR = 3.1) alveolar recording of O_2. d) Adult forearm recording (SNR = 0.9) with no O_2 gas present.

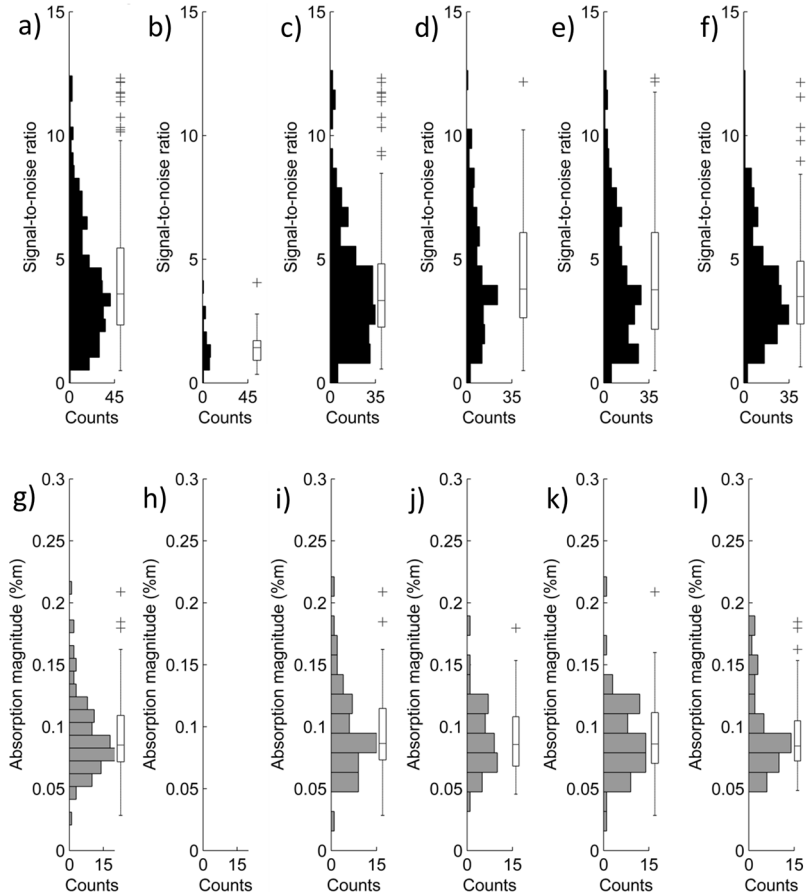

Figure 30.
Histograms showing values of signal-to-noise ratio (SNR) (a-f; black) and absorption magnitude (g-l; grey) for measurements of oxygen (O_2) gas in lungs (a, g), skeletal muscle (b, h), left lungs (c, i), right lungs (d, j), female lungs (e, k) and male lungs (f, l). Absorption magnitude values were calculated for measurements with values of SNR ≥5. Corresponding median values with 1st and 3rd quartiles, range and outliers are reported as boxplots.

Discussion

This thesis deals with different clinical aspects of O_2 and oxygenation. Actually, the oxygen is followed from its free form in the alveoli to its bound form as oxyhemoglobin in the capillaries.

The reason why completely different kinds of subjects were chosen for studies of free and bound O_2 is that probing the light has limited penetration (few centimeters), making deeper air-containing structures in adults inaccessible with the present equipment. However, since non-invasive measurement of free gas is particularly relevant in the smallest subjects - preterm infants – gas monitoring in infants is a most relevant field with future potential impact on intensive care medicine.

The major findings in the present thesis will now be discussed.

Tissue oxygenation, perfusion and blood volume (**I-II**)

We have noted that all three study techniques investigated (**I**) are influenced by tissue absorption as well as tissue scattering. Light scattering and frequency shifts are basic concepts of LDI (pp. 57-58), whereas values obtained by TVI or NIRS are influenced by absorption but also scattering. Scattering considerably influences oxygenation measurements, which are based on deeper tissue probing requiring longer path lengths (**I-II**). Determination of StO_2 by PTOFS, is based on absorption only, enabled by the use of time-resolved photon detection, and provides more realistic and accurate information on StO_2 (**II**).

There is no independent gold standard clinically available for determinations of StO_2 in deeper regions (e.g., brain or skeletal muscle tissue), since NIRS is the only feasible way of direct determination [45, 137, 143]. Available alternatives (pp. 27-28) are all based on indirect estimations.

The PTOFS technique, based on time-resolved detection of photons from ultra-short and spectrally broad-banded pulses of light, enables spectral information to be obtained at specific wavelengths by using a tunable filter. For optimal comparison between this technique and conventional CW-NIRS, oxygenation data was obtained at the same two wavelengths (730 and 810 nm) with both study techniques. Clearly, use of more wavelengths would have reduced influence on the PTOFS results by other tissue components than HbO_2 or Hb^-, such as H_2O, lipids or melanin.

However, considering that measurements at each wavelength took approximately 15 seconds, it would have been too time-consuming to cover the entire spectrum accordingly. Since the CW-NIRS system enabled measurements at six-second intervals, and since the duration of each study event by necessity was brief, PTOFS measurements were limited to two wavelengths. Here frequency-domain NIRS, based on use of multiple lasers or LEDs [149], could have an advantage in reduced acquisition time as compared to PTOFS, and otherwise being basically equivalent.

Normalization of results obtained with either study technique in each subject to median baseline values (**I**) was done to reduce inter-individual variation and facilitate comparison of individual responses to the study events. Data obtained with time-resolved and continuous-wave techniques (**II**) was not normalized accordingly, since here a comparison on how well each technique can provide reliable values, despite inter-individual differences, was evaluated. Significantly lower IQR of results obtained by PTOFS compared with CW-NIRS (**II**) indicate that data accuracy is considerably improved by determination of StO_2 from tissue absorption only (**II**).

Time-resolved measurements are considered to provide more correct values on StO_2, since determination is based on absorption only. Our time-resolved baseline values of StO_2 at around 55-60 % should be more realistic than the ones obtained by CW-NIRS (at just above 80 %), since nearly 80 % of the total microvascular blood volume is located in veins and venules [8]. Our time-resolved values of StO_2 are also in accordance with findings by other groups [144, 187].

Different non-invasive optical techniques were compared (**I-II**), to evaluate their ability of detecting defined regional physiological perturbations resembling clinical confounders or major clinical deterioration. Laser Doppler imaging and TVI provide superficial information on dermal tissue perfusion and blood volume, respectively, whereas NIRS probes considerably deeper regions, including skeletal muscle tissue.

Our studies complement recent other work on NIRS responses to various perturbations, including venous occlusion [188-190], arterial occlusion and consecutive RH [191], as well as issues of repeatability [192] and reproducibility [193].

*Influence of repositioning (**I**)*

In contrast to CW-NIRS measurements on StO_2 (**I-II**), values obtained by LDI or TVI were consistently more influenced by potentially confounding regional perturbations – like repositioning of a limb (**I**) – not reflecting clinical deterioration. This relative advantage of NIRS should be born in mind in clinical settings, where few false bedside alarms improve the quality of care. Prolonged elevation of the lower limb (typically 25 min) has been reported to decrease local StO_2 [194]. Very recently, lower limb elevation, both in volunteers with a simulated leg injury (using a pressure cuff of 50 mmHg) and in an uncompromised control group, was shown to gradually decrease regional StO_2 with increasing elevation angle [195].

Influence of temperature (I)

Hypothermia is common in emergency, perioperative and intensive care medicine. Local and superficial cold-induced vasodilation [196], confirmed by increased dermal capillary blood flow and blood volume (**I**), resulted from rapid and marked external regional cooling (**I**). Parallel changes in local perfusion and blood volume in response to external cooling (**I**) imply that the local blood flow velocity did not change. That values of StO_2 obtained by NIRS (probing deeper regions) did not reflect transient external local cooling (**I**) seems to be a relative advantage of this technique for clinical bedside use. In contrast, regional hypothermia in response to severe shock, due to e.g., major bleeding (mainly resulting from precapillary arteriolar constriction promoting capillary absorption of interstitial fluid and vital organ perfusion), is associated with higher vascular resistance and lower regional blood flow – detectable by NIRS as a reduction of StO_2 [125]. It should also be considered in clinical applications that values obtained by all study techniques evaluated, particularly LDI, reflected vasodilation and hyperperfusion associated with regional hyperthermia induced by rapid external warming (**I**). These observations are in accordance with recent findings [197] in volunteers subjected to external heating.

Influence of leg lift (II)

Elevation of both legs was part of the study design (**II**) to resemble initial bedside management in severe hypotension. No resulting change in StO_2 was detected by either technique in our healthy subjects, in accordance with their originally uncompromised medical conditions.

Influence of venous occlusion (II)

How impaired tissue perfusion, with pooling of deoxygenated venous blood, affects StO_2 was tested with the regional venous occlusion event, intended to resemble moderate fluid overloading. As expected, StO_2 levels decreased significantly, as detected by both study techniques (**II**).

Influence of gradual venous-through-arterial occlusion (I-II)

All study techniques evaluated responded strongly (in the order of 50 %) to gradual venous-through-arterial occlusion (**I**), experimentally designed to resemble hemodynamic changes associated with progressive compartment syndrome including tissue edema and reduced nutritional blood flow. Similarly, reduced values of StO_2 were obtained by CW-NIRS and PTOFS in response to gradual veno-arterial occlusion (**II**), as earlier observed (**I**).

We also confirmed over-shoots in StO_2 on rapid release of the pressure cuff – reflecting RH (**I-II**) [24], induced by rapid inflow of blood through dilated precapillary arterioles and opening of closed capillary beds [135] (p. 26). Reactive hyperemia can be considered as a test of microcirculatory reactivity [198], evaluating how well a tissue is able to adjust the extraction of O_2 after a hypoxic stimulus. This ability has been shown to be reduced in septic patients [135, 199].

Tissue oxygenation levels obtained by CW-NIRS responded well to gradual vascular occlusion (**I**), also when compared with values obtained by PTOFS (**II**). For those comparisons (Fig. 22), physiological regional perturbations resembling major hemodynamic changes potentially associated with medically deteriorated conditions (**II**) replaced previously evaluated minor physiological events normally not associated with clinical deterioration (**I**).

That values of systolic and diastolic arterial blood pressure (measured invasively distally to the inflatable cuff) gradually approached each other during venous-through-arterial occlusion (**I**), as shown in Fig. 25, reflects gradually reduced regional perfusion pressure levels. Early increase in regional diastolic blood pressure is considered to mainly reflect increased transcapillary hydrostatic and interstitial tissue pressure levels induced by venous congestion. The observed slight delay in return of DAP to baseline levels, after release of the occlusion pressure, most likely results from the increased interstitial pressure levels. To our knowledge, these changes have not previously been reported in humans.

Influence of arterial occlusion (II)

Instant arterial occlusion, rapidly blocking inflow of arterial blood, was included in the study design to resemble arterial thromboembolism, compression, injury, or extensive vasocontriction (**II**). Levels of StO_2, determined by both techniques, rapidly approached levels similar to those determined at 150 mmHg occlusion pressure during the venous-through-arterial occlusion, with approximately half of the decrease occurring after half of the five-minute occlusion period.

Influence of skin melanin content and adipose tissue thickness (I-II)

An interesting aspect of non-invasive optical techniques for physiological probing is the influence of skin pigmentation on the measurements. Our observation that higher values of blood volume were obtained by TVI in the only subject with enhanced skin melanin content (**I**) is quite understandable, considering that visible wavelengths of light were used for tissue probing. The algorithm for assessing blood volume with TVI is based on the fact that blood absorbs more green than red light, whereas surrounding tissue has similar absorption characteristics in the green and red spectral regions (Fig. 14). However, since melanin also absorbs more green than red light [94], as shown in Fig. 12, the blood volume appears to be higher in subjects with darker skin or pronounced sun tan. This should be taken into future consideration. That LDI, in contrast, was insensitive to skin pigmentation is reasonable, since measurements are done at a single wavelength without involving spectroscopic aspects. The NIRS technique is also largely insensitive to melanin content (**I-II**), related to the fact, that the wavelengths used are much longer than for TVI, and thus in a region where melanin absorption is considerably lower [143] (Fig. 12).

Efforts were made to understand the influence of cutaneous melanin content and subcutaneous ATT on CW-NIRS and PTOFS measurements (**II**). Since values of StO_2 obtained by PTOFS consistently had smaller IQR levels compared with CW-

NIRS, it is obvious that PTOFS is less sensitive. The discussion below is based mainly on results obtained in individual subjects differing in cutaneous melanin content and subcutaneous ATT (Fig. 27), since there were too few subjects for statistical analysis.

Melanin, located in the epidermis, has a high absorption of light at shorter wavelengths (e.g., 400 nm), with gradually reduced absorption at longer wavelengths [94], as shown in Fig. 12. Recently, the melanin skin volume fraction has been estimated (by multiphoton microscopy and frequency domain spectroscopy), to be approximately 5 % in non-sun-exposed skin type I and approximately 20 % in sun-exposed skin type VI [200]. Evaluation problems may arise in CW-NIRS measurements in subjects with extremely high cutaneous levels of melanin content, due to signal loss during vascular occlusion [201]. Individually obtained values of StO_2 (Fig. 27) indicate that cutaneous melanin content influenced the CW-NIRS signals associated with various physiological perturbations at higher levels of ATT. This does not seem to apply for PTOFS (**II**). This makes sense, since the time-resolved technique extracts the values from the shape of the dispersion curve of transmitted light, rather than from the light intensity, as is the case for the continuous-wave technique. Even dramatic reductions of detected light intensity levels, due to strong absorption by melanin, would not significantly alter the path of the remaining, unabsorbed light and consequently not the time dispersion of the detected light (**II**).

It is well known that subcutaneous ATT can influence CW-NIRS measurements [129, 185]. Since the effective light penetration into tissue, within the tissue optical window, is estimated to one third to half the distance between emitted and detected light [128], high levels of ATT mean that the detected light reflects probing of mostly subcutaneous fat, rather than muscle tissue. According to individual values of StO_2 (Fig. 27), we note that both study techniques seem to be sensitive to increasing ATT, with smaller response to physiological perturbations noted (**II**). Subcutaneous adipose tissue, having a lower baseline metabolism than skeletal muscle tissue [202], represents more of the tissue volume probed at higher ATT [185]. Accordingly, the mean optical path length that light has traveled through muscle tissue decreases, resulting in an underestimation of muscle StO_2 [203]. Monte Carlo simulations (computer modeling of the movements of individual photons) suggest that very little light passes through skeletal muscle tissue at ATT levels above 15 mm [204]. Recently, a correction curve was proposed for time-resolved measurements on muscle tissue, suitable for ATT between 2 and 6 mm [203].

*Influence of myoglobin (**I-II**)*

One aspect, that also needs to be addressed, is that NIRS signals can be influenced by myoglobin (Mb), since Mb and Hb have similar spectral absorption characteristics [202]. However, within a given volume of muscle tissue, the concentration of Hb is about 1.5 times higher than that of Mb. Hemoglobin has four bindings sites for O_2 (Fig. 2) compared with one binding site in Mb [205, 206]. Many researchers suggest that Mb contributes to less than 20 % of measured StO_2 in muscle tissue [129, 205-

207]. However, recent research indicates that Mb might contribute to ~50-70 % of NIRS signals [208]. This is of course a serious statement, which should be investigated further.

Detection of oxygen gas and water vapor (III-IV)

Our studies showed that H_2O vapor (**III**) as well as O_2 gas (**IV**) could be detected in full-term healthy infants.

The main reason why H_2O vapor signals were considerably stronger with correspondingly better SNR, is the considerably higher absorption strength ($\sigma(\lambda)$) of H_2O vapor, resulting in a more prominent absorption imprint (larger $\Delta I/I_0$) in the detected light. Furthermore, the actual thickness of overlaying tissue is important, and possibilities of shallower tissue depths were higher for the abdominal measurements.

The locations chosen for alveolar O_2 monitoring were light injection in the midclavicular line and detection in the armpit on the same side (**IV**). Those locations are not necessarily the most desirable ones for future determination of O_2 gas content and distribution in preterm or full-term infants. However, since H_2O vapor signals were initially detectable here (**III**), indicating light propagation through air-filled cavities, the same geometry was chosen for detection of O_2 gas (**IV**). A main reason for successful detection was the use of much higher O_2 probing light levels, to increase the SNR (**IV**).

The observation, that while detection of O_2 gas was possible at least once in each infant (**IV**), but sometimes not, implies that non-optimal sites were sometimes used for emission and/or detection of light.

As could be expected, no significant differences were found between body sides, or between infants of opposite genders. All these findings were also valid for the measured absorption magnitudes (%m). Several of these aspects are shown in Fig. 30. More surprisingly, there was no significant difference in signal quality between infants differing in body weight within an approximate range of 3.0-4.0 kg.

Detection of O_2 gas is of course encouraging, but clearly determination of O_2 concentrations would be the desired goal. Concentration values might be obtained based on normalization to H_2O vapor (Eq. 18, p. 68). However, this would require identical path lengths probed for the two wavelengths, which is unfortunately not the case, especially not for the "reflection" geometry available, (p. 48).

One reason for this problem is that light is absorbed considerably more by liquid H_2O at 937 nm (used to detect H_2O vapor) than at 760 nm (used to detect O_2 gas). This will result in fewer photons with longer path lengths at 937 nm. If a "transmission" type of arrangement is used, the detected photons must have passed the gas-containing cavities, and these problems are not very severe, as noted in frontal

and maxillary sinus measurements in humans [175]. However, the "reflection mode" had to be used (**III-IV**), because of the size of the full-term infants, leading to the H_2O vapor light missing some of the gas.

One solution to this problem is to identify and use H_2O vapor absorption lines closer to the ones of O_2. Such lines, although weaker, can be found at about 820 nm (Fig. 12).

Moreover, the favorable "transmission" geometry could also be found for pulmonary measurements in very preterm infants or, if the irradiation is done from inside the upper airways, also in larger children, and even adults (pp. 89-91). This might ultimately lead to less use of radiography in certain areas of intensive care medicine.

Conclusions

Optical techniques, being non-invasive and providing data in real-time, are attractive as potential tools for surveillance of critical illness, in particular concerning oxygenation.

Based on results obtained in the present thesis, the main conclusions are:

1. The CW-NIRS, LDI, and TVI techniques can non-invasively provide complementary information on regional hemodynamic changes in dermal and skeletal muscle tissue in humans, since CW-NIRS mainly responded to venous-through-arterial occlusion (**I-II**), reactive hyperemia (**I-II**), and heating (**I**), whereas LDI and TVI rather reflected repositioning, cooling, and heating, in addition to veno-arterial occlusion (**I**).
2. The CW-NIRS technique better than LDI or TVI reflects major regional hemodynamic changes, since it responded prominently to venous-through-arterial occlusion and RH (**I-II**).
3. The CW-NIRS technique is less sensitive to bedside confounders compared to LDI and TVI, since it responded far less to local repositioning or cooling (**I**).
4. The CW-NIRS and PTOFS techniques both respond to major hemodynamic changes, since values of tissue oxygenation obtained by either technique similarly reflected various extents of local venous or arterial occlusion (**II**).
5. More accurate and realistic absolute values of tissue oxygenation are obtained by the PTOFS technique than by CW-NIRS, as judged from lower inter-individual variation and better agreement of tissue oxygenation levels with previous reports (**II**).
6. High dermal adipose tissue thickness strongly attenuates muscle tissue responses obtained by CW-NIRS as well as PTOFS, as shown by lower tissue oxygenation signal response to physiological provocations at increasing subcutaneous adipose tissue thickness levels (**II**).
7. The CW-NIRS and LDI techniques are less sensitive than TVI to skin contents of melanin, since results based on those techniques were less influenced than results obtained by TVI in subjects with darker skin color (**I**).

8. At increasing adipose thickness levels PTOFS seemed to be less sensitive to melanin content than CW-NIRS (**II**).
9. The novel GASMAS technique is able to monitor physiological gases *in situ*, since we were, for the first time, able to record useful signals on water vapor non-invasively from lungs as well as intestines in three full-term infants (**III**).
10. Oxygen can be non-invasively monitored *in situ* in the human body, since, for the first time, signals were obtained in each individual in a group of newborn infants (**IV**). This opens up a new field of non-invasive medical measurements of oxygen *in situ*.
11. Oxygen concentration determinations in the alveoli require a knowledge of the optical path length, which might be determined from the water vapor signal, where the corresponding concentration is known. However, this could not be achieved with the present setup, but indications for a solution are given (**IV**).

Future perspectives

Future work along the main directions of this thesis work would primarily focus on development and clinical testing of improved, more user-friendly and reliable equipment for monitoring in severe illness.

Monitoring of tissue oxygenation

Regarding the broad-band NIRS method, more widespread use of time-resolved techniques, PTOFS and frequency-domain NIRS, for monitoring of severely ill or injured patients should be encouraged. With the rapid development of more compact and cheaper laser sources, as well as electronics and computers, this is a quite realistic scenario. In particular, incorporating more laser wavelengths might prevent confounding tissue components from interfering with oxygenation measurements.

Future clinical scientific work should preferably be directed to bedside measurements in critically ill or injured patients with true and severe pathophysiological problems. Clearly, technical performance must always be balanced to price and ease of operation in the clinical setting.

Monitoring of free oxygen gas *in situ*

An important long-term goal of all our efforts on gas monitoring is to be able, ultimately, to reduce potentially detrimental radiological investigations by using harmless optical measurements in connection with the severe diseases of early infancy - respiratory distress syndrome (RDS) and necrotizing enterocolitis (NEC). The demonstrated capability to detect lung gases gives the hope that this could materialize in the future.

Regarding preterm and full-term infants, stronger pulmonary signals, enabled by more powerful continuous-wave lasers, are desirable. Furthermore, use of a monitoring wavelength of H_2O vapor closer (say, at 820 nm) to that of O_2 would enable more robust determination of the O_2 gas concentration based on assumed equal path lengths (Eq. 18, p. 68) of O_2 and H_2O vapor *in situ*. In addition, applying laser illumination from inside the lungs, as recently proposed (Figs 31 and 32) [209],

might result in much higher recorded levels of light, and also stronger recorded gas signals, since almost all detected photons are forced to pass air-containing tissue. This also again favors the validity of the H_2O vapor assumption (Eq. 18). Although internal irradiation would mean that the advantage of non-invasiveness is lost, it should be borne in mind that most premature infants who might benefit from this kind of surveillance do have an endotracheal tube, which could be combined with light delivery [209] to envision true 24-hour cot-side monitoring.

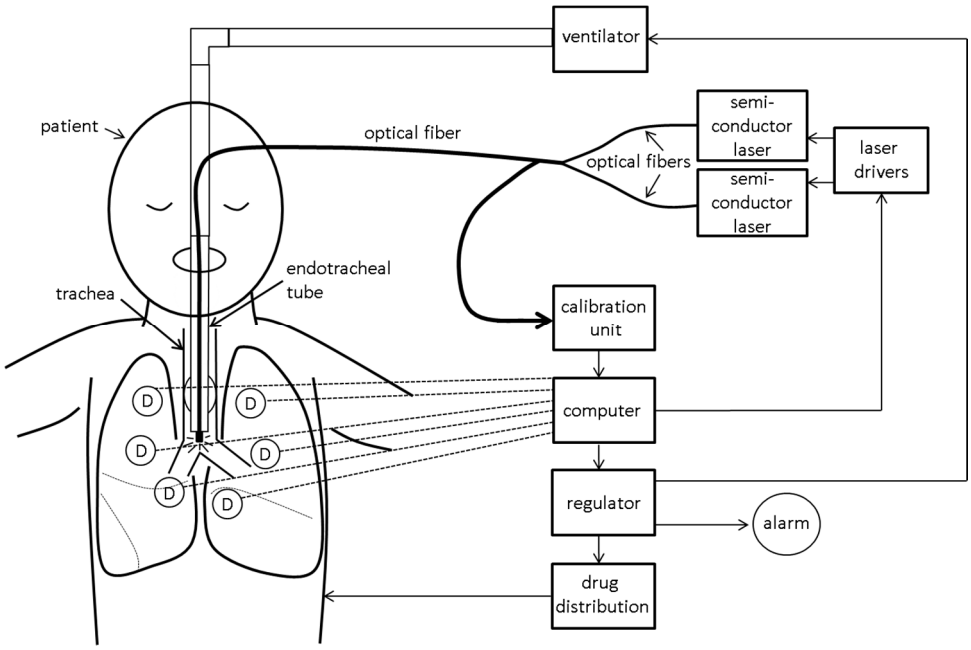

Figure 31.
Schematic diagram showing possible implementation of internal laser illumination for medical gas analysis. The patient is connected to the ventilator by the endotracheal tube. Semi-conductor lasers for detection of oxygen (O_2) (at 760 nm) and water (H_2O) vapor (at 820 nm), interconnected to laser drivers, are controlled by a computer. Emitted laser light is merged and sent in through the endotracheal tube to illuminate the lung from the inside. Detectors (D) in defined positions on the outside of the thoracic cavity are used to record the diffusely spread light, carrying information on gas concentration and distribution. Based on measured values, the computer might also be used to adjust a regulator for interactive control of ventilator settings and administration of drugs. Activation of an alarm system may alert hospital staff of alveolar O_2 levels outside defined threshold limits. Modified from [209].

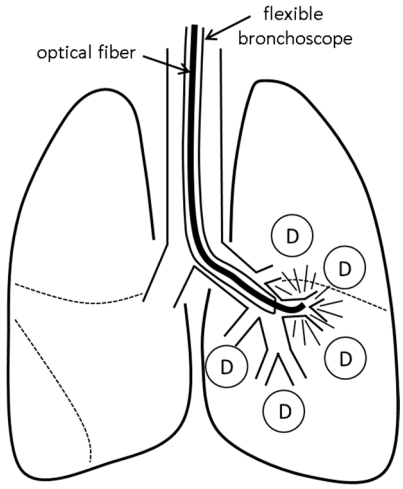

Figure 32.
Schematic diagram showing a possible implemantation of laser light coupling for studies of lung function through the working channel of a flexible bronchoscope. The diffusely spread light is detected at the skin surface by single or multiple detectors (D). Modified from [209].

Actually, efforts on the European level are now being initiated to develop a clinically useful system in a new collaboration between our group and industrial companies, as funded within the EU EUROSTARS program. In particular, higher power semi-conductor lasers at the relevant wavelengths (presently not available) are being developed by industry, and realistic practical equipment will be constructed.

Such efforts might also make it possible to find valuable additional applications of medical GASMAS. These might include adult lungs, intestines, necrotic tumor differentiation and various indications of decay, such as caput necrosis. Regarding adult-lung monitoring, which might become realistic with internal light administration (Figs 31 and 32), intensive care situations, such as adult respiratory distress syndrome and severe pneumonia come to mind. Again, severely ill intensive care patients are mostly tracheally intubated.

An additional future aspect, which would require high-quality signals/short measuring times, could be studies of dynamics, e.g., the response on a short-time scale to an abrupt change in F_iO_2, or even to follow the oxygenation during the breathing cycle.

In view of the positive ongoing developments there could be real hopes for the early work, described in this thesis, to bear rich fruits in intensive care, for infants as well as adults.

Acknowledgements

It is a true honor to thank all those, who through their support have made this dissertation possible. I would like to express my great appreciation to all of you, with special gratitude to:

Jonas Åkeson, my main supervisor, for the opportunity to pursue this work under enthusiastic leadership, and for sharing your deep knowledge in anesthesiology and intensive care medicine. Thank you for always believing in me and for constant encouragement! I much enjoyed the journey!

Stefan Andersson-Engels, my co-supervisor, for the wonderful possibility of interdisiplinary research, for sharing the many mysteries of biophotonics, and making difficult things seem easy.

Vineta Fellman, my co-supervisor, for guiding me through the field of neonatology, with your great experience and insight.

Patrik Lundin, for a most pleasant collaboration and friendship throughout the projects with measurements on the small ones. Your deep skills in advanced laser spectroscopy were a prerequisite for capturing the faint and elusive signals!

Alfi Shaharin, for your tireless work side-by-side with me capturing the time-resolved signals and processing the data into useful quantities. I much appreciate our friendship!

My additional co-authors, Arman Ahamed Subash, Lorenzo Cocola, Ida Ellerström, John Jahr, Dmitry Khoptyar, Marcus Larsson, Märta Lewander Xu, Gabriel Somesfalean, Katarina Svanberg, Sune Svanberg and Per Wollmer, for enjoyable and much appreciated collaboration.

Gert Nilsson, a pioneer in optical tissue monitoring, for important contributions at the onset of the project.

Rebecca Rylance, for excellent help on statistics and for a most precious friendship. You are so important to me!

Johan Lundberg and Bengt Roth, for providing work opportunities in the amazing field of anesthesiology and intensive care medicine, in Malmö and Lund.

Carolina Samuelsson, head of the Anesthesiology and Intensive Care clinic at SUS, Lund/Malmö, for much valued support in my work and research.

All my anesthesiologist colleagues at Skåne University Hospital, Lund/Malmö, for the wonderful working environment, for all rewarding interactions and the joy in the many times stressful work. Special thanks to Malin Rundgren, my clinical supervisor, for always encouraging me and keeping my mind sharp.

All co-workers at the Atomic Physics Division, for keeping me on a high level of technical understanding. Special thanks to Claes-Göran Wahlström for hosting me in the multidisciplinary environment. I much appreciate Åke Johansson for excellent and much needed computer assistance, as well as for interesting conversations, and Anne Petersson-Jungbeck and Jakob Testad for much contributing to a nice environment.

Haiyan Xie, for valuable help with some of the figures, and Petra Palm for help with manuscript lay-out.

Ann-Cathrine Berg for valuable assistance, and the staff at the postnatal ward for facilitating logistics, during the GASMAS measurements.

The staff at "Röda Stugan" - thank you for always being devoted and flexible in the day care of our children - in practice making projects like this possible.

All my dear friends (among them Lisa Bogentoft, Marie Båge, Malin Dahlsjö, Anna Forsman, Ebba von Geijer, Stina Gäre, my sister-in-law Malin Krite and Suzanne Wallberg) for all the fun times, all the wonderful travels and for always being there for me, in good as well as bad times!

Margareta Krite, my mother-in-law, for helping out whenever needed with William, Valdemar and Ragnhild, and for your appreciation and care.

Kristina Svanberg, my sister and bosom friend, for always being there and for all your love and help. The sky is the limit!

My highly loved parents, Katarina and Sune, for always supporting me throughout every step of my life, for believing in me and for encouraging me to always preform at my best. Thank you also for all the support with William, Valdemar and Ragnhild.

William, Valdemar and little Ragnhild, my three totally amazing children. Thank you for your endless love, your wonderful views on how life works, and for keeping everything in perspective.

Finally, Martin, my husband and solid rock, for always loving me, for taking me on adventures all around the world, for making every minute memorable and for all the fun times! You are the love of my life, forever.

Thank You All!

Grants

Region Skåne research funds for PhD students, and further funds to the Faculty of Medicine, Lund University.

The Swedish Research Council for support through direct grants, and a Linnaeus grant to the Lund Laser Centre, Lund University.

The BIOPTICHAL project under LASERLAB Europe with support to the Lund Laser Centre.

References

1. Scheele, C.W., *Chemische Abhandlung von der Luft und dem Feuer*, Uppsala, 1777.
2. Sternbach, G.L. and Varon, J., *The discovery and rediscovery of oxygen.* The Journal of Emergency Medicine, 2005. **28**: 221-224.
3. Severinghaus, J.W., *Priestley, the furious free thinker of the enlightenment, and Scheele, the taciturn apothecary of Uppsala.* Acta Anaesthesiologica Scandinavica, 2002. **46**: 2-9.
4. Gnaiger, E., Steinlechner-Maran, R., Méndez, G., Eberl, T., and Margreiter, R., *Control of mitochondrial and cellular respiration by oxygen.* Journal of Bioenergetics and Biomembranes, 1995. **27**: 583-596.
5. Nathan, A. and Singer, M., *The oxygen trail: tissue oxygenation.* British Medical Bulletin, 1999. **55**: 96-108.
6. West, J.B., *Marcello Malpighi and the discovery of the pulmonary capillaries and alveoli.* American Journal of Physiology - Lung Cellular and Molecular Physiology, 2013. **304**: L383-L390.
7. Androutsos, G., Karamanou, M., and Stefanadis, C., *William Harvey (1578-1657): Discoverer of blood circulation.* Hellenic Journal of Cardiology, 2012. **53**: 6-9.
8. Granger, H.J. and Shepherd, A.P., *Intrinsic microvascular control of tissue oxygen delivery.* Microvascular Research, 1973. **5**: 49-72.
9. Levick, J.R. and Michel, C.C., *Microvascular fluid exchange and the revised Starling principle.* Cardiovascular Research, 2010. **87**: 198-210.
10. Guyton, A. and Hall, J., *Textbook of Medical Physiology*. 10th ed., 2000, Philadelphia, Elsevier: p. 144-261.
11. Kam, P. and Power, I., *Principles of Physiology for the Anaesthetist*. 3rd ed., 2015, Boca Raton, CRC Press: p. 75-112.
12. Fahlke, C., Linke, W., Rassler, B., and Wiesner, R., *Fysiologisk Bildordbok.* 2012, Stockholm, Liber: p. 176-189.
13. Hsia, C.C.W., *Respiratory function of hemoglobin.* New England Journal of Medicine, 1998. **338**: 239-248.
14. Pittman, R.N., *Regulation of tissue oxygenation*. In: *Colloquium Series on Integrated Systems Physiology: From Molecule to Function*. 2011, Morgan & Claypool Life Sciences: p. 1-81.
15. Bohr, C., Hasselbalch, K., and Krogh, A., Ü*ber einen in biologischer Beziehung wichtigen Einfluss, den die Kohlensäurespannung des Blutes auf dessen Sauerstoffbindung übt.* Skandinavisches Archiv für Physiologie, 1904. **16**: 402-4012.
16. Murphy, P.J., *The fetal circulation.* Continuing Education in Anaesthesia, Critical Care & Pain, 2005. **5**: 107-112.
17. Christiansen, J., Douglas, C., and Haldane, J., *The absorption and dissociation of carbon dioxide by human blood.* Journal of Physiology, 1914. **48**: 244-271.

18. Koeppen, B.M., and Stanton, B.A., *Berne & Levy Principles of Physiology.* 6th ed., 2006, St. Louis, Elsevier Mosby.
19. McPherson, R.A. and Pincus, M.R., *Henry's clinical diagnosis and management by laboratory methods.* 2011, Philadelphia, Elsevier Saunders.
20. Bassett, D. and Howley, E.T., *Limiting factors for maximum oxygen uptake and determinants of endurance performance.* Medicine and Science in Sports and Exercise, 2000. **32**: 70-84.
21. Dempsey, J., Hanson, P., and Henderson, K., *Exercise-induced arterial hypoxaemia in healthy human subjects at sea level.* Journal of Physiology, 1984. **355**: 161-175.
22. Segal, S.S., *Regulation of blood flow in the microcirculation.* Microcirculation, 2005. **12**: 33-45.
23. Bagher, P. and Segal, S.S., *Regulation of blood flow in the microcirculation: role of conducted vasodilation.* Acta Physiologica, 2011. **202**: 271-284.
24. Sparks Jr, H.V. and Belloni, F.L., *The peripheral circulation: local regulation.* Annual Review of Physiology, 1978. **40**: 67-92.
25. Tagawa, T., Imaizumi, T., Endo, T., Shiramoto, M., Harasawa, Y., and Takeshita, A., *Role of nitric oxide in reactive hyperemia in human forearm vessels.* Circulation, 1994. **90**: 2285-2290.
26. The National Heart, Lung, and Blood Institute Acute Respiratory Distress Syndrome (ARDS) Clinical Trials Network, *Pulmonary-artery versus central venous catheter to guide treatment of acute lung injury.* New England Journal of Medicine, 2006. **354**: 2213-2224.
27. Osthaus, W.A., Huber, D., Beck, C., Roehler, A., Marx, G., Hecker, H., et al., *Correlation of oxygen delivery with central venous oxygen saturation, mean arterial pressure and heart rate in piglets.* Pediatric Anesthesia, 2006. **16**: 944-947.
28. Peters, S.G., Afessa, B., Decker, P.A., Schroeder, D.R., Offord, K.P., and Scott, J.P., *Increased risk associated with pulmonary artery catheterization in the medical intensive care unit.* Journal of Critical Care, 2003. **18**: 166-171.
29. Profant, M., Vyska, K., and Eckhardt, U., *The Stewart-Hamilton equations and the indicator dilution method.* SIAM Journal on Applied Mathematics, 1978. **34**: 666-675.
30. Sakka, S.G., Rühl, C.C., Pfeiffer, U.J., Beale, R., McLuckie, A., Reinhart, K., et al., *Assessment of cardiac preload and extravascular lung water by single transpulmonary thermodilution.* Intensive Care Medicine, 2000. **26**: 180-187.
31. Lopes, M.R., Oliveira, M.A., Pereira, V.O., Lemos, I.P., Auler, J.O., and Michard, F., *Goal-directed fluid management based on pulse pressure variation monitoring during high-risk surgery: a pilot randomized controlled trial.* Critical Care, 2007. **11**: R100.
32. Cannesson, M., Aboy, M., Hofer, C.K., and Rehman, M., *Pulse pressure variation: where are we today?* Journal of Clinical Monitoring and Computing, 2011. **25**: 45-56.
33. Reinhart, K., Kuhn, H.-J., Hartog, C., and Bredle, D., *Continuous central venous and pulmonary artery oxygen saturation monitoring in the critically ill.* Intensive Care Medicine, 2004. **30**: 1572-1578.
34. Goldman, R.H., Klughaupt, M., Metcalf, T., Spivack, A.P., and Harrison, D.C., *Measurement of central venous oxygen saturation in patients with myocardial infarction.* Circulation, 1968. **38**: 941-946.

35. Hoffman, G.M., Ghanayem, N.S., and Tweddell, J.S., *Noninvasive assessment of cardiac output.* Seminars in Thoracic and Cardiovascular Surgery: Pediatric Cardiac Surgery Annual, 2005. **8**: 12-21.
36. Ferrannini, E., *The theoretical bases of indirect calorimetry: a review.* Metabolism, 1988. **37**: 287-301.
37. Heard, S.O., *Gastric tonometry: the hemodynamic monitor of choice (pro).* Chest, 2003. **123**: 469S-474S.
38. Zhang, X., Xuan, W., Yin, P., Wang, L., Wu, X., and Wu, Q., *Gastric tonometry guided therapy in critical care patients: a systematic review and meta-analysis.* Critical Care, 2015. **19**: 22.
39. Singer, M., *Esophageal Doppler monitoring. In: Fuctional Hemodynamic Monitoring*. Pinsky M.R. and Payen D, (Eds) 2005, Berlin Heidelberg, Springer: p. 193-204.
40. Mythen, M. and Webb, A., *Perioperative plasma volume expansion reduces the incidence of gut mucosal hypoperfusion during cardiac surgery.* Archives of Surgery, 1995. **130**: 423-429.
41. Gan, T.J., Soppitt, A., Maroof, M., El-Moalem, H., Robertson, K.M., Moretti, E., et al., *Goal-directed intraoperative fluid administration reduces length of hospital stay after major surgery.* Anesthesiology, 2002. **97**: 820-826.
42. Conway, D.H., Mayall, R., Abdul-Latif, M.S., Gilligan, S., and Tackaberry, C., *Randomised controlled trial investigating the influence of intravenous fluid titration using oesophageal Doppler monitoring during bowel surgery.* Anaesthesia, 2002. **57**: 845-849.
43. Smith, I., Kumar, P., Molloy, S., Rhodes, A., Newman, P., Grounds, R., et al., *Base excess and lactate as prognostic indicators for patients admitted to intensive care.* Intensive Care Medicine, 2001. **27**: 74-83.
44. Spronk, P.E., Zandstra, D.F., and Ince, C., *Bench-to-bedside review: sepsis is a disease of the microcirculation.* Critical Care, 2004. **8**: 462.
45. Scheeren, T.W.L., Schober, P., and Schwarte, L.A., *Monitoring tissue oxygenation by near infrared spectroscopy (NIRS): background and current applications.* Journal of Clinical Monitoring and Computing, 2012. **26**: 279-287.
46. Goldman, D., Bateman, R.M., and Ellis, C.G., *Effect of decreased O_2 supply on skeletal muscle oxygenation and O_2 consumption during sepsis: role of heterogeneous capillary spacing and blood flow.* American Journal of Physiology - Heart and Circulatory Physiology, 2006. **290**: H2277-H2285.
47. Hampson, N.B., Piantadosi, C.A., Thom, S.R., and Weaver, L.K., *Practice recommendations in the diagnosis, management, and prevention of carbon monoxide poisoning.* American Journal of Respiratory and Critical Care Medicine, 2012. **186**: 1095-1101.
48. Johnson, D., *Perioperative methemoglobinemia.* Canadian Journal of Anesthesia/Journal Canadien d'Anesthésie, 2005. **52**: 665-668.
49. Hamel, J., *A review of acute cyanide poisoning with a treatment update.* Critical Care Nurse, 2011. **31**: 72-82.
50. Way, J.L., *Cyanide intoxication and its mechanism of antagonism.* Annual Review of Pharmacology and Toxicology, 1984. **24**: 451-481.
51. Kam, P. and Power, I., *Principles of Physiology for the Anaesthetist*. 3rd ed., 2015, Boca Raton, CRC Press: p. 113-185.
52. Bezemer, R., Karemaker, J.M., Klijn, E., Martin, D., Mitchell, K., Grocott, M., et al., *Simultaneous multi-depth assessment of tissue oxygen saturation in thenar and*

forearm using near-infrared spectroscopy during a simple cardiovascular challenge. Critical Care, 2009. **13**: S5.
53. Goldenberg, R.L., Culhane, J.F., Iams, J.D., and Romero, R., *Epidemiology and causes of preterm birth.* The Lancet, **371**: 75-84.
54. Slattery, M.M. and Morrison, J.J., *Preterm delivery.* The Lancet, 2002. **360**: 1489-1497.
55. Goldenberg, R.L. and Rouse, D.J., *Prevention of premature birth.* New England Journal of Medicine, 1998. **339**: 313-320.
56. Jobe, A. and Bancalari, E., *Bronchopulmonary dysplasia.* American Journal of Respiratory and Critical Care Medicine, 2001. **163**: 1723-1729.
57. Rees, S. and Inder, T., *Fetal and neonatal origins of altered brain development.* Early Human Development, 2005. **81**: 753-761.
58. Jobe, A.J., *The new BPD: an arrest of lung development.* Pediatric Research, 1999. **46**: 641-641.
59. Adams, F.H., Fujiwara, T., Emmanouilides, G.C., and Räihä, N., *Lung phospholipids of human fetuses and infants with and without hyaline membrane disease.* Journal of Pediatrics, 1970. **77**: 833-841.
60. Hallman, M., Merritt, T.A., Pohjavuori, M., and Gluck, L., *Effect of surfactant substitution on lung effluent phospholipids in respiratory distress syndrome: evaluation of surfactant phospholipid turnover, pool size, and the relationship to severity of respiratory failure.* Pediatric Research, 1986. **20**: 1228-1235.
61. Stoll, B.J., Hansen, N.I., Bell, E.F., Shankaran, S., Laptook, A.R., Walsh, M.C., et al., *Neonatal outcomes of extremely preterm infants from the NICHD Neonatal Research Network.* Pediatrics, 2010: 443-456.
62. Sweet, D.G., Carnielli, V., Greisen, G., Hallman, M., Ozek, E., Plavka, R., et al., *European consensus guidelines on the management of neonatal respiratory distress syndrome in preterm infants – 2010 update.* Neonatology, 2010. **97**: 402-417.
63. Rodriguez, R.J., *Management of respiratory distress syndrome: an update.* Respiratory Care, 2003. **48**: 279-287.
64. Subiramanian, S. and Sweet, D.G., *Management of neonatal respiratory distress syndrome.* Paediatrics and Child Health, 2012. **22**: 518-522.
65. Crowley, P., *Prophylactic corticosteroids for preterm birth.* The Cochrane Library, 1996. Issue 1: CD000065.
66. Speer, C.P., Sweet, D.G., and Halliday, H.L., *Surfactant therapy: past, present and future.* Early Human Development, 2013. **89**: S22-S24.
67. SUPPORT Study Group of the Eunice Kennedy Shriver NICHD Neonatal Research Network, *Early CPAP versus surfactant in extremely preterm infants.* New England Journal of Medicine, 2010. **362**: 1970-1979.
68. Verder, H., Robertson, B., Greisen, G., Ebbesen, F., Albertsen, P., Lundstrom, K., et al., *Surfactant therapy and nasal continuous positive airway pressure for newborns with respiratory distress syndrome.* New England Journal of Medicine, 1994. **331**: 1051-1055.
69. Bohlin, K., Gudmundsdottir, T., Katz-Salamon, M., Jonsson, B., and Blennow, M., *Implementation of surfactant treatment during continuous positive airway pressure.* Journal of Perinatology, 2007. **27**: 422-427.
70. Lovrenski, J., *Lung ultrasonography of pulmonary complications in preterm infants with respiratory distress syndrome.* Upsala Journal of Medical Sciences, 2012. **117**: 10-7.

71. Liu, J., *Lung ultrasonography for the diagnosis of neonatal lung disease.* The Journal of Maternal-Fetal & Neonatal Medicine 2014. **27**: 856-61.
72. Copetti, R., Cattarossi, L., Macagno, F., Violino, M., and Furlan, R., *Lung ultrasound in respiratory distress syndrome: a useful tool for early diagnosis.* Neonatology, 2008. **94**: 52-9.
73. Hall, E.J., *Lessons we have learned from our children: cancer risks from diagnostic radiology.* Pediatric Radiology, 2002. **32**: 700-706.
74. Don, S., *Radiosensitivity of children: potential for overexposure in CR and DR and magnitude of doses in ordinary radiographic examinations.* Pediatric Radiology, 2004. **34**: S234-41.
75. Neu, J. and Walker, W.A., *Necrotizing enterocolitis.* New England Journal of Medicine, 2011. **364**: 255-264.
76. Lin, P.W. and Stoll, B.J., *Necrotising enterocolitis.* The Lancet. **368**: 1271-1283.
77. Berseth, C.L., *Feeding strategies and necrotizing enterocolitis.* Current Opinion in Pediatrics, 2005. **17**: 170-173.
78. Lucas, A. and Cole, T., *Breast milk and neonatal necrotising enterocolitis.* The Lancet, 1990. **336**: 1519-1523.
79. Hsueh, W., Caplan, M.S., Qu, X.-W., Tan, X.-D., De Plaen, I.G., and Gonzalez-Crussi, F., *Neonatal necrotizing enterocolitis: clinical considerations and pathogenetic concepts.* Pediatric and Developmental Pathology, 2003. **6**: 6-23.
80. Claud, E. and Walker, W., *Hypothesis: inappropriate colonization of the premature intestine can cause neonatal necrotizing enterocolitis.* The FASEB Journal, 2001. **15**: 1398-1403.
81. Hoyos, A.B., *Reduced incidence of necrotizing enterocolitis associated with enteral administration of Lactobacillus acidophilus and Bifidobacterium infantis to neonates in an intensive care unit.* International Journal of Infectious Diseases, 1999. **3**: 197-202.
82. Smith, B., Bodé, S., Skov, T.H., Mirsepasi, H., Greisen, G., and Krogfelt, K.A., *Investigation of the early intestinal microflora in premature infants with/without necrotizing enterocolitis using two different methods.* Pediatric Research, 2012. **71**: 115-120.
83. Gephart, S.M., McGrath, J.M., Effken, J.A., and Halpern, M.D., *Necrotizing enterocolitis risk: state of the science.* Advances in Neonatal Care, 2012. **12**: 77-89.
84. Pietz, J., Achanti, B., Lilien, L., Stepka, E.C., and Mehta, S.K., *Prevention of necrotizing enterocolitis in preterm infants: a 20-year experience.* Pediatrics, 2007. **119**: e164-e170.
85. Danielsson, B. and Hwang, C.P., *Treatment of infantile colic with surface active substance (Simethicone).* Acta Paediatrica, 1985. **74**: 446-450.
86. Lucassen, P.L.B.J., Assendelft, W.J.J., Gubbels, J.W., van Eijk, J.T.M., van Geldrop, W.J., and Knuistingh Neven, A., *Effectiveness of treatments for infantile colic: systematic review.* BMJ, 1998. **316**: 1563-1568.
87. Svanberg, S., *Laser spectroscopy in medical diagnostics.* In*: Lasers for Medical Applications*. Jelínkova, H., (Ed.) 2013, Woodhead Publishing, Philadelphia: p. 286-324.
88. Skou, J.C., *The Identification of the Sodium-Potassium Pump. In: Nobel Lectures, Chemistry 1996-2000.* Ed. Grenthe, I. 2003, Word Scientific Publishing Co Singapore: p. 179-194.
89. Rolfe, P., *In vivo near-infrared spectroscopy.* Annual Review of Biomedical Engineering, 2000. **2**: 715-754.

90. Wang, L.V. and Wu, H.-I., *Biomedical Optics: Principles and Imaging*. 2012, John Wiley & Sons, Hoboken, NJ: p. 1-15.
91. Svaasand, L.O., Boerslid, T., and Oeveraasen, M., *Thermal and optical properties of living tissue: application to laser-induced hyperthermia.* Lasers in Surgery and Medicine, 1985. **5**: 589-602.
92. Parrish, J.A., *New concepts in therapeutic photomedicine; photochemistry, optical targeting and the therapeutic window.* Journal of Investigative Dermatology, 1981. 77: 45-50.
93. Boulnois, J.-L., *Photophysical processes in recent medical laser developments: a review.* Lasers in Medical Science, 1986. **1**: 47-66.
94. Jacques, S.L. and McAuliffe, D.J., *The melanosome: threshold temperature for explosive vaporization and internal absorption coefficient during pulsed laser irradiation.* Photochemistry and Photobiology, 1991. **53**: 769-775.
95. Beer, A., *Bestimmung der Absorption des rothen Lichts in farbigen Flüssigkeiten.* Annalen der Physik und Chemie, 1852. **86**: 78-88.
96. Contini, D., Martelli, F., and Zaccanti, G., *Photon migration through a turbid slab described by a model based on diffusion approximation. I. Theory.* Applied Optics, 1997. **36**: 4587-4599.
97. Sassaroli, A. and Fantini, S., *Comment on the modified Beer-Lambert law for scattering media.* Physics in Medicine and Biology, 2004. **49**: N255-N257.
98. Kocsis, L., Herman, P., and Eke, A., *The modified Beer–Lambert law revisited.* Physics in Medicine and Biology, 2006. **51**: N91.
99. Jacques, S.L., Roman, J.R., and Lee, K., *Imaging superficial tissues with polarized light.* Lasers in Surgery and Medicine, 2000. **26**: 119-129.
100. O'Doherty, J., Henricson, J., Anderson, C., Leahy, M.J., Nilsson, G.E., and Sjöberg, F., *Sub-epidermal imaging using polarized light spectroscopy for assessment of skin microcirculation.* Skin Research and Technology, 2007. **13**: 472-484.
101. O'Doherty, J., McNamara, P., Clancy, N.T., Enfield, J.G., and Leahy, M.J., *Comparison of instruments for investigation of microcirculatory blood flow and red blood cell concentration.* Journal of Biomedical Optics, 2009. **14:** 034025-1-034025-13.
102. Zhai, H., Chan, H.P., Farahmand, S., Nilsson, G.E., and Maibach, H.I., *Tissue viability imaging: mapping skin erythema.* Skin Research and Technology, 2009. **15**: 14-19.
103. Henricson, J., Nilsson, A., Tesselaar, E., Nilsson, G., and Sjöberg, F., *Tissue viability imaging: microvascular response to vasoactive drugs induced by iontophoresis.* Microvascular Research, 2009. **78**: 199-205.
104. Bergkvist, M., Henricson, J., Iredahl, F., Tesselaar, E., Sjöberg, F., and Farnebo, S., *Assessment of microcirculation of the skin using Tissue Viability Imaging: a promising technique for detecting venous stasis in the skin.* Microvascular Research, 2015. **101**: 20-25.
105. Jubran, A., *Advances in respiratory monitoring during mechanical ventilation.* CHEST Journal, 1999. **116**: 1416-1425.
106. Palmisano, B.W. and Severinghaus, J.W., *Transcutaneous PCO_2 and PO_2: a multicenter study of accuracy.* Journal of Clinical Monitoring, 1990. **6**: 189-195.
107. Nitzan, M., Romem, A., and Koppel, R., *Pulse oximetry: fundamentals and technology update.* Medical Devices: Evidence and Research, 2014. 7: 231.

108. Yoshiya, I., Shimada, Y., and Tanaka, K., *Spectrophotometric monitoring of arterial oxygen saturation in the fingertip.* Medical and Biological Engineering and Computing, 1980. **18**: 27-32.
109. Babchenko, A., Davidson, E., Ginosar, Y., Kurz, V., Faib, I., Adler, D., et al., *Photoplethysmographic measurement of changes in total and pulsatile tissue blood volume, following sympathetic blockade.* Physiological Measurement, 2001. **22**: 389-396.
110. Perkins, G.D., McAuley, D.F., Giles, S., Routledge, H., and Gao, F., *Do changes in pulse oximeter oxygen saturation predict equivalent changes in arterial oxygen saturation?* Critical Care, 2003. **7**: R67.
111. Fouzas, S., Priftis, K.N., and Anthracopoulos, M.B., *Pulse oximetry in pediatric practice.* Pediatrics, 2011. **128**: 740-752.
112. Martin, D.S. and Grocott, M.P.W., *Oxygen therapy in critical illness: precise control of arterial oxygenation and permissive hypoxemia.* Critical Care Medicine, 2013. **41**: 423-432.
113. Chen, J. and Smith, L.E., *Retinopathy of prematurity.* Angiogenesis, 2007. **10**: 133-140.
114. Saugstad, O.D. and Aune, D., *Optimal oxygenation of extremely low birth weight infants: a meta-analysis and systematic review of the oxygen saturation target studies.* Neonatology, 2014. **105**: 55-63.
115. Barker, S.J., Curry, J., Redford, D., and Morgan, S., *Measurement of carboxyhemoglobin and methemoglobin by pulse oximetry: a human volunteer study.* The Journal of the American Society of Anesthesiologists, 2006. **105**: 892-897.
116. Schramm, W.M., Bartunek, A., and Gilly, H., *Effect of local limb temperature on pulse oximetry and the plethysmographic pulse wave.* International Journal of Clinical Monitoring and Computing, 1997. **14**: 17-22.
117. Hynson, J.M., Sessler, D.I., Belani, K., Washington, D., McGuire, J., Merrifield, B., et al., *Thermoregulatory vasoconstriction during propofol/nitrous oxide anesthesia in humans: threshold and oxyhemoglobin saturation.* Anesthesia & Analgesia, 1992. **75**: 947-952.
118. Talke, P. and Stapelfeldt, C., *Effect of peripheral vasoconstriction on pulse oximetry.* Journal of Clinical Monitoring and Computing, 2006. **20**: 305-309.
119. Agashe, G.S., Coakley, J., and Mannheimer, P.D., *Forehead pulse oximetry: headband use helps alleviate false low readings likely related to venous pulsation artifact.* Journal of the American Society of Anesthesiologists, 2006. **105**: 1111-1116.
120. Berkenbosch, J.W. and Tobias, J.D., *Comparison of a new forehead reflectance pulse oximeter sensor with a conventional digit sensor in pediatric patients.* Respiratory Care, 2006. **51**: 726-731.
121. Brimacombe, J. and Keller, C., *Successful pharyngeal pulse oximetry in low perfusion states.* Canadian Journal of Anaesthesia, 2000. **47**: 907-909.
122. Brimacombe, J., Keller, C., and Margreiter, J., *A pilot study of left tracheal pulse oximetry.* Anesthesia & Analgesia, 2000. **91**: 1003-1006.
123. Chen, G., Zhu, Z., Liu, J., and Wei, W., *Esophageal pulse oximetry is more accurate and detects hypoxemia earlier than conventional pulse oximetry during general anesthesia.* Frontiers of Medicine, 2012. **6**: 406-410.
124. Jöbsis, F., *Noninvasive, infrared monitoring of cerebral and myocardial oxygen sufficiency and circulatory parameters.* Science, 1977. **198**: 1264-1267.

125. Crookes, B.A., Cohn, S.M., Bloch, S., Amortegui, J., Manning, R., Li, P., et al., *Can near-infrared spectroscopy identify the severity of shock in trauma patients?* Journal of Trauma - Injury Infection and Critical Care, 2005. **58**: 806-816.
126. Schwarte, L.A., Stevens, M.F., and Ince, C., *Splanchnic perfusion and oxygenation in critical illness*. In: *Intensive Care Medicine*, Vincent J.-L., (Ed.) 2006, Springer, New York: p. 627-640.
127. Pellicer, A. and del Carmen Bravo, M. *Near-infrared spectroscopy: a methodology-focused review*. Seminars in Fetal and Neonatal Medicine, 2011. **16**: 42-49.
128. Cui, W.J., Kumar, C., and Chance, B., *Experimental study of migration depth for the photons measured at sample surface.* Proceedings SPIE, 1991. **1431**: 180-191.
129. Ferrari, M., Muthalib, M., and Quaresima, V., *The use of near-infrared spectroscopy in understanding skeletal muscle physiology: recent developments.* Philosophical Transactions of the Royal Society of London A: Mathematical, Physical and Engineering Sciences, 2011. **369**: 4577-4590.
130. Holzle, F., Loeffelbein, D.J., Nolte, D., and Wolff, K.D., *Free flap monitoring using simultaneous non-invasive laser Doppler flowmetry and tissue spectrophotometry.* Journal of Cranio-Maxillofacial Surgery, 2006. **34**: 25-33.
131. Pham, T.H., Coquoz, O., Fishkin, J.B., Anderson, E., and Tromberg, B.J., *Broad bandwidth frequency domain instrument for quantitative tissue optical spectroscopy.* Review of Scientific Instruments, 2000. **71**: 2500-2513.
132. Svensson, T., Alerstam, E., Khoptyar, D., Johansson, J., Folestad, S., and Andersson-Engels, S., *Near-infrared photon time-of-flight spectroscopy of turbid materials up to 1400 nm.* Review of Scientific Instruments, 2009. **80**: 063105.
133. Wolf, M., Ferrari, M., and Quaresima, V., *Progress of near-infrared spectroscopy and topography for brain and muscle clinical applications.* Journal of Biomedical Optics, 2007. **12**: 062104-1-062104-14.
134. Smith, M., *Shedding light on the adult brain: a review of the clinical applications of near-infrared spectroscopy.* Philosophical Transactions of the Royal Society of London A: Mathematical, Physical and Engineering Sciences, 2011. **369**: 4452-4469.
135. Creteur, J., Carollo, T., Soldati, G., Buchele, G., De Backer, D., and Vincent, J.-L., *The prognostic value of muscle StO2 in septic patients.* Intensive Care Medicine, 2007. **33**: 1549-1556.
136. Cohn, S.M., Crookes, B.A., and Proctor, K.G., *Near-infrared spectroscopy in resuscitation.* Journal of Trauma and Acute Care Surgery, 2003. **54**: S199-S202.
137. Wolf, M. and Greisen, G., *Advances in near-infrared spectroscopy to study the brain of the preterm and term neonate.* Clinics in Perinatology, 2009. **36**: 807-834.
138. Ruf, B., Bonelli, V., Balling, G., Hörer, J., Nagdyman, N., Braun, S.L., et al., *Intraoperative renal near-infrared spectroscopy indicates developing acute kidney injury in infants undergoing cardiac surgery with cardiopulmonary bypass: a case–control study.* Critical Care, 2015. **19**: 27.
139. Hyttel-Sorensen, S., Austin, T., van Bel, F., Benders, M., Claris, O., Dempsey, E., et al., *A phase II randomized clinical trial on cerebral near-infrared spectroscopy plus a treatment guideline versus treatment as usual for extremely preterm infants during the first three days of life (SafeBoosC): study protocol for a randomized controlled trial.* Trials, 2013. **14**: 1-8.
140. Hyttel-Sorensen, S., Pellicer, A., Alderliesten, T., Austin, T., van Bel, F., Benders, M., et al., *Cerebral near infrared spectroscopy oximetry in extremely preterm infants: phase II randomised clinical trial.* BMJ, 2015. **350**: g7635.

141. Pellicer, A., Greisen, G., Benders, M., Claris, O., Dempsey, E., Fumagally, M., et al., *The SafeBoosC phase II randomised clinical trial: a treatment guideline for targeted near-infrared-derived cerebral tissue oxygenation versus standard treatment in extremely preterm infants.* Neonatology, 2013. **104**: 171-178.
142. Villringer, A. and Chance, B., *Non-invasive optical spectroscopy and imaging of human brain function.* Trends in Neurosciences, 1997. **20**: 435-442.
143. Lipcsey, M., Woinarski, N.C., and Bellomo, R., *Near infrared spectroscopy (NIRS) of the thenar eminence in anesthesia and intensive care.* Annals of Intensive Care, 2012. **2**: 11.
144. Hamaoka, T., Katsumura, T., Murase, N., Nishio, S., Osada, T., Sako, T., et al., *Quantification of ischemic muscle deoxygenation by near infrared time-resolved spectroscopy.* Journal of Biomedical Optics, 2000. **5**: 102-105.
145. Matcher, S.J. and Cooper, C.E., *Absolute quantification of deoxyhemoglobin concentration in tissue near-infrared spectroscopy.* Physics in Medicine and Biology, 1994. **39**: 1295-1312.
146. Liebert, A., Wabnitz, H., Grosenick, D., Moller, M., Macdonald, R., and Rinneberg, H., *Evaluation of optical properties of highly scattering media by moments of distributions of times of flight of photons.* Applied Optics, 2003. **42**: 5785-5792.
147. Patterson, M.S., Chance, B., and Wilson, B.C., *Time resolved reflectance and transmittance for the noninvasive measurement of tissue optical properties.* Applied Optics, 1989. **28**: 2331-2336.
148. Sevick, E.M., Chance, B., Leigh, J., Nioka, S., and Maris, M., *Quantification of time-resolved and frequency-resolved optical-spectra for the determination of tissue oxygenation.* Analytical Biochemistry, 1991. **195**: 330-351.
149. Tromberg, B.J., Shah, N., Lanning, R., Cerussi, A., Espinoza, J., Pham, T., et al., *Non-invasive in vivo characterization of breast tumors using photon migration spectroscopy.* Neoplasia, 2000. **2**: 26-40.
150. Taroni, P., Danesini, G., Torricelli, A., Pifferi, A., Spinelli, L., and Cubeddu, R., *Clinical trial of time-resolved scanning optical mammography at 4 wavelengths between 683 and 975 nm.* Journal of Biomedical Optics, 2004. **9**: 464-473.
151. Wolf, M., Ferrari, M., and Quaresima, V., *Progress of near-infrared spectroscopy and topography for brain and muscle clinical applications.* Journal of Biomedical Optics, 2007. **12**: 062104-1-062104-14.
152. Hebden, J.C., *Advances in optical imaging of the newborn infant brain.* Psychophysiology, 2003. **40**: 501-510.
153. Koga, S., Poole, D.C., Fukuoka, Y., Ferreira, L.F., Kondo, N., Ohmae, E., et al., *Methodological validation of the dynamic heterogeneity of muscle deoxygenation within the quadriceps during cycle exercise.* American Journal of Physiology - Regulatory, Integrative and Comparative Physiology, 2011. **301**: R534-R541.
154. Chin, L.M.K., Kowalchuk, J.M., Barstow, T.J., Kondo, N., Amano, T., Shiojiri, T., et al., *The relationship between muscle deoxygenation and activation in different muscles of the quadriceps during cycle ramp exercise.* Journal of Applied Physiology, 2011. **111**: 1259-1265.
155. Khoptyar, D., Subash, A.A., Johansson, S., Saleem, M., Sparén, A., Johansson, J., et al., *Broadband photon time-of-flight spectroscopy of pharmaceuticals and highly scattering plastics in the VIS and close NIR spectral ranges.* Optics Express, 2013. **21**: 20941-20953.
156. Whitaker, D.K., *Time for capnography – everywhere.* Anaesthesia, 2011. **66**: 544-549.

157. Kodali, B.S. and Urman, R.D., *Capnography during cardiopulmonary resuscitation: current evidence and future directions.* Journal of Emergencies, Trauma and Shock, 2014. **7**: 332-40.
158. Soto, R.G., Fu, E.S., Vila, H., and Miguel, R.V., *Capnography accurately detects apnea during monitored anesthesia care.* Anesthesia and Analgesia, 2004. **99**: 379-382.
159. Bhavanishankar, K., Moseley, H., Kumar, A.Y., and Delph, Y., *Capnometry and anesthesia.* Canadian Journal of Anaesthesia, 1992. **39**: 617-632.
160. Cheng, E.Y., Woehlck, H., and Mazzeo, A.J., *Capnography in critical care medicine.* Journal of Intensive Care Medicine, 1997. **12**: 18-32.
161. McCurdy, M.R., Bakhirkin, Y., Wysocki, G., Lewicki, R., and Tittel, F.K., *Recent advances of laser-spectroscopy-based techniques for applications in breath analysis.* Journal of Breath Research, 2007. **1**: 014001.
162. Lundberg, J., Farkas-Szallasi, T., Weitzberg, E., Rinder, J., Lidholm, J., Änggåard, A., et al., *High nitric oxide production in human paranasal sinuses.* Nature Medicine, 1995. **1**: 370-373.
163. Sjöholm, M., Somesfalean, G., Alnis, J., Andersson-Engels, S., and Svanberg, S., *Analysis of gas dispersed in scattering media.* Optics Letters, 2001. **26**: 16-18.
164. Sigrist, M.W. (Ed.), *Air Monitoring by Spectroscopic Techniques*1994. New York: John Wiley & Sons.
165. Svanberg, S., *Gas in scattering media absorption spectroscopy – from basic studies to biomedical applications.* Laser & Photonics Reviews, 2013. **7**: 779-796.
166. Lewander, M., Guan, Z., Persson, L., Olsson, A., and Svanberg, S., *Food monitoring based on diode laser gas spectroscopy.* Applied Physics B, 2008. **93**: 619-625.
167. Zhang, H., Huang, J., Li, T., Wu, X., Svanberg, S., and Svanberg, K., *Studies of tropical fruit ripening using three different spectroscopic techniques.* Journal of Biomedical Optics, 2014. **19**: 067001-1-067001-8.
168. Andersson, M., Persson, L., Sjöholm, M., and Svanberg, S., *Spectroscopic studies of wood-drying processes.* Optics Express, 2006. **14**: 3641-3653.
169. Svensson, T., Andersson, M., Rippe, L., Svanberg, S., Andersson-Engels, S., Johansson, J., et al., *VCSEL-based oxygen spectroscopy for structural analysis of pharmaceutical solids.* Applied Physics B, 2008. **90**: 345-354.
170. Svensson, T., Adolfsson, E., Burresi, M., Savo, R., Xu, C.T., Wiersma, D.S., et al., *Pore size assessment based on wall collision broadening of spectral lines of confined gas: experiments on strongly scattering nanoporous ceramics with fine-tuned pore sizes.* Applied Physics B, 2013. **110**: 147-154.
171. Mei, L., Somesfalean, G., and Svanberg, S., *Pathlength determination for gas in scattering media absorption spectroscopy.* Sensors, 2014. **14**: 3871-3890.
172. Buck, A.L., *New equations for computing vapor pressure and enhancement factor.* Journal of Applied Meteorology, 1981. **20**: 1527-1532.
173. Persson, L., Andersson, M., Cassel-Engquist, M., Svanberg, K., and Svanberg, S., *Gas monitoring in human sinuses using tunable diode laser spectroscopy.* Journal of Biomedical Optics, 2007. **12**: 054001-1-054001-8.
174. Lewander, M., Guan, Z.G., Svanberg, K., Svanberg, S., and Svensson, T., *Clinical system for non-invasive in situ monitoring of gases in the human paranasal sinuses.* Optics Express, 2009. **17**: 10849-10863.
175. Lewander, M., Lindberg, S., Svensson, T., Siemund, R., Svanberg, K., and Svanberg, S., *Non-invasive diagnostics of the maxillary and frontal sinuses based on diode laser gas spectroscopy.* Rhinology, 2012. **50**: 26-32.

176. Lindberg, S., Lewander, M., Svensson, T., Siemund, R., Svanberg, K., and Svanberg, S., *Method for studying gas composition in the human mastoid cavity by use of laser spectroscopy.* Annals of Otology Rhinology and Laryngology, 2012. **121**: 217-223.
177. Zhang, H., Huang, J., Li, T., Svanberg, S., and Svanberg, K., *Optical detection of middle ear infection using spectroscopic techniques: phantom experiments.* Journal of Biomedical Optics, 2015. **20**: 057001-1-057001-8.
178. Öberg, P.A., *Laser-Doppler flowmetry.* Critical Reviews in Biomedical Engineering, 1990. **18**: 125-163.
179. Rådegran, G., *Limb and skeletal muscle blood flow measurements at rest and during exercise in human subjects.* Proceedings of the Nutrition Society, 1999. **58**: 887-898.
180. Wårdell, K., Jakobsson, A., and Nilsson, G.E., *Laser Doppler perfusion imaging by dynamic light scattering.* IEEE Transactions on Biomedical Engineering, 1993. **40**: 309-316.
181. Allen, J. and Howell, K., *Microvascular imaging: techniques and opportunities for clinical physiological measurements.* Physiological Measurement, 2014. **35**: R91.
182. Daly, S.M. and Leahy, M.J., *'Go with the flow': a review of methods and advancements in blood flow imaging.* Journal of Biophotonics, 2013. **6**: 217-255.
183. Cole, A.L., Herman, R.A., Heimlich, J.B., Ahsan, S., Freedman, B.A., and Shuler, M.S., *Ability of near infrared spectroscopy to measure oxygenation in isolated upper extremity muscle compartments.* Journal of Hand Surgery, 2012. **37**: 297-302.
184. Soller, B.R., Ryan, K.L., Rickards, C.A., Cooke, W.H., Yang, Y., Soyemi, O.O., et al., *Oxygen saturation determined from deep muscle, not thenar tissue, is an early indicator of central hypovolemia in humans.* Critical Care Medicine, 2008. **36**: 176-182.
185. van Beekvelt, M.C.P., Borghuis, M.S., van Engelen, B.G.M., Wevers, R.A., and Colier, W.N.J.M., *Adipose tissue thickness affects in vivo quantitative near-IR spectroscopy in human skeletal muscle.* Clinical Science, 2001. **101**: 21-28.
186. Fitzpatrick, T.B., *The validity and practicality of sun-reactive skin type-I through type-VI.* Archives of Dermatology, 1988. **124**: 869-871.
187. De Blasi, R.A., Palmisani, S., Alampi, D., Mercieri, M., Romano, R., Collini, S., et al., *Microvascular dysfunction and skeletal muscle oxygenation assessed by phase-modulation near-infrared spectroscopy in patients with septic shock.* Intensive Care Medicine, 2005. **31**: 1661-1668.
188. Cross, T.J., van Beekvelt, M., Constantini, K., and Sabapathy, S., *Measurement of regional forearm muscle haemodynamics via the near-infrared spectroscopy venous occlusion technique: the impact of hand circulatory occlusion.* Physiological Measurement, 2014. **35**: 2563-2573.
189. Cross, T.J. and Sabapathy, S., *The impact of venous occlusion per se on forearm muscle blood flow: implications for the near-infrared spectroscopy venous occlusion technique.* Clinical Physiology and Functional Imaging, 2015. doi: 10.1111/cpf.12301.
190. Woinarski, N.C., Suzuki, S., Lipcsey, M., Lumsden, N., Chin-Dusting, J., Schneider, A.G., et al., *Near-infrared spectroscopy of the thenar eminence to estimate forearm blood flow.* Critical Care and Resuscitation, 2013. **15**: 323-326.
191. Monthé-Sagan, K., Fischer, M.-O., Saplacan, V., Gerard, J.-l., Hanouz, J.-L., and Fellahi, J.-L., *Near-infrared spectroscopy to assess microvascular dysfunction: a prospective pilot study in cardiac surgery patients.* Journal of Critical Care, 2016. **31**: 264-268.

192. Hyttel-Sorensen, S., Hessel, T.W., and Greisen, G., *Peripheral tissue oximetry: comparing three commercial near-infrared spectroscopy oximeters on the forearm.* Journal of Clinical Monitoring and Computing, 2014. **28**: 149-155.
193. Lacroix, S., Gayda, M., Gremeaux, V., Juneau, M., Tardif, J.-C., and Nigam, A., *Reproducibility of near-infrared spectroscopy parameters measured during brachial artery occlusion and reactive hyperemia in healthy men.* Journal of Biomedical Optics, 2012. **17**: 077010-1-077010-5.
194. Svendsen, L.B., Flink, P., Wojdemann, M., Riber, C., Mogensen, T., and Secher, N.H., *Muscle oxygen saturation during surgery in the lithotomy position.* Clinical Physiology, 1997. **17**: 433-438.
195. Palanca, A.A., Yang, A., and Bishop, J.A., *The effects of limb elevation on muscle oxygen saturation: A near-infrared spectroscopy study in humans.* Physical Medicine and Rehabilitation, 2015. doi:10.1016/j.pmrj.2015.07.015.
196. Daanen, H.A.M., *Finger cold-induced vasodilation: a review.* European Journal of Applied Physiology, 2003. **89**: 411-426.
197. Davis, S.L., Fadel, P.J., Cui, J., Thomas, G.D., and Crandall, C.G., *Skin blood flow influences near-infrared spectroscopy-derived measurements of tissue oxygenation during heat stress.* Journal of Applied Physiology, 2006. **100**: 221-224.
198. Vallet, B., *Vascular reactivity and tissue oxygenation*. Intensive Care Medicine, 1998. **24**: p. 550-563.
199. Doerschug, K.C., Delsing, A.S., Schmidt, G.A., and Haynes, W.G., *Impairments in microvascular reactivity are related to organ failure in human sepsis.* American Journal of Physiology - Heart and Circulatory Physiology, 2007. **293**: H1065-H1071.
200. Saager, R.B., Balu, M., Crosignani, V., Sharif, A., Durkin, A.J., Kelly, K.M., et al., *In vivo measurements of cutaneous melanin across spatial scales: using multiphoton microscopy and spatial frequency domain spectroscopy.* Journal of Biomedical Optics, 2015. **20**: 066005-1-066005-10.
201. Wassenaar, E.B. and Van den Brand, J.G.H., *Reliability of near-infrared spectroscopy in people with dark skin pigmentation.* Journal of Clinical Monitoring and Computing, 2005. **19**: 195-199.
202. Yu, G., Durduran, T., Lech, G., Zhou, C., Chance, B., Mohler, E.R., et al., *Time-dependent blood flow and oxygenation in human skeletal muscles measured with noninvasive near-infrared diffuse optical spectroscopies.* Journal of Biomedical Optics, 2005. **10**: 024027-1024027-12.
203. Ohmae, E., Nishio, S., Oda, M., Suzuki, H., Suzuki, T., Ohashi, K., et al., *Sensitivity correction for the influence of the fat layer on muscle oxygenation and estimation of fat thickness by time-resolved spectroscopy.* Journal of Biomedical Optics, 2014. **19**: 067005-1-067005-11.
204. Matsushita, K., Homma, S., and Okada, E. *Influence of adipose tissue on muscle oxygenation measurement with an NIRS instrument*. Proceedings SPIE **3194**, 1998: 159-165.
205. Quaresima, V., Ferrari, M., Franceschini, M.A., Hoimes, M.L., and Fantini, S., *Spatial distribution of vastus lateralis blood flow and oxyhemoglobin saturation measured at the end of isometric quadriceps contraction by multichannel near-infrared spectroscopy.* Journal of Biomedical Optics, 2004. **9**: 413-420.
206. Binzoni, T., Quaresima, V., Barattelli, G., Hiltbrand, E., Gürke, L., Terrier, F., et al., *Energy metabolism and interstitial fluid displacement in human gastrocnemius during short ischemic cycles.* Journal of Applied Physiology, 1998. **85**: 1244-1251.

207. Mancini, D.M., Bolinger, L., Li, H., Kendrick, K., Chance, B., and Wilson, J.R., *Validation of near-infrared spectroscopy in humans.* Journal of Applied Physiology, 1994. 77: 2740-2747.
208. Davis, M.L. and Barstow, T.J., *Estimated contribution of hemoglobin and myoglobin to near infrared spectroscopy.* Respiratory Physiology & Neurobiology, 2013. **186**: 180-187.
209. Krite Svanberg, E. and Svanberg, S., *Equipment and method for internal laser illumination for medical gas analysis,* Swedish Patent Application No 1500335-3. August 2015.